Capacity Quantification of Two-Way Arching Reinforced Masonry Walls under Blast Loads

By

Brent Wybenga,

B.Tech., Dipl. (Arch.) Tech

A Thesis

Submitted to the School of Graduate Studies

In Partial Fulfillment of the Requirements

For the Degree of

Master of Applied Science

McMaster University

MASTER OF APPLIED SCIENCE (2014) McMaster University

(CIVIL ENGINEERING) Hamilton, Ontario

Title:	Capacity Quantification of Two-Way Arching Reinforced Masonry Walls under Blast Loads
Author:	Brent Wybenga, B.Tech., Dipl. (Arch.) Tech
Supervisors:	Dr. Wael El-Dakhakhni and Dr. Waleed Mekky
Number of pages:	xv, 118

Abstract

The focus of this study is on evaluating the performance of nine, one-third scale, arching, reinforced masonry (RM) walls subjected to blast loads and three, one-third scale arching, RM walls subjected to out-of-plane static airbag loads. These RM walls were supported on four sides to enforce two-way arching allowing the ability to monitor individual response to varying levels of blast loads and standoff distances. The uniformity of the blast pressure and impulse were ensured by a specifically designed test enclosure, diminishing the wrap-around and clearing effects, allowing valuable data to be documented. The damage levels noted, ranged from Superficial to Blowout compared directly to the CSA S850-12 performance limits. The outcome of this experiment demonstrates the beneficial effect of two-way arching on the flexural behaviour of RM walls under impulsive loading. The use of two-way arching RM walls significantly reduces structural damage and increases out-of-plane resistance, which in turn enhances the overall structural integrity and building preservation. Further, when subjected to blast, two-way arching RM walls considerably reduces debris and their dispersal, thus increasing public safety and minimizing hazard levels. When using the experimental test data results to calibrate finite element models (FEM), more analytical data points can be obtained and therefore getting a larger range of scaled distances and trials. The validation of the LS-DYNA model can be used as an alternative to the costly experimental data, as the information collected concluded that the FEM gave damage patterns and failure modes that were comparable with experimental results. The test data collected provides a better understanding of RM wall response to blast loads and to the ongoing Masonry

Blast Performance Database (MBPD) project at McMaster University. The generated MBPD will in turn contribute to masonry design clauses in the future editions of the recently introduced Canadian Standards CSA S850-12 “Design and Assessment of Buildings Subjected to Blast Loads”.

Acknowledgements and Dedication

Thank you to Dr. El-Dakhakhni, my Research Supervisor; his extensive knowledge and guidance, academically and technically, have made this dissertation possible. Both Mr. Wheeler and Mr. Heerema, technicians at the Applied Dynamics Laboratory, who kindly dedicated their time and expertise in finalizing this project. Dr. Mekky for his invaluable skills and assistance in LS-DYNA. My parents, who shared the importance of thoroughness and dedication to every task, and their belief in my success. A special thank you to my wife Sarah, for believing in me, encouraging me, and supporting me throughout this project. Your understanding, support and love are always deeply appreciated. Throughout my studies there have been many others who have supported me; thank you for your help, wisdom, understanding, and confidence in me.

The funding provided by McMaster University Centre for Effective Design of Structures (CEDS) and the Ontario Research and Development Challenge Fund (ORDCF), the Natural Sciences and Engineering Research Council of Canada (NSERC), the Canadian Concrete Masonry Producers Association (CCMPA) and the Canada Masonry Design Centre (CMDC) has made this research possible. The Ontario Masonry Contractors Association (OMCA) generously provided masons for completion of this project, the Canadian Explosives Research Laboratory (CERL) provided their time and expertise in conducting the field blast tests and the Canadian Forces provided the range where the testing was conducted.

Table of Contents

List of Figures

List of Tables

List of Symbols

A_s = area of reinforcing steel;

c = distance from extreme compression fibre to the neutral axis;

COV = coefficient of variation;

d = distance from extreme compression fibre to centroid of tension reinforcement;

E = total energy of the explosive;

E_s = modulus of elasticity of steel;

FEM = finite element model;

f'_m = average compressive strength of masonry prisms;

F_y = yield strength of steel;

h_w = wall height;

I = moment of inertia;

I_s = positive blast impulse;

l = length;

M_u = moment resistance;

$P(t)$ = blast pressure;

P_a = ambient pressure;

P_o = overpressure;

P_s = peak incident pressure;

R = actual distance from the centre of explosion;

$SDOF$ = single degree of freedom;

t = time of interest;

T_d = positive phase duration;

t_w = wall thickness;

W = charge mass;

Z = scaled distance;

$q_{n\,\inf}$ = out-of-plane resistance;

q_u = ultimate out-of-plane load;

α = shape modifier;

β_1 = ratio of depth of rectangular compression block to depth to neutral axis;

δ = displacement;

ε_s = strain in reinforcing steel; and

λ_2 = slenderness parameter

1 Introduction

1.1 Background

This thesis examines the mechanics of two-way arching reinforced masonry infill walls' response to free-field blast loading. This research is critical to the development of new reliable information for engineers, architects and designers, as well as to facilitate the assessment of the current masonry blast design provisions in North America. This information is necessary to ensure the structural integrity of new and existing masonry structures. Whereby documenting the effect of blast loads on reinforced masonry walls, in a controlled environment, yields high quality data that may be used to verify design clauses in future editions of blast design standards.

A large percentage of the world's population resides and/or works in buildings constructed with masonry infill walls. Customarily, masonry infill panels are an attractive choice for exterior wall partition construction because they are easily constructed in place around existing structural or mechanical elements at an affordable cost. Deliberate and accidental explosions have made it necessary for a review of the vulnerability of existing masonry construction and consideration of different design strategies for new construction. Blast loads, whether deliberate or accidental, can result in extreme strains of building elements that can undermine the overall integrity of the entire structure. Physical experimental tests, which utilize duplicate blast load conditions are very useful to predict anticipated behavior. There is a concern that current building standards and guidelines predicting the mechanics of reinforced masonry infill walls

under out-of-plane action from non-blast loads are in need of review and update to address the unique nature of blast loads. Historically, blast effect data were considered pertinent information for government and military purposes only. However, the documentation of this data is presently becoming essential for design of critical civilian facilities as well. In order to have a real benefit and practical use, this data needs to be collected in a controlled setting. Recently, in response to this growing demand, relevant guidelines for analysis and design of buildings subjected to blast loads have been published in both Canada by the Canadian Standards Association (CSA) Design and Assessment of Buildings Subjected to Blast Loads *CSA S850* (2012) standards and in the United States through the American Society of Civil Engineers (ASCE) Blast Protection of Buildings *ASCE 59* (2011) standards.

It is expected that test results generated under controlled and documented boundary conditions gives high quality, reliable data that can be used to interpret the effects of blast loads on reinforced masonry infill walls. The challenge, however, is to duplicate real life scenarios that facilitates accurate and useful data collection. Experimental testing with blast loads poses multiple obstacles to researchers, such as: extensive and cost prohibitive testing, construction, labour, transportation to test sites, and other logistical procedures, such as managing a controlled environment, explosives, and test range site availability. Although the behavior of masonry walls subjected to blast loads have been experimentally investigated and analyzed by a number of researchers in the past, most of these studies have been to predict the capacity of unreinforced masonry (URM) walls

subjected to out-of-plane blast loads or the effectiveness of different retrofitting techniques (Abou-Zeid et al., 2011 and Myers et al. 2004). Abou-Zeid et al. (2011) investigated the blast resistance of arching URM walls and concluded that masonry walls that can resist loads through an arching mechanism significantly improved the performance and structural resistance relative to non-arching URM walls. The focus of this paper will be to examine the mechanics of two-way arching reinforced masonry infill walls' response to free-field blast loading. The response parameters of interest include wall deflections and their failure modes. The experimental blast results of nine masonry infill wall specimens, confined by four rigid supports (simulating upper and lower rigid floor beams, and side columns), subjected to blast loading will be reported in detail in this thesis, as well as any arching effects and its significance to masonry wall performance.

1.2 Research Significance and Objectives

The documentation of the effect of blast loading on two-way arching reinforced masonry walls in a controlled environment will provide significant blast performance data to facilitate blast design guidelines and evaluate the structural integrity of existing buildings.

The principal objectives of this research are to perform experimental out-of-plane blast and static testing on arching reinforced masonry infill walls with different reinforcement ratios, boundary conditions and scaled distances, and to explore the use of finite element models to generate essential data for the Masonry Blast Performance Database (MBPD)

at McMaster University to support the development of input of future design clauses in the CSA S850 standard.

1.3 Scope and Methodology

This thesis is focused on experimentally investigating the structural performance of one-third scale, two-way arching reinforced masonry walls subjected to free-field blast loading. The first phase of the test program involved static air-bag tests of three, one-third scale, reinforced masonry walls with an airbag. The results from the first phase were compared with theoretically predicted capacities determined with the yield line method and flexural theory. The second phase of this test program involved free-field blast tests of nine, one-third scale, reinforced masonry walls. The final phase of this experimental investigation included the development of a finite element model in LS-DYNA code. This model was compared to results from the free-field blast tests based on: the walls' failure modes, and damage patterns.

1.4 Thesis Organization

This thesis contains six chapters, outlined as follows:

Chapter 1 introduces the background of the study, research significance and objectives, the scope and methodology and the organization and layout of the written dissertation. It also provides a literature review based on the main topics presented in the thesis,

providing general information and brief historical significance. Specific topics include: masonry construction, blast loading and finite element modelling of blast loads.

Chapter 2 describes the experimental program, the design details of masonry wall specimens, material properties, design and construction of test facilities, external and internal instrumentation and comprehensive test procedures.

Chapter 3 presents the experimental test results, including the static airbag testing of three test specimens, and a comparison to an analytical yield line estimate and the American Masonry Standards Joint Committee (MSJC) design code approach to predict the out-of-plane arching capacities of masonry walls.

Chapter 4 provides the displacements, rotations, failure modes and crack patterns in each of the nine masonry specimens tested under blast loading.

Chapter 5 discusses the development of the finite element (FE) model of the wall specimens and the most significant stages and components involved in creating the model. This chapter also provides results from the corresponding FE simulations of the experimental tests and compares the damage patterns and failure modes between the FE simulations and the physical test data.

Chapter 6 concludes the research with the conclusions and recommendations of the dissertation.

1.5 Literature Review

In the following section, pertinent literature reviewed by the author will be presented as it relates to masonry construction, blast loads, experimental testing and numerical modelling. Further more, to determine ways to enhance structural integrity, the behaviours of reinforced masonry, blast and blast loading must be explored and evaluated. Finally, as physical blast testing may not be practical nor financially feasible, numerical modeling must be considered and heavily relied upon.

1.5.1 Masonry Construction

Masonry, whether chosen for its aesthetic, versatile, or durable nature, is readily available and a cost-effective material. Masonry is a durable construction material and is utilized in the form of concrete, fire clay, or stone in the form of blocks, bricks or other modular units. The durability of a masonry assemblage is determined by several factors including; the quality of the materials and the workmanship and the type and detailing of reinforcing materials utilized.

The compressive strength of concrete masonry assemblages vary from approximately 7 MPa to 34 MPa (Hamid and Drysdale (2005)) based on the raw materials of the unit, orientation in stacking, block strength, grout strength, etc. Although unreinforced

masonry (URM) is commonly used for non-loadbearing construction of low-rise buildings in North America, it can be vulnerable under dynamic loads. Loadbearing URM can be particularly vulnerable to the effects of out-of-plane loading when such loads exceed the threshold of elastic behaviour in the masonry. Reinforced masonry (RM) can be used to improve the out-of-plane wall behaviour. Many studies have been conducted regarding the reinforcement of masonry and there are design standards, which give designers minimum requirements of the design, analysis and detailing of masonry structures in place in Canada, CSA (Canadian Standards Association), and the Masonry Standards Joint Commission (MSJC) in the United States. The damage, both to personnel and structures, can be reduced through examination of failure modes, capacity quantification and crack patterns under specific blast testing.

1.5.2 Out-of-Plane Wall Behaviour Enhancement

To date, there have been various studies performed to quantify, improve and enhance the out-of-plane behavior of masonry walls. Most of the research is based on expanding the knowledge and database for the capacities of URM walls to seismic or blast events. Hrynyk and Myers (2008) tested a series of arching URM walls with retrofit techniques to out-of-plane static loading. The infill walls were retrofitted with a combination of fiber-reinforced polymer (FRP) grids and polyurea material. The study found that the walls failed prematurely due to a lack of anchorage between the strengthened walls and surrounding structure. A simplified model was developed to estimate the out-of-plane capacity, finding that the model predictions agreed with the experimental work. Varela-

Rivera et al. (2012) tested six full-scale confined masonry walls to out-of-plane airbag incremental uniform loading. The out-of-plane experimental strengths were compared to an analytical model based on the spring-strut, failure line, and yield line methods and again the experimental out-of-plane strengths were well predicted with the model based on the spring-strut method. Results were underestimated based on the yield and failure line methods, and were overestimated with the model based on the compressive strut method. Hamed and Rabinovitch (2006) studied the out-of-plane behavior of masonry walls that were externally strengthened with GFRP strips. This study found that by restraining longitudinal elongation out-of-plane deflection could be significantly decreased.

The arching mechanism is a simple and economic approach to enhance the strength of new and existing reinforced masonry walls to out-of-plane loads, including blast. McDowell et al. (1956) first developed the arching mechanism theory based on the assumption that URM walls fully restrained by rigid supports may crack in the middle and form two rigid segments as depicted in Fig. 1.1. The restraining action of the rigid supports produces large in-plane compressive (thrust) forces within the wall and prevents debris formation due to increased friction and interlocking forces between masonry courses. In order for this arching action to take place and fully develop, it is critical that the wall is fully restrained at the rigid supports (Hamid and Drysdale 2005) with no gap. As a result, arching can increase the capacity and significantly enhance the performance of reinforced masonry walls. Abou-Zeid et al. (2011), concluded that the capacity of

URM walls subjected to out-of-plane blast loads was significantly improved due to the arching effect. Also, the arching effect reduced the hazard from flying debris in the tested URM. The arching mechanism can potentially reduce the hazard level for building occupants during a blast load by reducing the number of fragments and flying debris from within a building or structure.

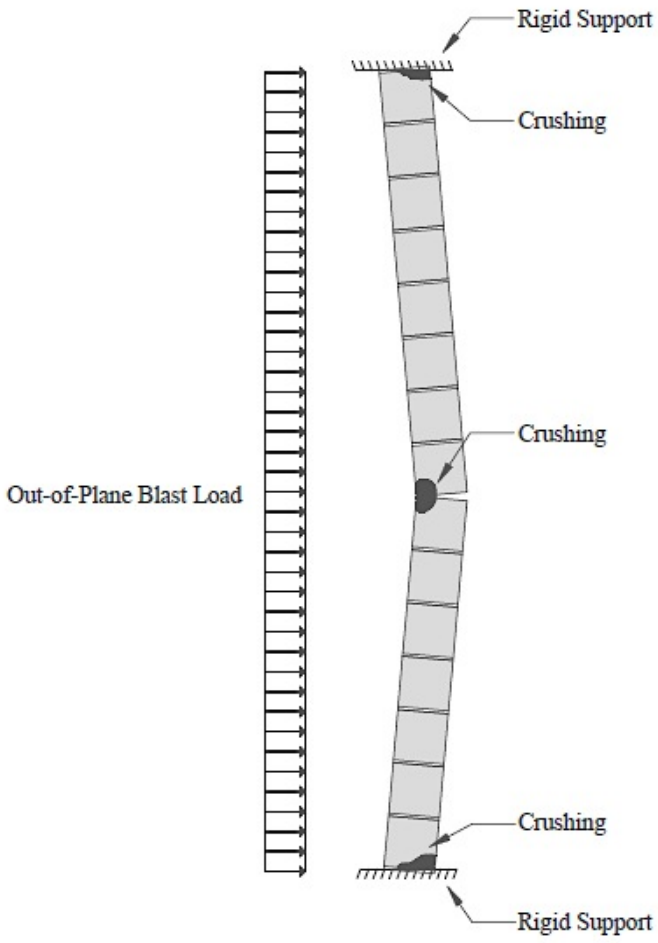

Figure 1.1: Arching Mechanism

1.5.3 Blast Loading

1.5.3.1 Explosions

Strehlow and Baker (1976) describe explosions as:

"In general, an explosion is said to have occurred in the atmosphere if energy is released over a sufficiently small time and in a sufficiently small volume so as to generate a pressure wave of finite amplitude traveling away from the source. This energy may have originally been stored in the system in a variety of forms; these include nuclear, chemical, electrical or pressure energy, for example. However, the release is not considered to be explosive unless it is rapid enough and concentrated enough to produce a pressure wave that one can hear. Even though many explosions damage their surroundings, it is not necessary that external damage be produced by the explosion. All that is necessary is that the explosion is capable of being heard."

The above definition of explosions, refer to free-field explosions, which can be further categorized into three different groups; nuclear, physical and chemical. In a nuclear explosion, the energy released arises in the form of an atomic nuclei. Physical explosions are considered to be an explosion due to compressed gas, and chemical explosions are the rapid oxidation of fuel elements forming an explosive compound (Mays and Smith 1995). As the blast wave gradually moves away from the detonation point, its pressure drops significantly and becomes equal to the atmospheric pressure. The important two types of blast conditions are free-air blast loads and surface blast loads. Free-air blasts

are when the charge centre is at a significant distance from any surface resulting in a spherical blast wave. Surface blasts are when the blast is on the ground or in close proximity to the ground resulting in a hemispherical wave.

1.5.3.2 Scaling

Scaling laws can be used to extrapolate results obtained from reduced scale testing to the prototype (full-scale) case (Harris and Sabnis 1999). One of the most common scaling methods used in blast load normalization and quantification is the Hopkinson-Cranz cubed root scaling first developed by Hopkinson (1915) as given in Eq. 1, which is used to predict the dimensionless properties of blast waves from large-scale explosions based on much smaller tests performed (Baker et al. 1973). The scaled-distance dimensionless parameter Z can be produced from the same blast source and detonated in the same atmosphere.

$$Z = \frac{R}{W^{1/3}} \tag{1}$$

Where Z is the scaled-distance parameter, R is the distance from the centre of the explosion (standoff distance) and W is the explosive charge mass (Baker et al. 1973).

In a controlled test, the Hopkinson-Cranz cubed root scaling can be used to considerably reduce the amount of explosive required for testing and to expedite and simplify free-field

high explosive testing giving self-similar blast wave characteristics with the most important of which is peak overpressure. This has important effects on both the safety on explosive testing and cost.

1.5.3.3 Idealizaion of the pressure-time profile

Figure 1.2 shows an ideal incident blast wave signature. An ideal blast wave is comprised of two main phases during the pressure time history, a positive phase and a negative phase. In a typical study of blast waves, the negative phase of the blast wave is usually ignored because its effects are generally insignificant compared to the effects of the positive phase when considering structural behaviour (Baker et al. 1983). The main properties being the peak reflective pressure, P_s, which is the instantaneous rise to the highest reflective pressure, the positive phase duration, T_d, of the explosion, and the positive impulse, I_s, which is the area under the positive time history curve. Prior to shock front arrival, the pressure is ambient P_a.

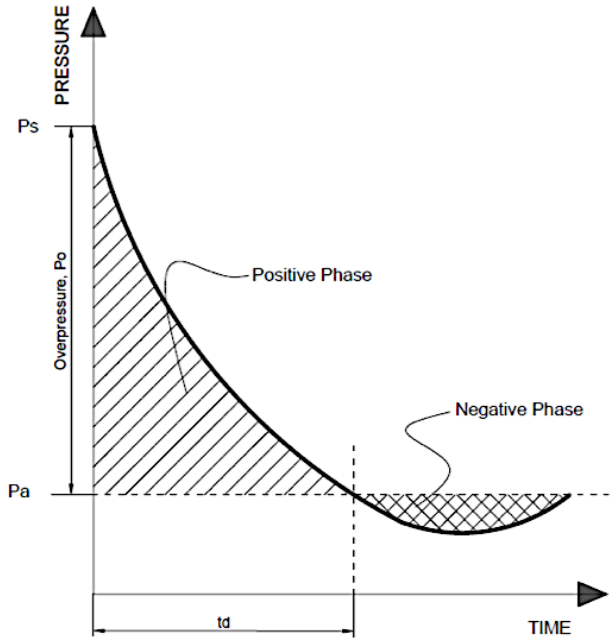

Figure 1.2: Ideal Blast Wave

The modified Friedlander equation shown in equation 2 below (Baker et al. 1983) can be used to confirm the maximum peak pressure, positive phase duration and positive impulse of the recorded pressure transducer of the experimental blast. In blast research, it is typical to fit the experimental data with the Modified Friedlander equation and a regression analysis because of the non-ideal behaviour of the free-field blast tests. The impulse is calculated from the area under the Modified Friedlander curve. Fitting the Modified Friedlander equation over the full positive phase can yield reliable interpolation to the experimental data, which in turn can be used later in a numerical and finite element analysis. Blast waves are dependent on environmental conditions like atmospheric properties and the surface of the ground, creating a difference in experimental measured results and theoretical predicted values.

$$P(t) = P_s \left[1 - \frac{t}{T_d}\right] e^{-\alpha(t/T_d)} \quad (2)$$

where *P(t)* is the blast pressure at any time *t*, and is a function of the peak overpressure P_s and the positive phase duration T_d and α is the curve fitting parameter (Baker et al. 1983).

1.5.3.4 TNT Equivalency

Trinitrotoluene (TNT) equivalency is a method of representing the energy released by any material in an explosion in terms of the equivalent mass of TNT needed to produce an explosion of equal size. The TNT equivalent of an alternate explosive material can be calculated as the ratio of mass of TNT to the mass of the alternate material that results in the same magnitude of blast wave at the same distance of charge. The main reason for selecting TNT as a reference is that there is a large amount of experimental data from military and academic research associated with this explosive.

The most accurate method in calculating the TNT equivalence would be to conduct experimental tests and compare the pressure and impulse from the alternative explosive material with those obtained from the TNT of equal identical mass. Some TNT equivalence conversion factors found from common explosives can be found in Table 1.1 (Baker et al. 1983).

Table 1.1: Sample TNT Equivalent factors (Baker et al. 1983)

Explosive	Mass Specific Energy (kJ/kg)	TNT Equivalent $(E/M)_x / (E/M)_{TNT}$
Comp B (60% RDX, 40% TNT)	5190	1.148
PETN	5800	1.282
Pentolite 50/50 (50% PETN, 50% TNT)	5110	1.129
TNT	4520	1
C-4 (91% RDX, 9% plasticizer)	4870	1.078
ANFO	3228	0.67
Blasting Gelatin	4520	1

1.5.4 Structural Response of Masonry Walls to Blast Loading

Analyzing the dynamic response of reinforced masonry walls to explosive loading can be very complex and can involve the effect of high strain rates, non-linear material behavior and uncertainties of blast load calculations. The primary purpose for the study of the structural response of reinforced masonry walls to blast loads are life safety consequences related to potential structural failures. The immediate goal being to reduce hazards to occupants or bystanders with a secondary objective to minimize the economic implications. The most common method in analyzing the response of masonry walls is to study the response under experimental blast field-testing. There is a growing database on blast free field-testing on masonry walls, which is generating valuable data due to the high concern of accidental or deliberate explosions. Several researchers have conducted tests on one-way unreinforced masonry specimens as well as retrofitting techniques in an effort to mitigate the high risk of the walls blowing inside the structure and fatally

injuring occupants. For instance, Baylot et al. (2005) conducted a series of blast tests to predict the blast response of lightly attached concrete masonry walls. Unreinforced quarter-scaled masonry walls were tested and the walls hazard level was determined based on debris horizontal velocity. The tests conducted provided a set of experimental data that were used to validate numerical models and to develop engineering tools for predicting the response of CMU walls (Baylot et al., 2005). Dennis et al. (2002) summarized the results of a series of quarter-scale CMU wall experiments conducted in 1999 and developed an FE model for predicting the response of masonry walls to blast loads. Landry (2003) performed a number of simulations similar to those by Dennis et al. (2002) to validate the high level of protection pressure-impulse (P-I) diagrams. Landry (2003) and Dennis et al. (2002) found that there was good agreement between the FE results and the results of P-I diagrams. Forsen (1985) studied the response of one-way masonry walls in various Swedish construction practices. Forsen's test results compared well to the P-I results obtained from a single-degree-of-freedom (SDOF) analyses. Abou-Zeid et al. (2011) tested eight full-scale unreinforced concrete masonry walls tested under free field blast loads. They found that the effectiveness of providing an arching action is a cost-effective hardening technique to enhance the blast capacity of URM walls. Based on the review of the masonry experimental study's above, it's clear that there is a need for research concerning two-way reinforced masonry walls subjected under blast loads.

1.5.5 Analysis Techniques

Due to time constraints, high economic costs and the high computing power, numerical modeling techniques are considered an alternative to experimental testing techniques. The two main modeling methods used in the quantification of building parts and materials to blast loading are single degree of freedom (SDOF) models, which are analytical techniques, and Finite Element Analysis (FEA) models, which are numerical techniques.

A pressure-impulse (P-I) diagram is an easy way to calculate and relate a specific damage level to a combination of blast pressures and impulses (Smith and Hetherington, 1994) using SDOF analysis. P-I diagrams are typically derived for a particular structural type (e.g. concrete block, wood stud) or a particular structural element (e.g. column, walls) in a form similar to the example provided in Fig. 1.3. A P-I diagram, also called an iso-damage curve (Mays and Smith 1995), is divided into different areas based on the level of damage anticipated. The example P-I diagram in Fig. 1.3 shows two regions: Region (I) – Damage, corresponds to the structural damage and Region (II) – No Damage, refers to no or minor damage on the structure. The P-I diagram specifies the possible combinations of pressure and impulse that will cause a defined failure or specific damage level.

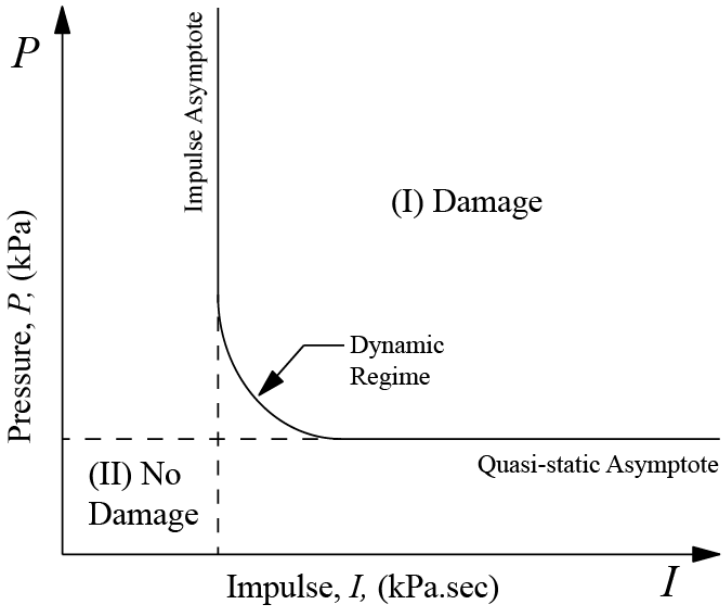

Figure 1.3: Typical Pressure-Impulse Diagram

The focus of this thesis will be on FEA numerical technique. FEA is a computer-generated model of a material or designed part that is stressed and analyzed for specific results like stress, strain, force, displacement, accelerations, etc. FEA uses a system of nodes, within a mesh. The accurate modeling of reinforced masonry wall behavior subjected to blast loads is a difficult problem to solve because of the isotropic material and the material interaction. Seyedrezai (2011) used LS-DYNA (LSTC, 2007) FE software to model full scale one-way arching of URM walls to blast loads based on experimental fieldwork done by Abou-Zeid et al. (2011). The simulated blast load profile was generated in LS-DYNA based on the ConWep blast load (Hyde, 1990). and was incorporated in LS-DYNA by Randers-Pehrson and Bannister (1997). Seyedrezai (2011) concluded that developed finite element model was valid and reliable to predict the true

response of the wall subjected to blast loads. Another FEM analysis using LS-DYNA was done by Eamon et al. (2004). This LS-DYNA model was developed from a series of experiments that were conducted at the U.S. Army Engineer Research and Development Center to determine the response of a one-way quarter-scale concrete masonry units (CMU) walls to the detonation of an explosive charge. They concluded that the FE analysis slightly over predicts the maximum static capacity of the CMU wall when the average CMU properties were used, and provided a good estimate of the load deflection function.

1.5.6 Concluding Remarks

The proposed research proposes to investigate two-way arching of third-scale reinforced masonry walls to out-of-plane blast loading. From the literature reviewed above, it is clear that additional research needs to be conducted to quantify the out-of-plane arching response of reinforced masonry walls under to blast loads and this has not be done previously to the best of the author's knowledge.

2 Experimental Program

2.1 Introduction

The experimental program described in this chapter is part of a larger test program aimed at generating a masonry blast performance database (MBPD) by McMaster University. This thesis focuses on the response of nine one-third scale, fully-grouted reinforced masonry infill walls, experiencing two-way arching and tested under three different levels of blast loading. Two-way represents the response of the wall and that it is restrained along all four sides to evoke bending about both major axes. In addition, three walls were tested under static loading to establish the static resistance function of the walls and compare against the blast loading and for dynamic modelling. This chapter of the thesis will describe the design details and construction of the wall specimens, constituent material properties and the live blast-testing program. The blast charge weights were designed to investigate three groups of walls possessing different reinforcement ratios at three different scaled distances. The blast charge weights were 5, 10 and 25 kg of Pentex ™ Booster, which has a 1.2 equivalency ratio of TNT based on total energy (Baker 1983). For the remainder of the paper, all blast charge weights will be presented in terms of the equivalent TNT explosive charge weights.

The test matrix was designed to simulate different varieties of blast threats, however, the primary motivation behind this research program is to simulate a vehicular bomb at curb-side to a structure as depicted in Figure 2.1. A large-size bomb (1000 kg) separated by a very small distance (15 m) can cause significant damage or even a complete collapse of

an unprotected structure. For the scenario used for this research program, a 15 m standoff distance was assumed with TNT charge weights that very from 100 to 1,000 kg in size.

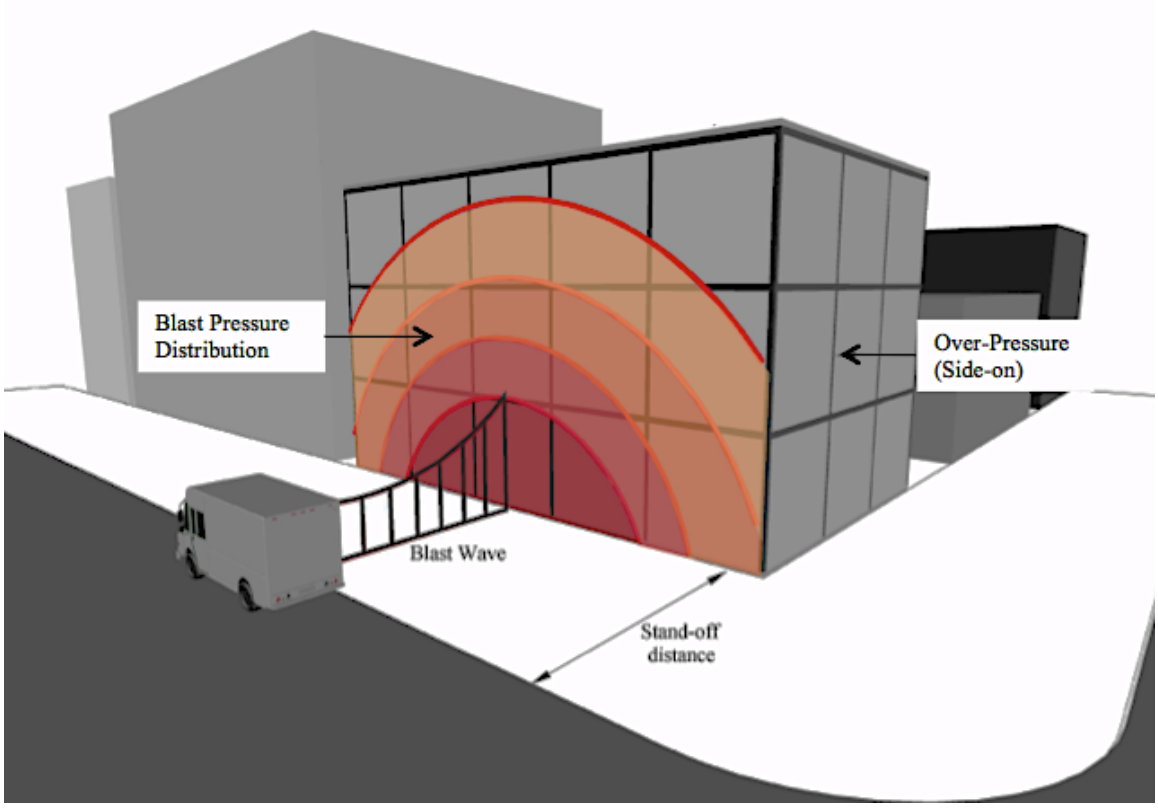

Figure 2.1: Blast Scenario

2.2 Design of Masonry Walls

A total of twelve walls were constructed as 3 different groups contained four identically detailed walls, WBL, WBM and WBH. The vertical reinforcement ratios were selected to represent a Low (WBL), Medium (WBM) and High (WBH) reinforcement ratios, as described in Table 2.1, and based on practical design limits prescribed in the masonry design standard CSA S304.1-04 and conforming to CSA S850-12 (2012) and ASCE 59-

11 (2011) blast standards. The wall specimens represent full-scale infill masonry walls 3.0 m tall by 3.0 m long, with rigid steel beams and columns surrounding it and forcing two-way arching to develop. All the wall specimen groups are designed to facilitate a two-way arching flexural response (restraint about both axes) and are fully-grouted.

Table 2.1: Masonry Wall Specimen Types

Wall Designation	**WBL**	**WBM**	**WBH**
Reinforcement	Every Other Cell	Every Cell	Every Cell
Vertical RFT. Ratio	8 D4 (0.31%)	15 D4 (0.59%)	15 D7 (1.07%)
Horizontal RFT. Ratio	7 D4 (0.29%)	15 D4 (0.59%)	15 D7 (1.07%)

2.3 Construction of Masonry Walls

The wall specimens are depicted in Figure 2.2 and were constructed at the Canada Masonry Design Centre (CMDC) in Mississauga, ON. The construction of the masonry walls was done over a three-week period by a professional mason, provided by the CMDC. All the masonry wall specimens were to represent reinforced masonry infill walls from a steel framed structure with reinforced masonry infill walls. The wall specimens were constructed with a half running bond, which is typical North American construction practice. All wall specimens were 15 courses tall by 7.5 masonry blocks long, with an average 3.5 mm mortar joint, making their overall dimensions 1,000 mm high by 1,000 mm long.

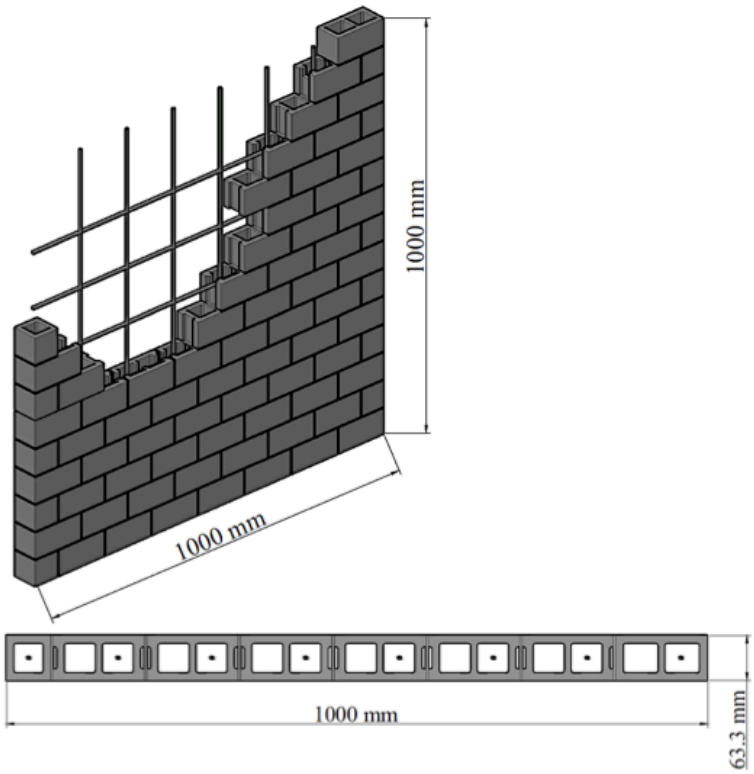

Figure 2.2: WBL Masonry Specimen and Plan View

There were 3 types of third-scale masonry blocks used in the construction of the walls; regular stretcher units (with frogged ends), full end units (without frogs), and half end units (without frogs). A special modification to the blocks had to be done by notching the top 25 mm to the webs, to provide room for the horizontal shear reinforcement and to allow for it to be completely surrounded by the grout. Walls were detailed to have symmetrical reinforcement patterns along both axes. The third-scale masonry blocks were used to represent a test done on a full scale prototype wall and providing comparable representation of actual construction and results (Harris and Sabins, 1999). All twelve masonry test specimens were built at the same time and in the same construction process. The mason constructed each wall on the steel C-Channels, indicated in Fig. 2.3a, which

were used to represent the steel frame and which had the vertical reinforcing bars welded to it. Grouting of the walls was done in two stages to enhance the quality control: the first stage occurred after the first 8 courses were constructed, with the grout stopped half way through the 8^{th} course to facilitate a shear key with the upper half of the wall, the second stage occurred after the remaining 7 courses were laid. The shear key is used in order to prevent the formation of a cold joint and potential slip plane at the mid-height of the wall. While grouting the walls a wood guide with drilled holes was used to keep the reinforcement vertical and at the proper spacing during grouting as indicated in Fig. 2.3b. This was extremely important for the walls because of the tight construction tolerances associated with one third-scale masonry. The different stages in building the masonry walls at the CMDC are shown in Fig. 2.3.

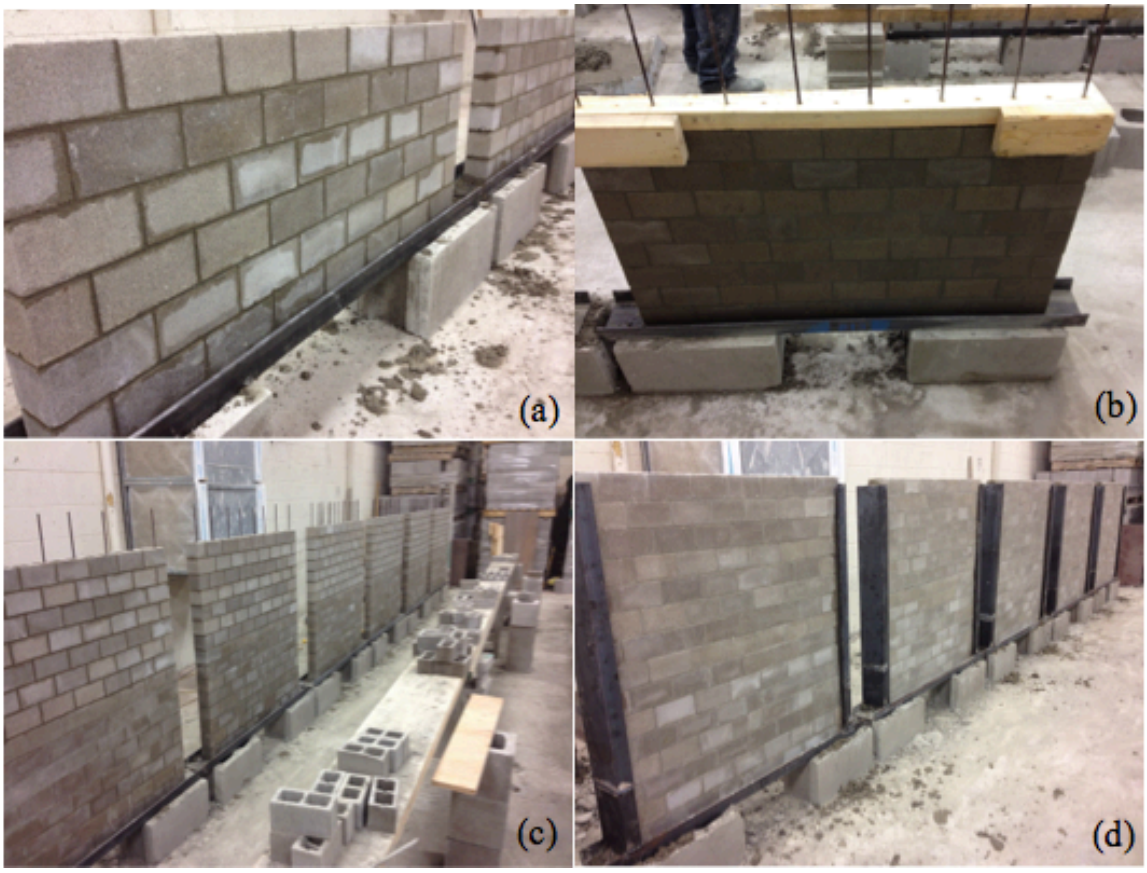

Figure 2.3: Masonry Wall Construction; a) Start of Construction, b) Grouting First Half, c) Second Half of wall construction, and d) C-Channels

2.4 Material Properties

The one third-scale concrete blocks, shown in Figure 2.4, were manufactured at McMaster University's Applied Dynamics Laboratory (ADL). Approximately 1,500 blocks were used for the construction of these walls. The third-scale concrete blocks were produced in accordance to the procedure described in an earlier research study done at McMaster University (Banting et al. 2010). The dimensions given in Fig. 2.4 represent a

one-third true replica model of the North American standard 20 cm concrete masonry unit (190 mm x 190 mm x 390 mm).

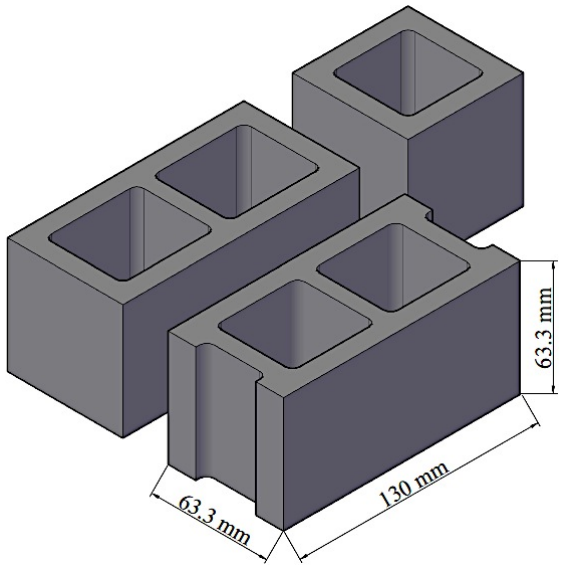

Figure 2.4: Third-Scale Concrete Blocks

2.4.1 Reinforcement Properties

The twelve experimental walls were designed as two-way action walls, and as such, the reinforcement was symmetrical in both vertical and horizontal directions. Two sizes of reinforcing steel were used in the construction of the masonry walls; D4 and D7 deformed wire with nominal cross sectional areas of 25 mm^2 and 45 mm^2, respectively. The reinforcement samples were tested under tensile loading until fracture in a universal test machine at McMaster University. The three samples of the third-scale reinforcement were tested according to ASTM A615-12 (2011). Figure 2.5 and Figure 2.6 contains a plot of the stress-strain data for the D7 and D4 tensile tests, respectively. The average

yield strengths for the D4 reinforcement was tested to be 478 MPa (COV=1%) and the D7 reinforcement was 484 MPa (COV=4%).

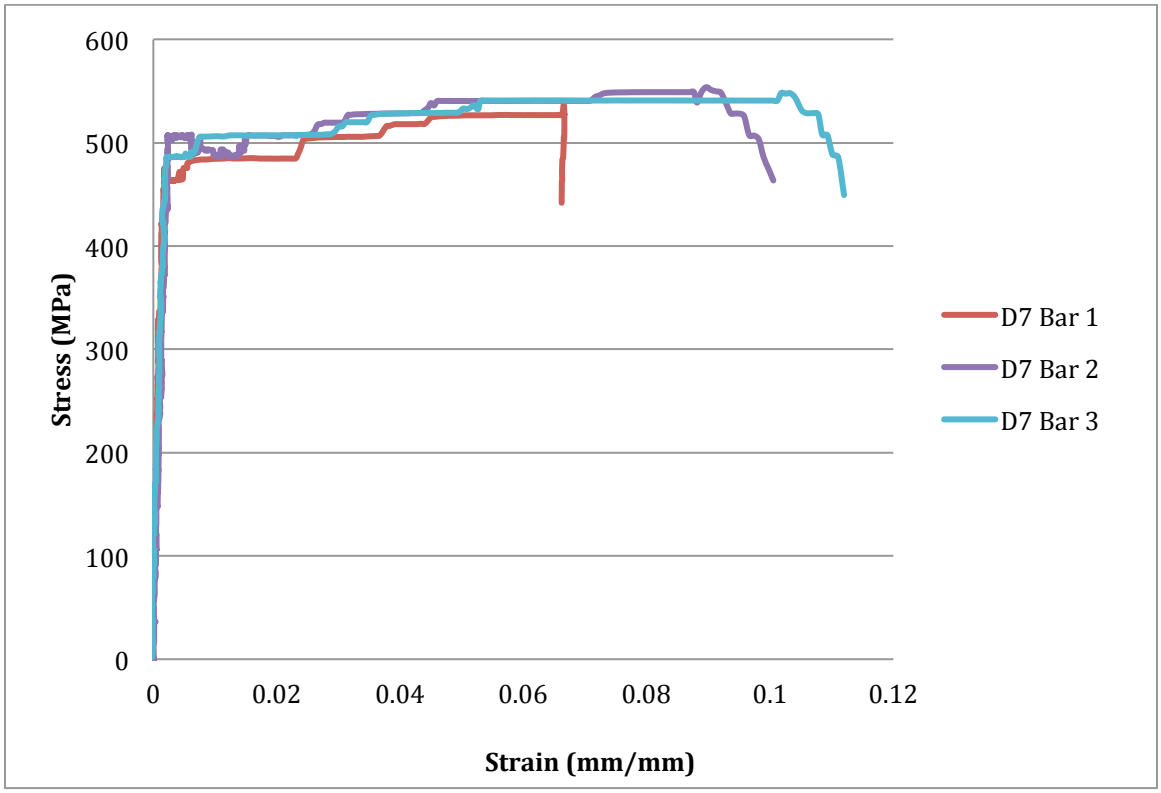

Figure 2.5: Stress-Strain Relationship of D7 Reinforcement

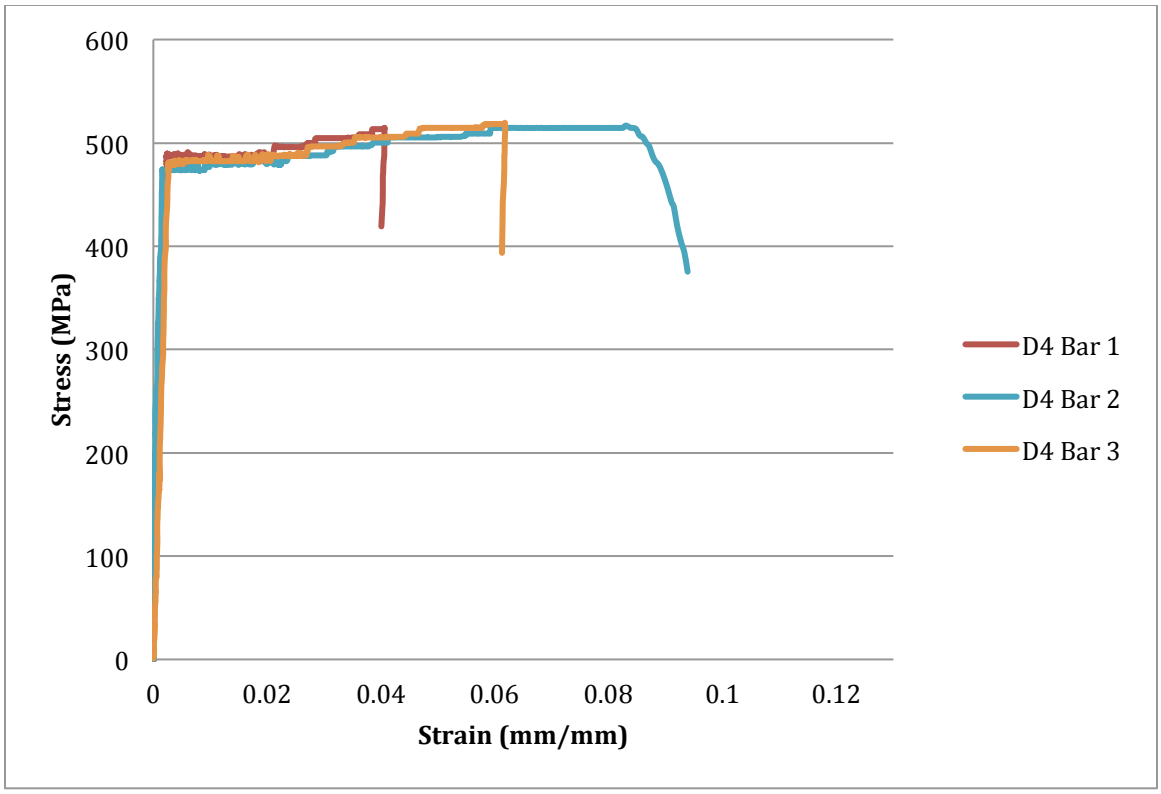

Figure 2.6: Stress-Strain Relationship of D7 Reinforcement

2.4.2 Mortar Properties

Sand was dried and sieved and put in barrels prior to the construction of the masonry walls in order to have precise material measurements and weight. Three 50 mm mortar cubes were tested every batch of mortar according to CSA A179 (2004). With a total of 18 mortar cubes tested giving an average of 28.4 MPa with a COV of 3.7%. In the laboratory, where the weather and humidity conditions are controlled, in full-scale construction, the mortar should have a target flow of approximately 100-115%. Before every batch of mortar was mixed and used, a flow table test was conducted according to CSA A179 (2004) make sure there was proper workability for the masons and so no

additional water was added during the construction. As mortar sits, its workability decreases, so the mortar was thrown out after 2 hours to make sure the water cement ratio stayed constant and no water was added. The average mortar flow measured was 125% with a COV of 5.3%. All mortar was batched by weight for better quality control with the proportions of Type-S Portland cement: Lime: Dry sand: Water to 1: 0.2: 3.53: 0.85.

2.4.3 Grout Properties

The grout was mixed and poured into the masonry walls in 2 lifts. Three 100 mm grout cylinders were cast for each grout mix made. The grout cylinders were then tested on the universal test machine at the Applied Dynamics Laboratory of McMaster University. The grout mix was prepared using the dry material weights and with the proportions of Cement: Lime: Dry sand: Water to 1:0.04:3.9:0.85. Grout cylinders strength had an average value 23.3 MPa with a COV of 9% as indicated in Table 2.2.

Table 2.2: Grout Strength

Test	Time	Failure Load (kN)	Stress (MPa)
1	9:00 AM	17.5	22.3
2	11:00 AM	19.4	24.7
3	2:00 PM	16.4	20.9
4	4:00 PM	16.2	20.6
5	8:00 AM	20.3	25.8
6	10:00 AM	19.4	24.7
7	1:00 PM	19.1	24.4
Average			**23.3**
COV			**9%**

2.4.4 Block Properties

The selected scale blocks measured 130 mm in length by 63 mm wide and 63 mm high. The face shells of the blocks have an average taper thickness from 11 – 12.34 mm. The compressive tests were performed in the universal test machine. To evaluate the masonry block compressive strength, 18 random one third-scale masonry blocks were tested with an average compressive strength of masonry of 20.3 MPa and a coefficient of variation (COV) of 11% according to CSA A165.1 (2004) and S304.1-04. The masonry block compressive strength was based on the average net cross-sectional area 4789 mm^2. Table 2.3 provides the compressive strengths of the third-scale concrete blocks.

Table 2.3: Block Compressive Strength

Specimen No.	Load (kN)	Stress (MPa)
1	91.7	19.2
2	105.0	21.9
3	95.5	19.9
4	82.0	17.1
5	106.0	22.1
6	96.7	20.2
Avg.		**20.1**
COV		**9%**

Specimen No.	Load (kN)	Stress (MPa)
1	93.5	19.5
2	87.0	18.2
3	95.5	19.9
4	101.5	21.2
5	103.7	21.7
6	107.5	22.4
Avg.		**20.5**
COV		**8%**

Specimen No.	Load (kN)	Stress (MPa)
1	80.0	16.7
2	92.0	19.2
3	86.7	18.1
4	119.5	24.9
5	117.5	24.5
6	89.5	18.7
Avg.		**20.4**
COV		**17%**

Total Avg.	**20.3**
COV	**11%**

2.4.5 Prism Properties

The four course high, stack bond, fully grouted masonry prims were tested in accordance to CSA S304 with an average compressive strength of 18.7 MPa with a COV of 10.2%. Three masonry prisms were constructed and tested for every batch of mortar made throughout the construction process. The same professional mason built these masonry prisms at the same time the masonry walls were constructed. The masonry prisms were also grouted at the same time the walls were being grouted to make sure all the materials were the same in each wall and in each prism. The masonry prisms were built and tested to establish an experimentally determined strength for the masonry that is comparable to the masonry static strength in the blast loading and also for any analytical models later on. All the masonry prisms were capped using gypsum. This was done to provide a level bearing area for the compressive loading done on the universal testing machine.

2.5 Boundary Conditions

The test specimen was used to simulate an exterior steel framed structure with masonry infill wall panels. These infill wall panels were built with no gap between the wall and the surrounding frame, thus forcing two-way arching action to develop. To simulate the steel frame with no gap and in order to facilitate modeling later on, a 5x9 C-Channel was used to construct the wall on top of and when the masonry wall was finished another C-Channel was mortared in place on top of the wall. Two vertical C-Channels were welded to the top and bottom C-Channels shown in Fig. 2.7(a). Figure 2.7(b) shows the round 25

mm solid steel cylinder around the entire perimeter of blast frame to create a knife-edge support for the steel frame surrounding the walls during blast testing.

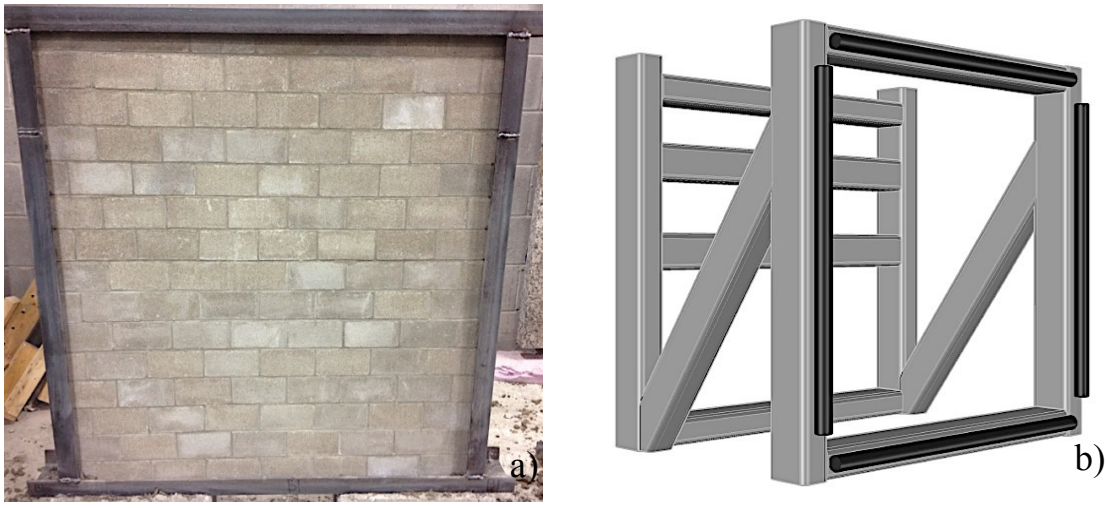

Figure 2.7: Boundary Condition; a) Wall and b) Blast Test Frame

2.6 Design and Construction of Test Set-up

The experimental setup was built in the ADL and transported to the test range at a Canadian Forces Base in Ontario. The blast frame was placed at a constant 5.0 m standoff distance from the centre of the explosive charge. The blast frame was fabricated to hold each of the masonry wall specimens during the blast testing as well as for ease of loading and unloading each wall at the Canadian Forces Base. A vertically standing square reaction test frame with 2 diagonal supports was constructed as shown in Figure 2.7 b). Hollow rectangular steel sections (HSS) were used to create this test frame with a thickness of 11.1 mm. At the back of the steel reaction frame, lighter HSS sections were

welded in place horizontally. These were welded at half and quarter height of the test frame for a mounting surface for the instrumentation. 6.4 mm steel plates were welded to the HSS on all sides to enclose the reaction frame. Hinges for ease of access, were attached and welded to the roof of the reaction bunker. The hinges on the lid are used to allow access in the reaction bunker for the installation of the instrumentation for each test. Two triangular supports were welded to the top of the frame to hold the parapet wall. In addition, three C-Channels were welded to each side of the reaction bunker to allow wing walls to be attached. The wing and a parapet walls were attached to the frame to increase the surface area and used to minimize the clearing effect that occurs in free field explosions. This facilitates a uniform pressure on the wall specimen and prevents the blast wave from propagating around the edges of the wall (Baker et al. 1983). In addition, a steel box enclosure (bunker) formed the rest of the test frame behind the wall to prevent the wrap-around effect. The exterior of the bunker was in turn supported by a 1.5 m cube concrete barrier blocks to shield the rear and side faces of the frame. The completed reaction bunker with the parapet and wing walls is shown in Figure 2.8.

Figure 2.8: Blast Test-Frame; a) Without wing Walls, and b) With wing walls

2.7 Measurements and Instrumentation

2.7.1 External Instrumentation

In the experimental test set-up mounted to the blast test frame were three piezoelectric surface pressure transducers. These three pressure transducers measured and recorded the reflected blast pressure profile on each wall during each test. One pressure transducer located at the top centre of the wall on the parapet and one located both sides of the wing-walls. The pressure transducers located on the wing walls were placed at mid height, as close to the wall specimen as possible to provide relevant readings. There was a thin layer of silicone applied to the pressure transducer to shield them from the blast flame during each shot. These pressure transducers were used to measure the reflected blast pressure profile from the blast wave. Four external pressure transducers were set-up around the test frame to record the incident blast pressure wave. In addition, one pressure

transducer was also located inside the blast frame to verify that no over-pressure developed inside the test bunker during the blast load. There was several incident blast wave pressure transducers placed around the blast test arena. The reflected and incident blast wave pressures were collected using a data acquisition system located 20 m away from the bunker location.

2.7.2 Internal Instrumentation

Four linear displacement potentiometers were internally mounted in the test reaction frame to measure the lateral displacements of the wall specimen from the blast load as shown in Fig. 2.9.

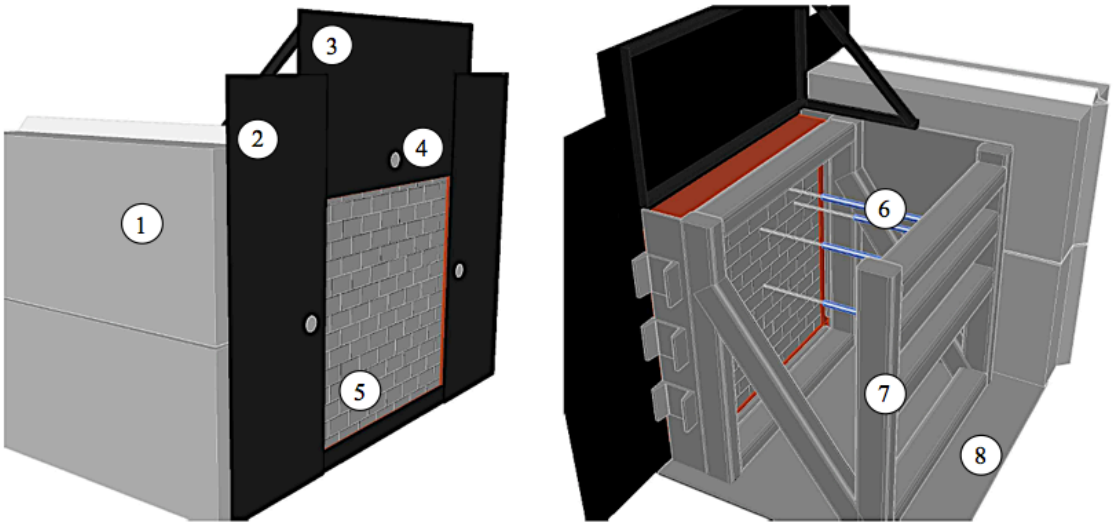

1 – Concrete barrier blocks	5 – Reinforced masonry wall
2 – Steel wing-walls	6 - Linear displacement potentiometers
3 - Parapet	7 - Steel test frame enclosure
4 - Piezoelectric pressure transducers	8 – Test frame base

Figure 2.9: The Blast Bunker: a) Exterior; and b) Interior

The linear potentiometers have a maximum stroke of 300 mm and were placed at critical locations (placed at the top - centre, ¾ wall height - ¾ wall width, ¾ wall height – centre, centre - centre) shown in Figure 2.10 below to capture the entire wall deformation profile in both the horizontal and vertical directions as well as to verify symmetry. The linear displacement potentiometers were attached with a ball bearing connection to allow rotations in all directions during the explosion and to prevent the displacement potentiometers from being damaged during the blast event.

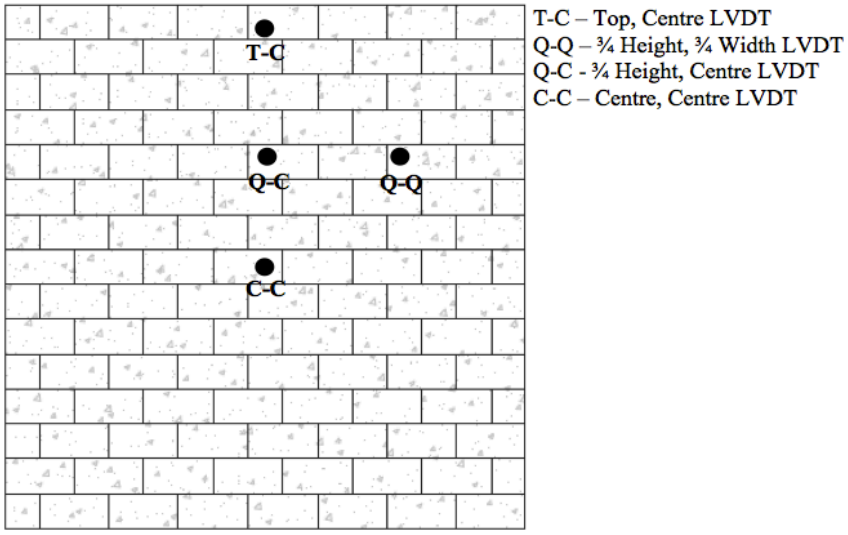

Figure 2.10: Interior Instrumentation Layout

2.8 Test Arena

As mentioned previously, the experimental program was selected as part of a larger test program aimed at producing a large masonry blast performance database (MBPD) of experimental results. There were five other similar test programs being conducted at the

same time, therefore a blast test arena had to be set up to provide an efficient way to test all of the walls simultaneously. The blast test arena was laid out in a semi-circle as shown in Figure 2.11. The semi-circle had a radius of 5.0 m and was constructed on a level sand base. The explosive charge was set in the centre of the circle allowing each test set up to have a 5.0 m stand-off distance. One high-speed camera was placed on the opposite side of the walls to capture the blast event. This high-speed camera would allow the blast event to be slowed down and then each wall specimen could potentially be examined and better observed during each trial.

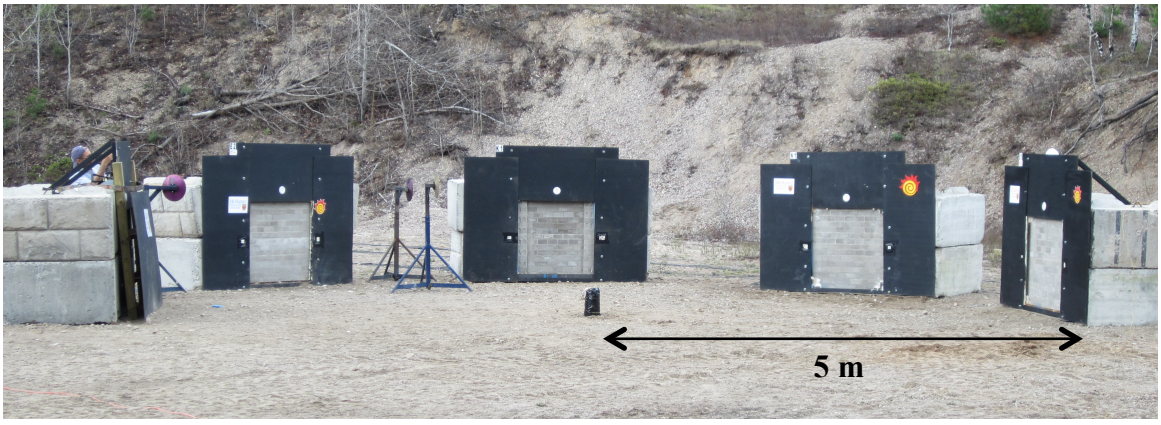

Figure 2.11: Blast Test Arena

2.9 Test Matrix

The test matrix was designed and selected to investigate and overall performance of two-way arching reinforced masonry walls with varying reinforcement ratios. Each of the three groups of 3 walls, defined previously with respect to their reinforcement ratio, are further divided according to different levels of blast load. Table 2.4 presents the test

matrix of the scaled reinforced masonry test specimens under the free field blast loading and shows the combination of reinforcement ratio, charge weight, equivalent charge weight and scaled distance for each blast trial. The reason for the selection of standoff distances and reinforcement ratios was to cover a wide range of threat situations and to evaluate the performance of the walls. It was also selected to provide different damage levels in the Canadian CSA S850-12 and American ASCE 59-11 blast standards.

Table 2.4: Shot Schedule

Group	Shot No.	Specimen	Pentex Charge Weight (kg)	Equivalent TNT Charge Weight (kg)	Scaled Distance ($m/kg^{1/3}$)
I	1	N/A	5	6	2.75
	2	WB6L	5	6	2.75
	3	WB6M	5	6	2.75
	4	WB6H	5	6	2.75
II	5	N/A	10	12	2.18
	6	WB12L	10	12	2.18
	7	WB12M	10	12	2.18
	8	WB12H	10	12	2.18
III	9	WB30L	25	30	1.61
	10	WB30M	25	30	1.61
	11	WB30H	25	30	1.61
	12	N/A	25	30	1.61

2.10 Summary and Conclusions

The details of the experimental program were presented in this chapter and focused on the material properties, material testing, construction, experimental test set-up, and instrumentation. Material testing was performed for each material in order to determine their properties. The Internal Instrumentation (LVDT's) were used to determine the lateral displacements and piezoelectric surface pressure transducers were used to record the reflected blast pressure profile in the experimental testing.

3 Static Airbag Experimental Testing and Analysis

3.1 Introduction

The static airbag tests conducted at McMaster University Applied Dynamics Laboratory were completed to compare the load-deflection profile and resulting damage pattern of the masonry walls with the blast testing. Three third-scale masonry walls possessing reinforcement ratios of 0.31%, 0.59% and 1.07%, as defined in Chapter 2 of this dissertation, were tested under incremental uniform pressures with a pneumatic airbag. In this chapter, results from the airbag test are compared to theoretical predictions that apply fundamental engineering theory: yield line method, a lower bound out-of-plane wall strength equation, FEMA 356 Arching equation and the American Masonry Standards Joint Committee (MSJC, 2013) code equations to consider the two-way arching effect.

The static testing is needed for a further analysis to calculate the resistance function for dynamic analysis (e.g. Single Degree Of Freedom (SDOF)) to verify the strain rate effects (dynamic strength of materials) in the reinforcement and concrete masonry, when comparing it to the experimental blast field-testing.

3.2 Test Set-up and Instrumentation

A key requirement to enhance the out-of-plane static resistance of the masonry wall specimens was to have a sufficiently rigid surrounding frame. To make use of the space

allotted at the laboratory, a self-reacting frame was considered. A steel reaction frame used for the experimental blast loading was already designed and fabricated, to make this static testing cost and time effective, the previously described steel reaction frame was retrofitted to make it a self-reacting frame for the static testing by sandwiching a steel and wood outer frame with an airbag in it and bolted it to the original steel frame as shown below in Figure 3.1.

The masonry wall specimens were tested under quasi-static conditions. These walls were tested by applying a uniformly distributed pressure from an airbag over the infill wall specimens. Inside the steel and wood shell it was lined with plywood to provide a smooth solid surface from which the airbag could apply even air pressure to the wall panel.

Figure 3.1: Construction of the test set-up

The loading of the specimens was applied by gradually inflating the airbag between the masonry specimens and the plywood backing of the outer steel reaction frame. As the uniform pressure was increased, the displacements of the masonry wall specimen were collected using the four LVDT's attached to the steel reaction frame. The LVDT's were placed in the same locations as the experimental field blast testing described in Chapter 2 (placed at the top - centre, ¾ wall height - ¾ wall width, ¾ wall height – centre, centre - centre) and this would ensure that the entire wall deformation, in both the horizontal and vertical directions would be recorded. A cross-section of the test set-up showing the LVDT's and self-reacting frame is shown in Figure 3.2.

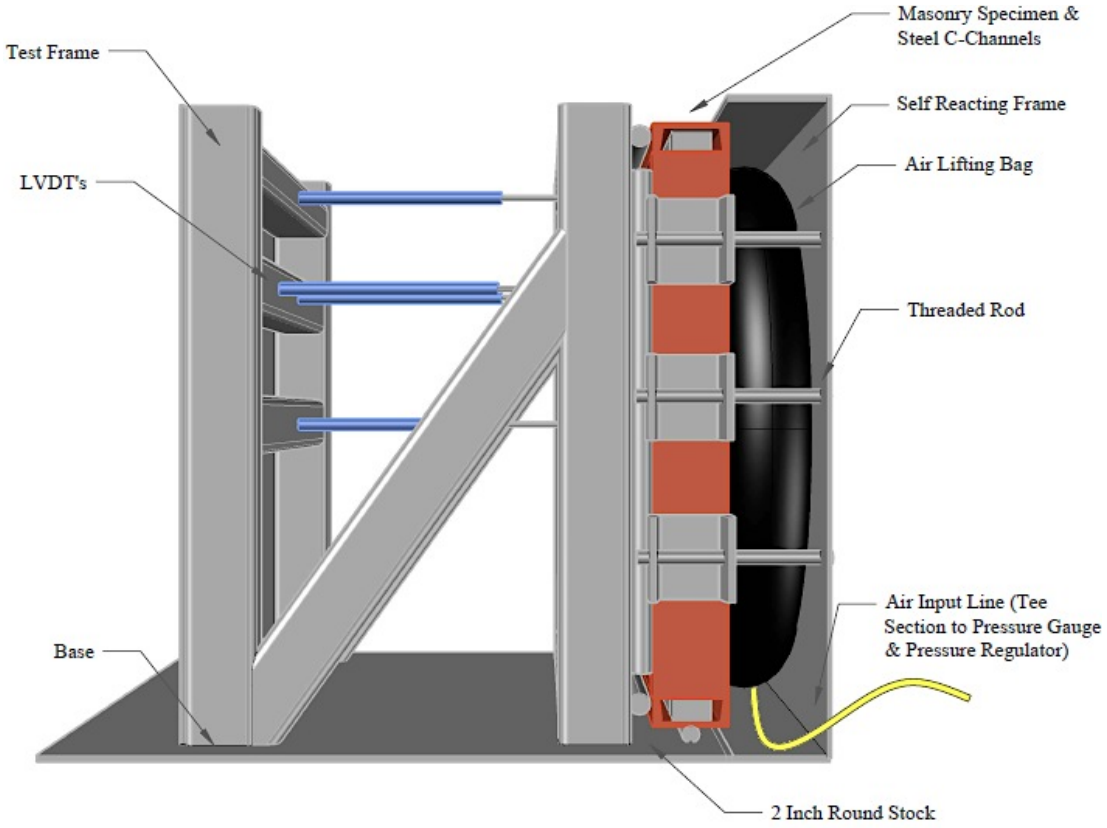

Figure 3.2: Cross section of the out-of-plane test set-up

3.3 Airbag and wall details

The pressure in the airbag was recorded using a digital pressure gauge on the air feed to the airbag. This pressure data was recorded using a data acquisition system at a sampling rate of one data point per second. The airbag was gradually inflated by controlling the flow using a digital pressure regulator as well as monitoring the pressure and displacement readings from the data acquisition system. The airbag was filled using a very slow rate to minimize the potentially brittle failure of a wall specimen from the sudden release of energy stored in the airbag and energy stored in the reinforced masonry wall. The airbag was installed tight against the masonry wall specimen to ensure that the

force of the airbag was always normal to the surface wall. The airbag was designed to be slightly (10% in length) smaller than the actual wall to apply no pressure on the boundary conditions.

3.4 Out-of-plane Analysis

The out-of-plane flexural capacity of the two-way arching reinforced masonry infill walls was calculated using an analytical yield line method as well as a lower bound out-of-plane wall, strength equation, since the walls are deforming and arching in two-ways. The three reinforced third-scale experimental walls were idealized into a simple case presented in Figure 3.3 to predict the out-of-plane flexural capacity. This simplification was determined based on an idealized perfect 2-way rigid arching mechanism developing in the wall. The walls were acting like two-way uniformly loaded beamless slabs (flat slab) with columns at the corners as well as the arching mechanism in both directions. The yield line method is a approach and assumes an elastic-perfectly plastic behaviour. The ultimate load is determined by virtual work or equations of equilibrium. Thus, the ultimate load calculated is usually high, meaning the walls will be more conservative than the actual static wall capacities (Park and Gamble 2000). The arching mechanism is calculated using an out-of-plane strength of an infill panel from equation 7-21 from FEMA 356 (2000). The equation from FEMA 356, 7-21 does not account for the tensile strains in the reinforcement and is used for calculating the capacity of arching URM walls. To the best of the author's knowledge, there are currently no

equations that calculate the arching capacity taking two-way reinforcement or any reinforcement at all into account.

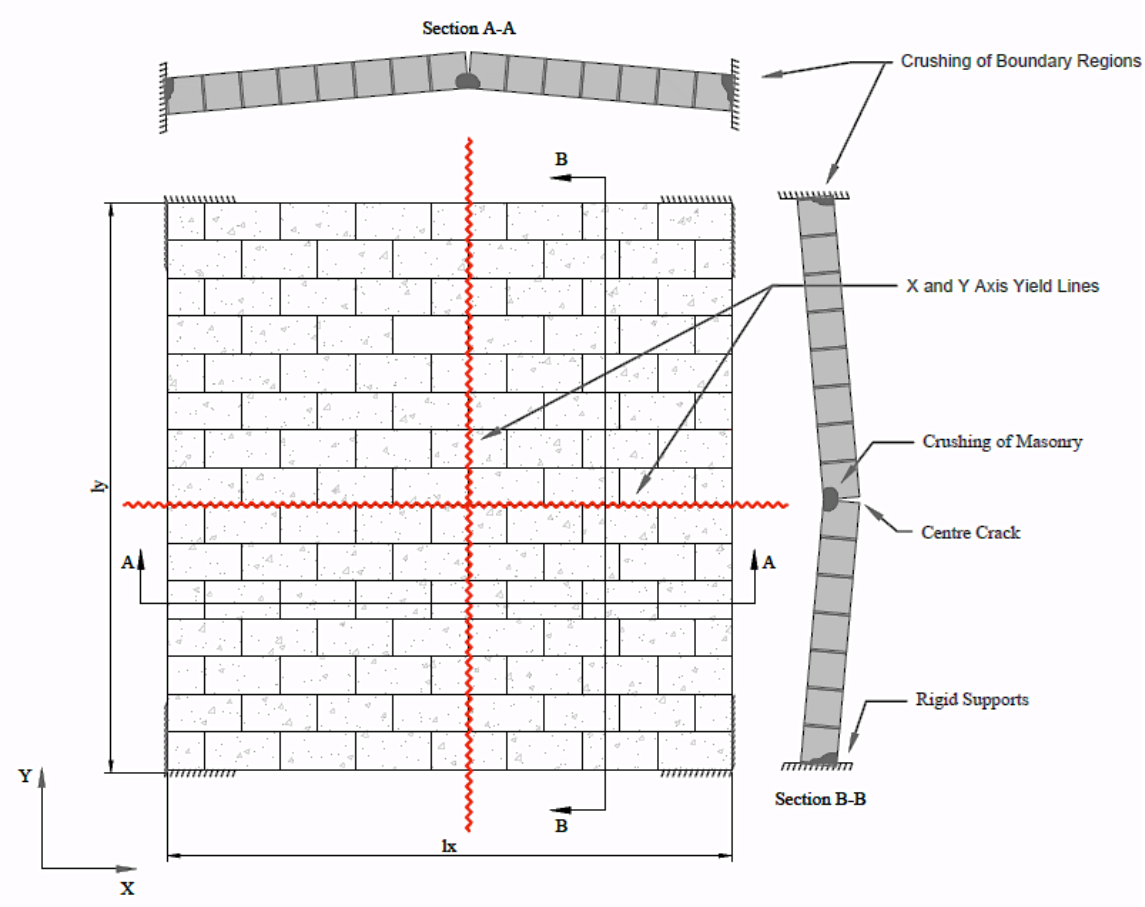

Figure 3.3: Idealized Out-Of-Plane Flexural Capacity

The first step in calculating the out-of-plane capacities was to determine the moment resistance per unit length *(M_u)* of the masonry infill walls in two orthogonal directions. It was determined that wall type WBL and WBM were under-reinforced and therefore the steel in the horizontal and vertical directions would be yielding when the uniform

maximum pressure was applied. When the reinforcing steel yields, equation 3 gives the moment resistance per unit length of the masonry infill walls.

$$M_u = A_s F_y \left[d - \frac{(\beta_1 c)}{2} \right] \quad (3)$$

Where A_s is the area of steel (mm^2), F_y is the yield strength (MPa), d is the distance from the extreme compression fibre to centroid of tension reinforcement, c is the distance from extreme compression fibre to the neutral axis and β_1 is the ratio of the depth of rectangular compression block to depth of neutral axis. For the third wall type, WBH with the highest reinforcement ratio, was under reinforced in the in-plane direction but not in its out-of-plane direction. As such the reinforcing steel would not to yield and therefore equation 4 is used.

$$M_u = A_s E_s \epsilon_s \left[d - \frac{(\beta_1 c)}{2} \right] \quad (4)$$

The next step in calculating the out-of-plane flexural capacity is applying the theory of virtual work. This is done by equating the external work (load x deflection) to the internal energy (moment x rotation) over the face of the masonry infill wall with an applied pressure. Finally, the maximum pressure can be solved of the masonry infill wall panel. Therefore the internal energy done is:

$$\Sigma M \theta_n l_0 = 2 \left[M_u \left(\frac{(2\delta)}{l} \right) l \right] = 4 M_u \delta \quad (5)$$

And the external work done is:

$$\Sigma U \Delta = 4 \left[\left(\frac{(q_u l^2)}{4} \right) \frac{\delta}{2} \right] = \left(\frac{(q_u l^2)}{2} \right) \delta \quad (6)$$

Which is the total load on each segment multiplied by the downward displacements of their centroids, therefore when equating the internal work equals the external work, the

combined ultimate load *(q_u)* calculated from in both orthogonal directions may be calculated as:

$$q_u = \frac{16M_u}{l^2} \quad (7)$$

Where M_u is the moment resistance per unit length (kN m) of the masonry infill and l is the length of infill (m).

This arching action is important to include because it can effectively enhance the out-of-plane later load resistance. There have been several analytical models developed to predict the out-of-plane capacity for arching of URM walls, which yield similar results (Dawe and Seah 1989, McDowell et al. 1956, and FEMA 356 2000). The ultimate arching out-of-plane lateral load (q_u) was calculated from FEMA 356 (2000). The arching out-of-plane lateral load was calculated using Equation 8.

$$q_u = \frac{0.7(f'_m)\lambda_2}{(h_w/t_w)} \quad (8)$$

Where t_w is the wall thickness (mm), h_w is the height (mm) f'_m is the compressive strength of the masonry prism and λ_2 is a slenderness parameter. A summary of the results of the simple yield line analysis as well as the arching of the concrete moment resistance can be found in Table 3.1.

The MSJC (2013) design code gives the equitation to calculate the capacity of the arching infill wall. The MSJC (2013) is based on the infill wall bearing against a rigid boundary with no gap and this approach also disregards the contribution of any reinforcement in the

infill wall. The MSJC (2013) infill wall resistance calculation is based on the work from Dawe and Seah (1989). Equation (9) below is used to calculate the out-of-plane resistance ($q_{n\,inf}$) for the masonry infill walls.

$$q_{n\,inf} = 729000\,(f'_m)^{0.75}\,t_{inf}^2\left[\frac{(\propto_{arch})}{(l_{inf})^{2.5}} + \frac{(\beta_{arch})}{(h_{inf})^{2.5}}\right] \tag{9}$$

where:

$$\propto_{arch} = \frac{1}{h_{inf}}(E_{bc}\,I_{bc}\,h_{inf}^2)^{0.25} < 50 \tag{10}$$

$$\beta_{arch} = \frac{1}{l_{inf}}(E_{bb}\,I_{bb}\,l_{inf}^2)^{0.25} < 50 \tag{11}$$

Where $q_{n\,inf}$ is the out-of-plane resistance (Pa), f'_m is the compressive strength of the masonry prism, t_w is the thickness of the infill (mm), h is the height of infill (mm), l is the length of infill (mm), E is the modules of elasticity (MPa) and I is the moment of inertia (mm^4). When using the MSJC design code to calculate the three infill walls capacities yields the same results because the MSJC design code ignores the reinforcement, all wall size and the boundary conditions are the same. The calculated capacity is 48.6 kPa for the three walls WBL, WBM and WBH in this test program.

Table 3.1: Out-of-plane flexural capacities

Wall	Yield Line Peak Capacity (kPa)	FEMA 356 Predicted Capacity (kPa)	MSJC (2013) Predicted Capacity (kPa)
WBL	41.6	26.5	48.6
WBM	68.8	26.5	48.6
WBH	98.2	26.5	48.6

As can be seen in Table 3.1, the arching capacities of the masonry infill are significantly increased and need to be statically tested to compare to the maximum calculated static out-of-plane capacities.

3.5 Experimental Static Test Results

This section of the dissertation presents the experimental out-of-plane test results of the three statically tested third scale masonry walls. After the experimental static airbag test was conducted, the airbag was removed from the test set-up and the crack patterns on both sides of the wall were recorded. A thorough explanation of each of the specimens damage sequence will be presented in the next sections, with detailed discussions on displacements, failure modes and crack patterns. The overall performance of the infill walls will be evaluated as well as the overall out-of-plane capacity. During the experimental testing the airbag was inflated at a rate of 0.01 psi per second (0.069 kPa per second).

This first specimen tested statically out-of-plane was WBL, which had the lowest reinforcement ratio 0.33%. It was constructed with D4 reinforcement bars in every other cell in both the horizontal and vertical directions. There were little observed cracks or any damage during the static out-of-plane test until the end of the test. The progression of the hairline cracks started from the centre and protruded towards the corners. This wall failed in a brittle way even though the pressure was increased gradually. Large cracks can be seen in Figure 3.4, with a diagonal "X" pattern. There were also horizontal cracks spanning from one edge to another as well as some vertical hairline cracks. This specimen is acting two-ways as evident by the symmetrical cracks. It was also arching due to the crushing of the masonry around the perimeter and the sudden release of energy. On the compression side of the wall (front face), the masonry was crushing and the face shells were spalling.

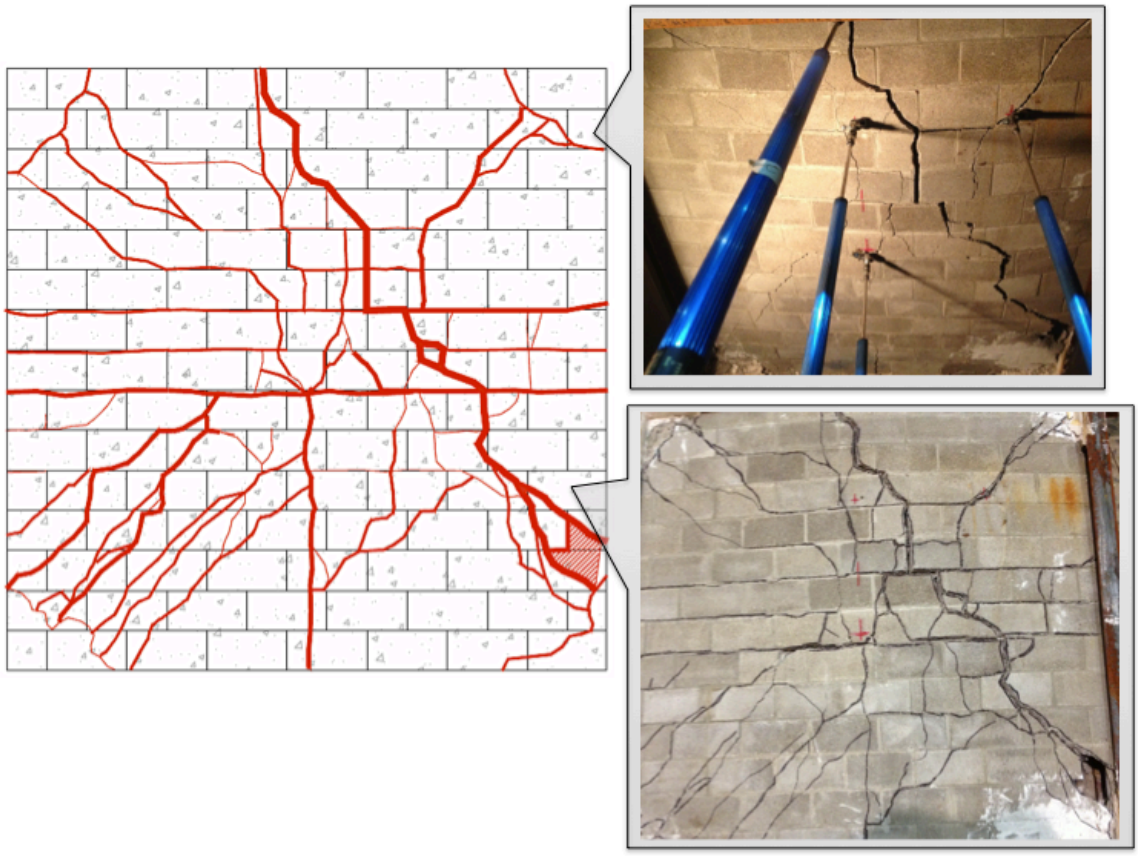

Figure 3.4: WBL, D4 Every Other Cell

Figure 3.5, shows the centre LVDT's pressure-displacement plot of the static out-of-plane test of wall WB. The pressure was maintained by a pressure regulator and provided a constant slow rate to capture all critical data points. The pressure-displacement curve shows an almost linear slope until the sudden release of energy. It was important to capture the descending branch of the pressure-displacement relationship for the statically tested wall, as it would be useful to generate the resistance function in a further SDOF analysis. The maximum pressure obtained by the first wall WBL was 156.3 kPa. In the out-of-plane static airbag results, it is important to point out the initial loading phase, in

which the airbag was first loaded. There was a slight gap in the wall because of compliance. This gap was removed, as at the beginning of the tests, the deflated airbag requires time to start filling, as before the airbag becomes capable of applying a uniform loading pressure against the wall. This removal of the time gap was done in all three of the static out-of-plane tests.

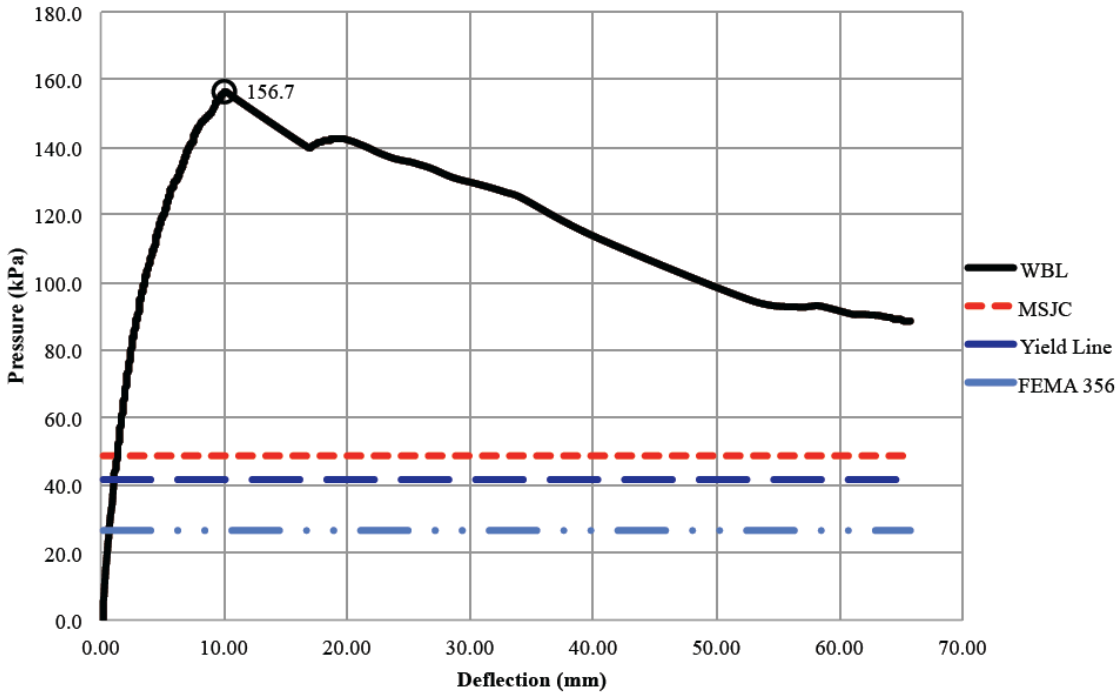

Figure 3.5: WBL Pressure – Displacement plot

This second masonry specimen tested statically out-of-plane was WBM; this was the medium reinforced wall with a reinforcement ratio of 0.62%. It was constructed with D4 reinforcement bars in every cell in both the horizontal and vertical directions. The same situation occured to this wall, as the previously tested wall. There were hairline cracks

until the sudden release of stored strain energy in the wall. The same "X" crack pattern was observed, with the cracks running diagonally from one corner to the opposite. There were two large horizontal bed joint cracks spanning from one side to the other at mid point of the tension face. On the compression side of the wall, there was severe cracking and spalling of the concrete around the gypsum corners. With the reinforcement in every cell, there was more crushing of the masonry around the perimeter from the arching mechanism. A detailed photograph of the second tested specimen WBM in the compression side, can be seen below in Figure 3.6.

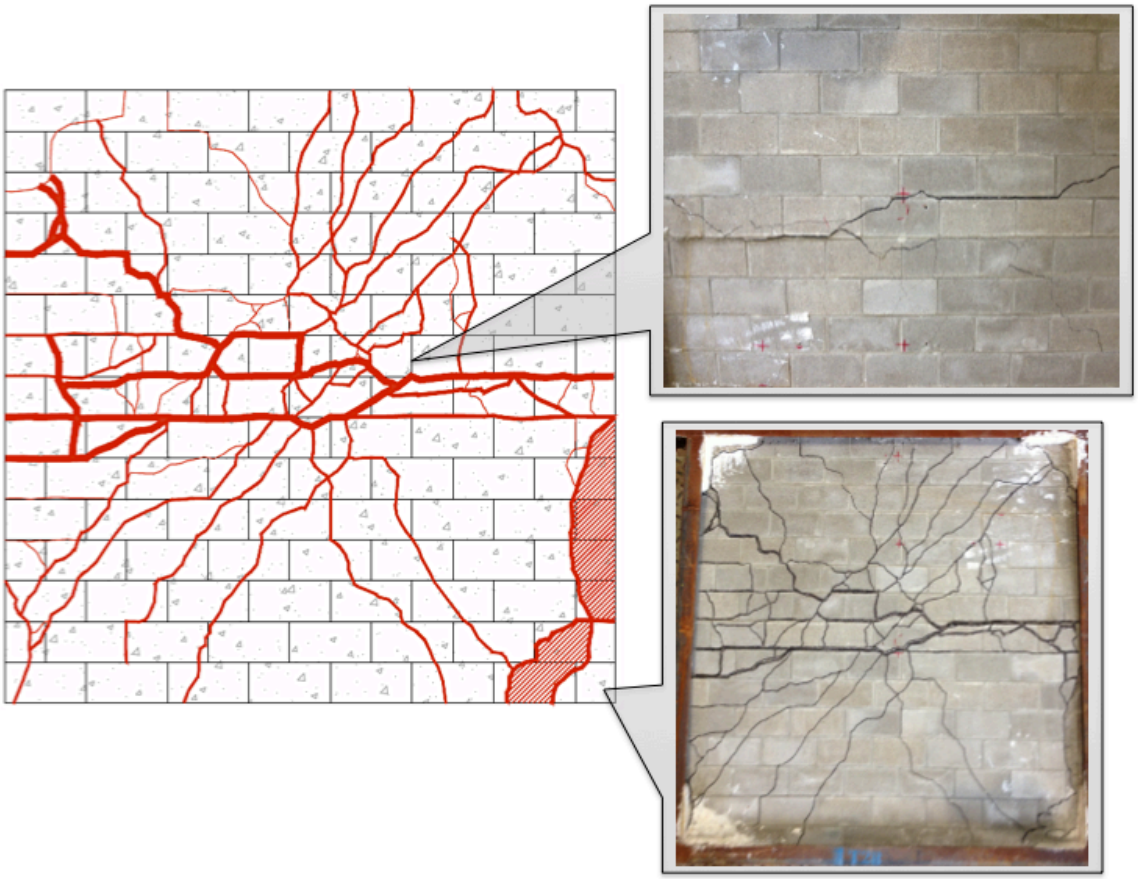

Figure 3.6: WBM, D4 Every Cell

The pressure-displacement plot was recorded from the centre LVDT, showing the largest deflections. The other three LVDT's that were placed on the wall prove that the wall was in fact bending in two-ways. As can be seen in Figure 3.7, the maximum pressure developed in WBM was 166.7 kPa before the wall was severely damaged. As also shown in the same figure below, this second wall picked some load up around 25mm of deflection. At 156 kPa the second wall WBM then lost all load and completely failed.

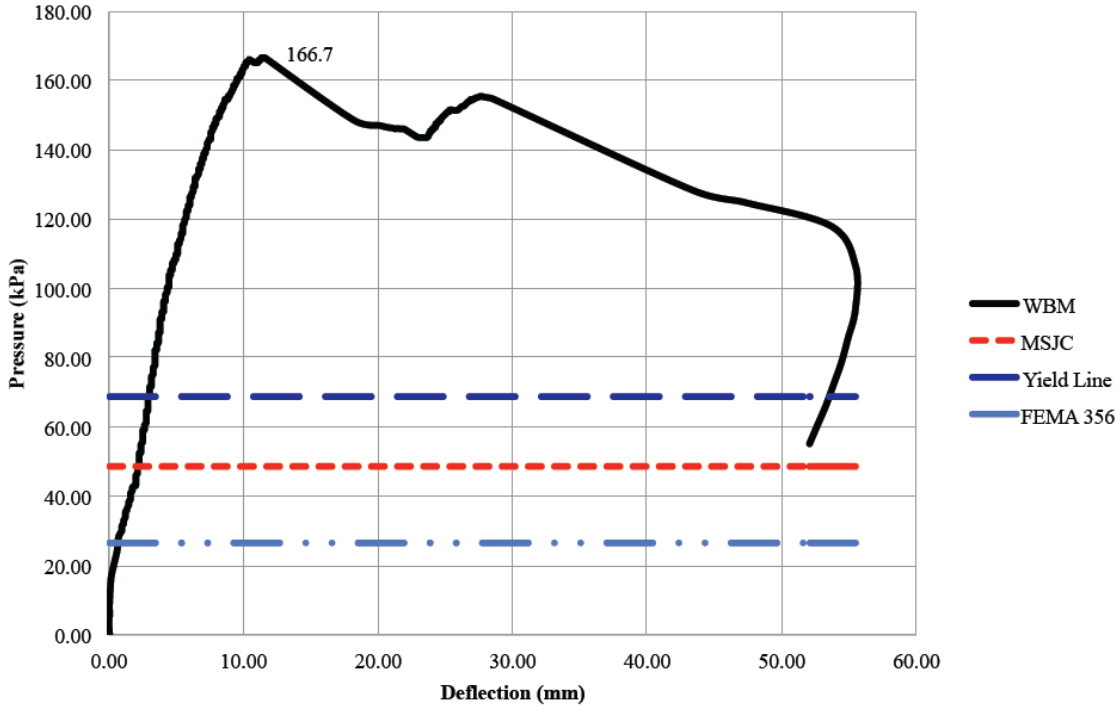

Figure 3.7: WBM Pressure – Displacement plot

Wall WBH underwent the highest deformation and capacity of the three masonry walls tested. The wall was loaded with the airbag at a rate of 0.01 psi per second (0.069 kPa

per second), attempting to minimize a high-energy release. There were hairline cracks spanning out from the centre of the wall towards the perimeter/boundary regions. Within a short time span, Wall WBH had a very large horizontal cracks spanning at mid height along the bed joint, for full length of the wall. The wall developed severe crushing of the masonry damage and blowout along the right perimeter of the test specimen (looking at the back of the wall) caused from the arching effect as is shown in Figure 3.8.

The wall was severely damaged then there was a sudden release of energy, after this, the air line was shut off and the pressure in the airbag further increased the deflection of the wall, until a total displacement of 150 mm was achieved, at which point severe cracking and spalling of the concrete occurred in the compression face. Figure 3.8, shows that the walls cracking pattern are symmetrical verifying that the wall is acting in two ways. One can also note that there is severe crushing of the masonry around the perimeter of the wall at the boundary conditions again validating that the wall is arching in both directions as well. This masonry crushing is the main failure mode of arching masonry walls.

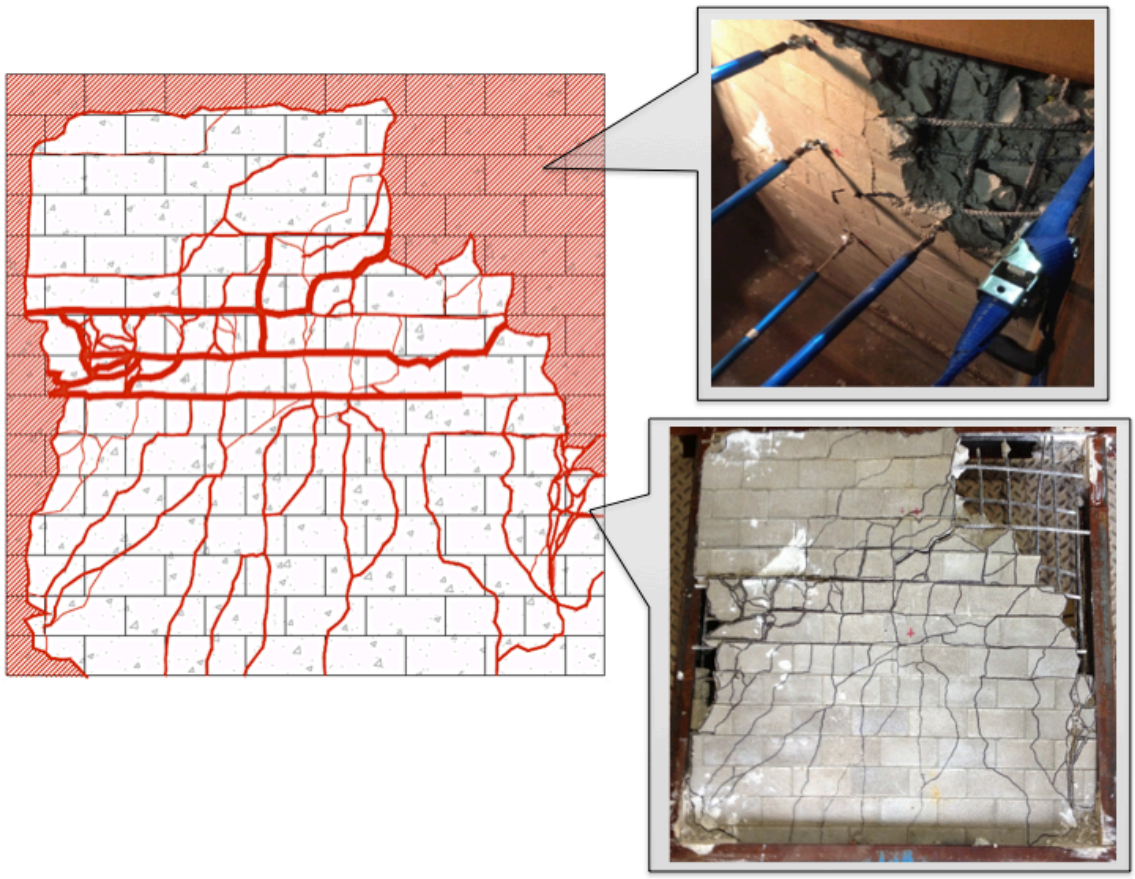

Figure 3.8: WBH, D7 Every Cell

As mentioned before, the pressure-displacement plot was recorded from the centre LVDT, which shows the largest deflections. The other three LVDT's displacements verify that the specimen is bending two-ways. The maximum pressure implemented by the airbag on the wall was 230 kPa before the wall was completely damaged. The capacity of WBH was significantly higher than the other two walls statically tested. The pressure-displacement curve can be seen in Figure 3.9.

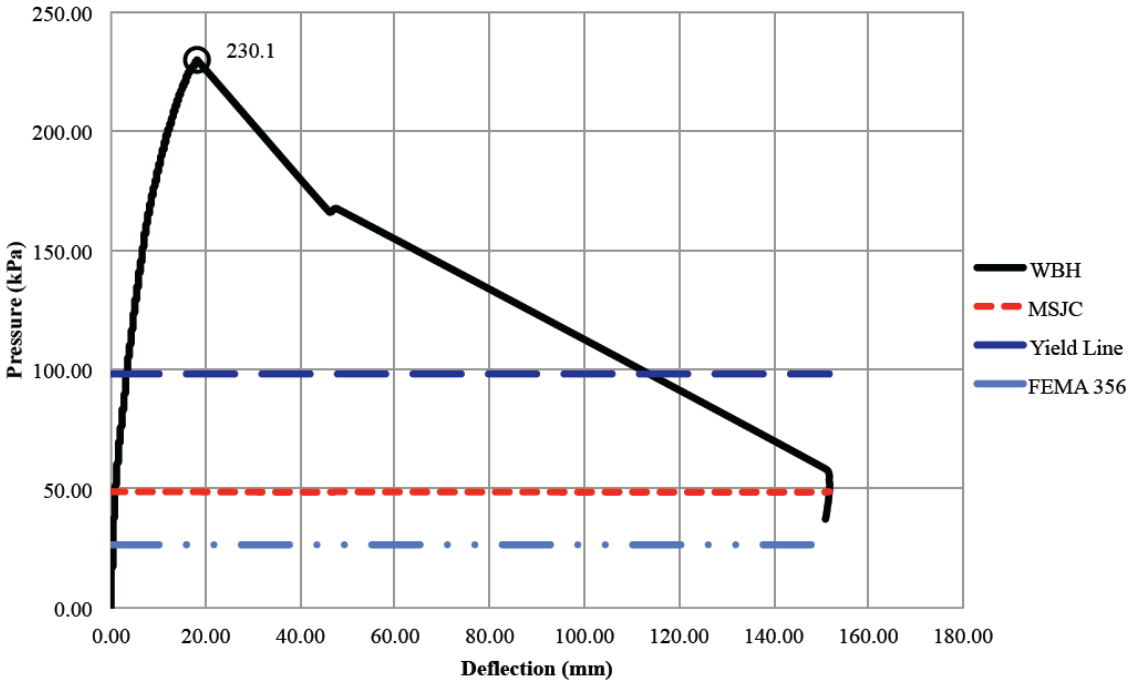

Figure 3.9: WBH Pressure – Displacement plot

3.6 Summary and Conclusions

Overall, the above three static out-of-plane airbag tests performed well. The static tests performed with higher capacities then originally expected. The calculated analytical capacities did not compared well to the three out-of-plane experimentally tested walls. This was because of an assumed conservatism built into the analytical equations. All the calculated methods underestimate the masonry infill wall capacities. These methods do not take into account the combined arching with rigid boundary conditions and that the masonry infill walls were acting in two ways while being fully reinforced.

4 Experimental Blast Test Results

4.1 Introduction

The results of the experimental blast test program are presented in this chapter. The deflection profiles are first discussed in detail, followed by the wall damage descriptions. The visual observations as well as the recorded displacements were used to discuss the formation of crack patterns and the development of wall failure modes. These wall cracks were traced (redrawn) to facilitate a better understanding of the failure modes. The recorded data was also used to generate the deflected shape of the wall specimens and to evaluate the maximum wall displacements and rotations. A full description of each wall is presented and documented with photographs showing the extent of cracking and observed failure mechanisms. The wall types in this dissertation are labeled with a "WB" as the specimens are part of a larger test program aimed at generating a masonry blast performance database. The character that follows the WB is to distinguish the level of reinforcement (**L**ow, **M**edium and **H**igh) and the number characterizes the charge size in kg.

4.2 Experimental Blast Wave Parameters

During the experimental testing, the blast wave properties were recorded for every blast trial using the pressure transducers located on the test frame, as mentioned before. These pressure transducers recorded the key parameters that contributed to the response of the wall. In the experimental testing, the blast wave properties are influenced by a number of

other properties such as ground surface and the atmospheric conditions. After the blast pressure data was collected, the experimental results were fitted for simplification with a modified Friedlander equation (Baker et al. 1983) to develop idealized blast load curves to be used in the finite element modeling later on in Chapter 5.

This is also a common practice because of the non-ideal behavior of experimental testing. The blast wave properties were also combined into three groups by the equivalent charge weight size (6 kg, 12 kg, and 30 kg) to get an average peak pressure and impulse. A sample pressure-time history can be seen Figure 4.1 with the experimental raw data and with the modified Friedlander equation fit (Baker et al. 1983).

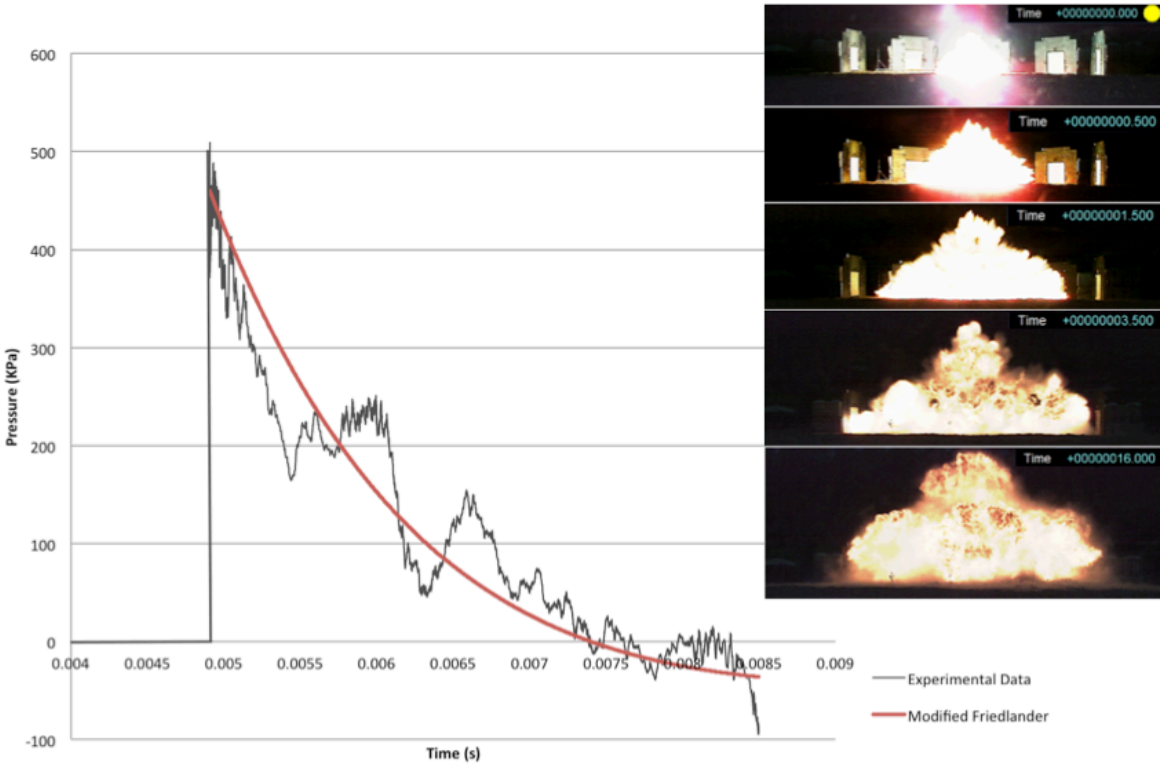

Figure 4.1: Experimental Pressure-Time history for Trial 3 with a modified Friedlander equation fit and a photograph of the evolution of the blast wave

Figure 4.1 also shows the evolution of the blast wave, captured from a high-speed camera where only select frames are shown to demonstrate the sequence. A closer look at the evolution of the blast wave shows that the experimental walls and test frame was completely engulfed by a fire-ball during the blast event.

The blast pressure experimental results were compared to the ConWep (Hyde 1990) predictions for verification. ConWep is a computer program based on a collection of experimental blast data and can imperially predict the blast wave parameters based on charge weight and standoff distances. The average experimental data and fitted modified

Friedlander results are compared in Table 4.1. From the results in the table below, it can be recognized that the two main blast wave parameters, peak pressure and impulse, were close to expected predicted parameters. Because of noise/ringing in the experimental test set-up, the pressure transducers gave slightly lower results when fitted to the modified Friedlander because of the high and low spikes in the data. In can been seen that in Table 4.1 below, the experimental data fitted with the modified Friedlander equation compared well to the predicted ConWep values within 18.6% for peak and 22.5% for the impulse.

Table 4.1: Pressure and Impulse estimates

	ConWep Predictions		**Positive phase duration modified Friedlander equation**			
TNT Charge Weights (Kg)	Peak Pressure (kPa)	Impulse (kPa ms)	Average Peak Pressure (kPa)	COV (%)	Average Impulse (kPa ms)	COV (%)
6	420	450	367	13.8	440	6.5
12	810	750	872	5.7	735	22.5
30	2010	1480	1882	18.6	1380	14.3

4.3 Failure Modes and Crack Patterns

The experimental test specimens were thoroughly inspected after each of the blast trials and all forms of damage was photographed and recorded. All cracks were outlined using permanent marker to facilitate retracing and drawing after the experimental testing. Sample crack patterns and photographs from the experimental test specimens are presented in this section. The typical failure mode in the two-way arching walls was

crushing of the masonry at the boundary regions. This crushing of the masonry is very significant under the largest (30 kg) explosive shots and can be seen in the Figures 4.2 – 4.8 below. This crushing near the boundary confirmed the development of the arching mechanism. Flexural cracking also occurred at the supports due to hogging moment resulting from the wall rotational restraints developed by the steel frame, followed by cracking at the walls central positive moment region. As a result, a three-hinged arch formed when the wall is viewed from its side. There we also spalling damage from the explosive loading on the masonry walls. The specifics of each explosive trial will be outlined in more detail in the sections below.

Wall WB6H was the only wall damaged in the first set of walls, which had the lowest reinforcement ratio. It was constructed with D4 reinforcement bars in every other cell in the horizontal and vertical directions. This reinforcement placement in every other cell represents 400 mm spacing in a full-scale concrete block wall.

The observed damage after the blast load was found to have a full-length horizontal hairline crack in the bed joint at mid-height, as well as a vertical hairline crack at its centre, spanning from one side to the other. This observed tension face of the masonry test specimen simulates the start of a typical flexure wall failure, showing the cross hair failure discussed in damage category in another section. As shown in Figure 4.2, the cracks are double symmetrical on all sides confirming that the wall is in fact acting two ways.

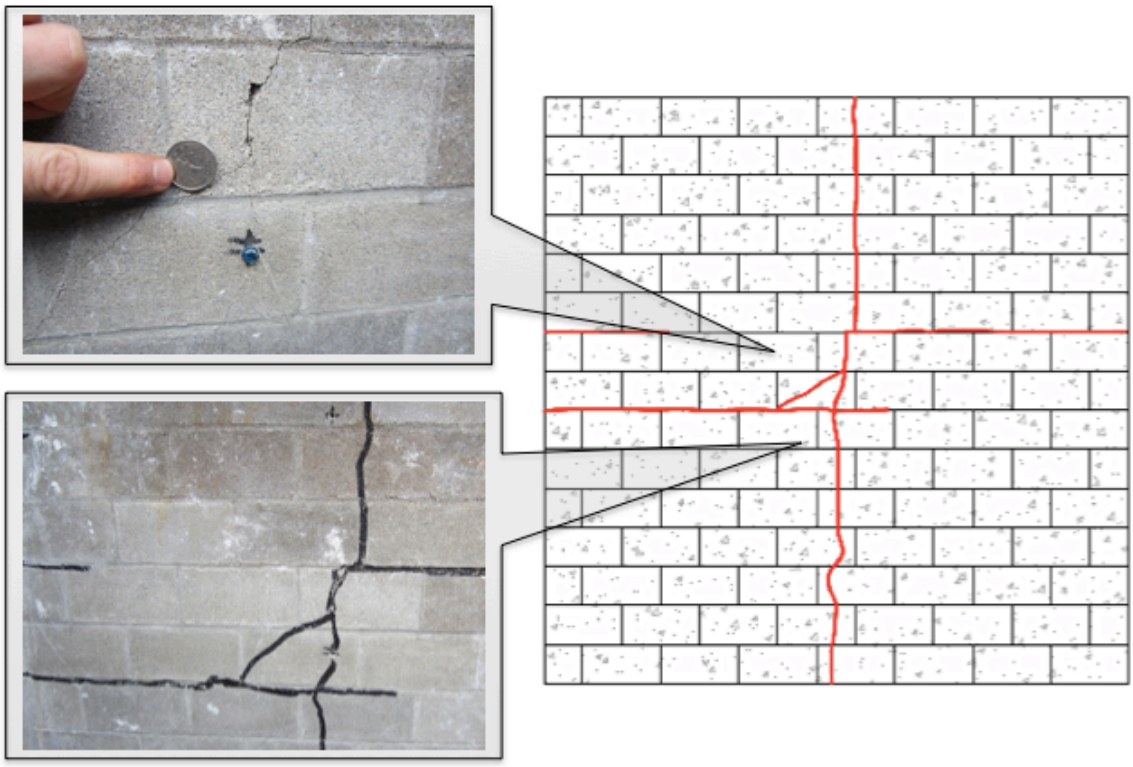

Figure 4.2: WB6L

Wall WB6M was constructed with D4 reinforcement in both horizontal and vertical directions in every cell. As mentioned previously, this wall specimen was subjected to 6 kg of equivalent TNT. After the tested wall was inspected, it was observed to have no damage or cracks on the wall. The third specimen that was tested was WB6H, with the high reinforcement ratio. The wall had D7 reinforcement bars in both the vertical and horizontal directions in every cell. No wall damage and deflections were observed.

Wall WB12L was the first wall tested in the second group with the lowest reinforcement ratio. There was a significant amount of damage compared to the 6 kg of equivalent TNT

shot, which was expected. Again, there was a flexural failure with the full-length vertical and horizontal cracks, however, this wall experienced a combined shear-flexure failure at its corners. The flexural cracks are more prominent and larger in the horizontal and vertical axis and the shear cracks are sometimes the diagonal cracks in the corners of the wall but there are sometimes breaching cracks. The walls crack patterns are completely symmetrical again ensuring that the wall is acting two-ways. There also was some minor crushing of the masonry in different locations around the perimeter of the test wall on the tension side showing that the arching mechanism is present. This wall specimen developed a flexure failure with combined shear failure in the corners shown in Figure 4.3. The Canadian CSA S850-12 and the American ASCE 59-11 blast standards do not give limits for shear failure or combined shear and flexure failures in blast loading.

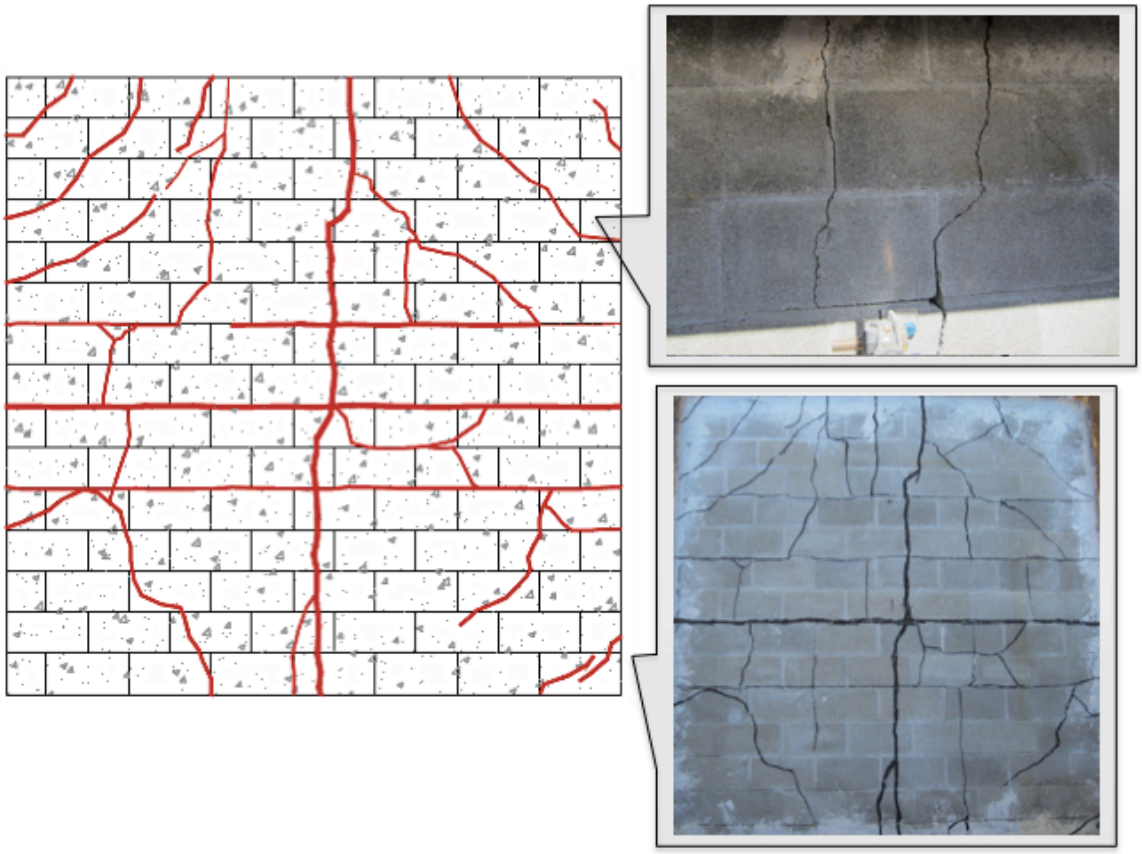

Figure 4.3: WB12L

Wall WB12M, with the medium reinforcement ratio, exhibited full-length horizontal cracks in the mortar bed joints from 8th through 10th courses of the wall and two vertical cracks spanning from mid-height to the top of the wall in the upper half. Figure 4.4 shows the tested walls crack patterns and damage details. In WB12M, large rock debris hit the corner of the wall from the blast event, causing a significant damage at the corner.

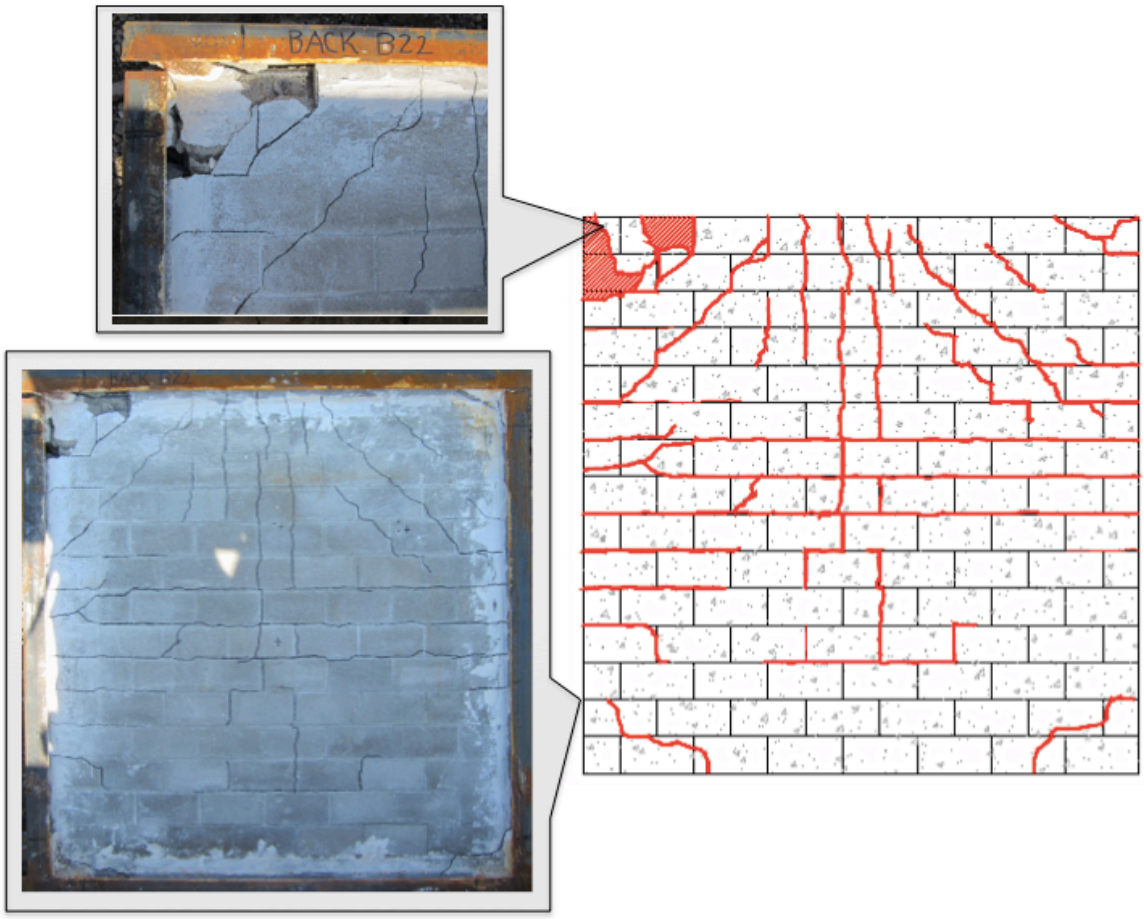

Figure 4.4: WB12M

The last wall, WB12H with the highest reinforcement ratio, experienced a similar flexural failure mode as wall WB12M. Again, mid-height horizontal cracks at the bed joints and a vertical crack in the centre spanning from mid-height to the top as shown in Figure 4.5.

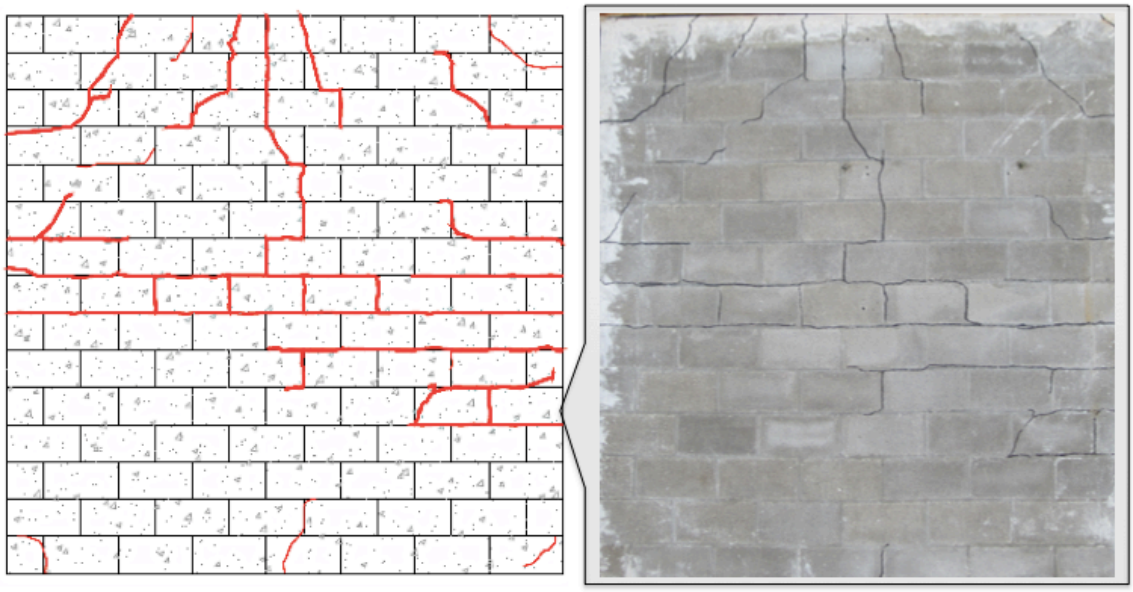

Figure 4.5: WB12H

Wall WB30H experienced full-length horizontal cracks on the tension side of the wall shown in Figure 4.6, extending from the 5th course to the 11th course. There was several of crushed CMU's around the perimeter of the test specimen, demonstrating the arching effects. The arching action at this high and close explosive charge weight makes the aching mechanism easy to see. The reinforcement was exposed at this point and can be seen in detail in Figure 4.6. It should be noted that, with the higher explosives charge weight, the boundary condition weld connecting the upper and right C-channel was blown apart causing more damage on that side then the opposite side.

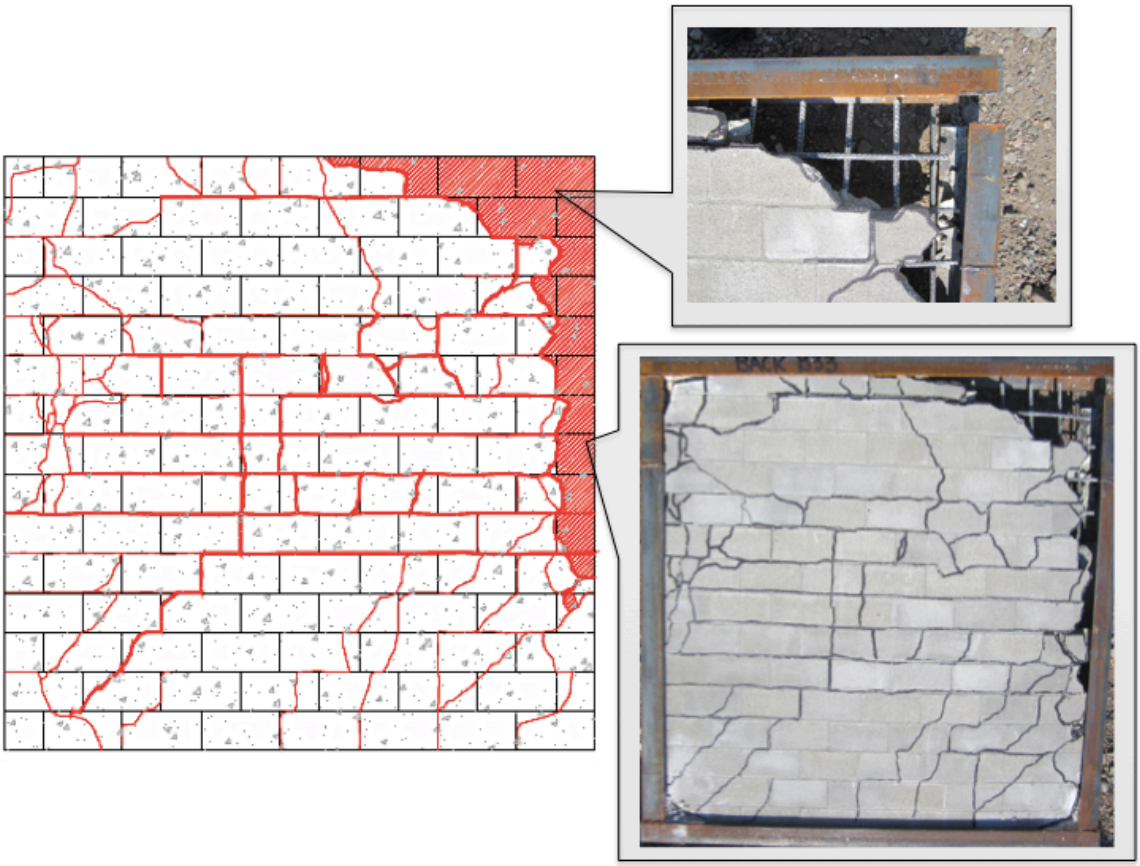

Figure 4.6: WB30H

The second wall tested with the 30 kg explosive charge weight was wall WB30M, having the medium reinforcement ratio with D4 reinforcement in every cell. As shown in Figure 4.7, this wall experienced extensive cracking with a grid of horizontal, vertical, and diagonal cracks protruding towards the centre of the wall from its boundaries. There was some shear present in the upper corner near the boundary. Again, the arching mechanism resulted with the crushing of the masonry around the perimeter of the wall specifically the left and right side of the wall.

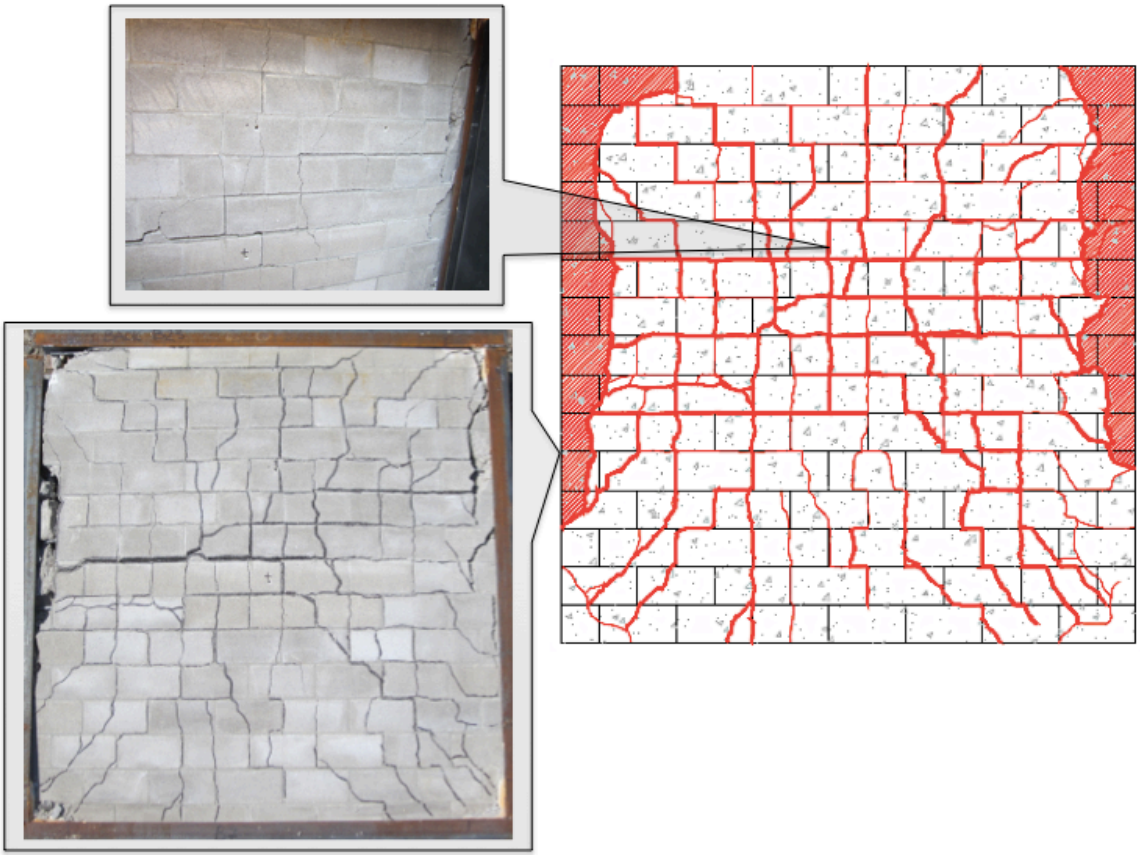

Figure 4.7: WB30M

Wall WB30L was the final wall tested in the 30 kg group of wall and the entire experimental program of two-way arching masonry walls. Wall WB30L had a very large horizontal crack spanning at mid height the full length of the wall and a large vertical crack at centre spanning the full length of the wall. This wall developed a flexure failure with very high rotations. Although the wall was classified as a "blowout" failure, the wall did not actually blow into the test frame. Also, there was little debris that flew inside the test frame. Which for reducing the hazard level for building occupants during a blast load and having very little debris fragments inside the building or structure is great. The

wall did develop severe crushing of the masonry damage and blowout along the left and right perimeter of the test specimen caused from the arching effect shown in Figure 4.8.

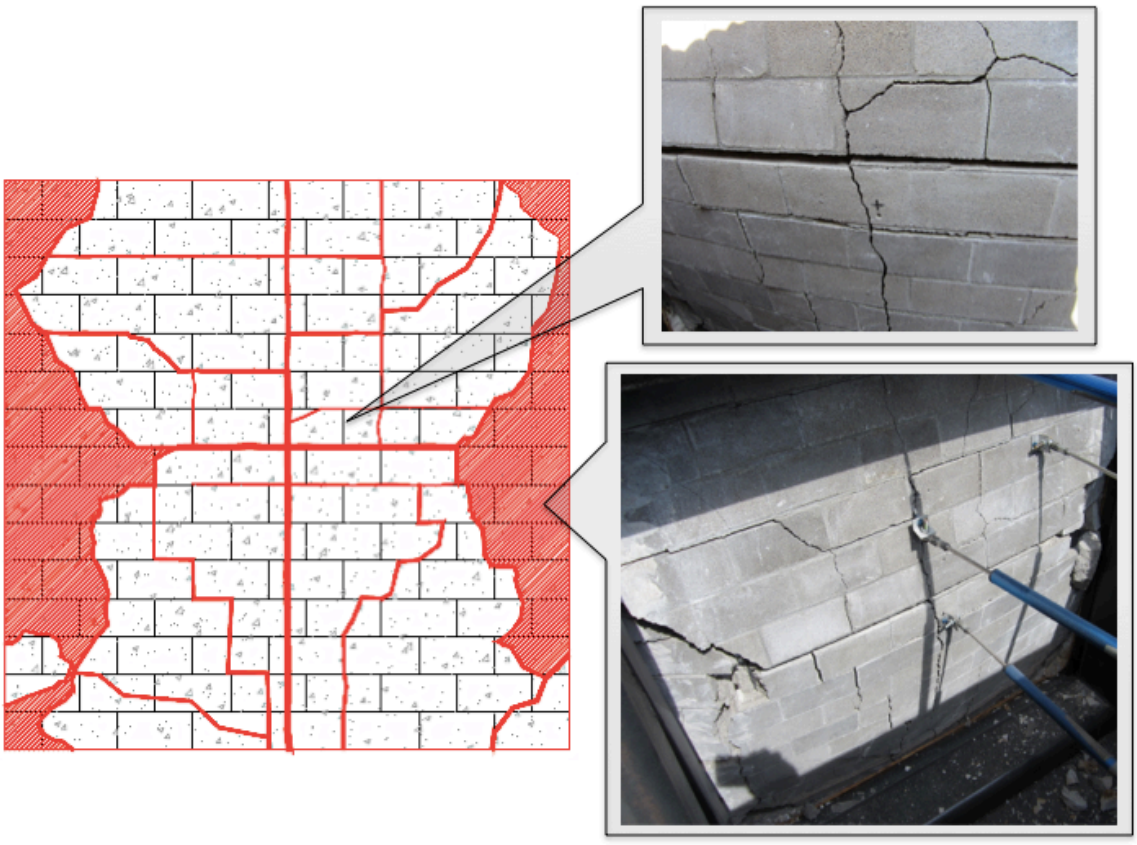

Figure 4.8: WB30L

4.4 Wall Displacements and Rotations

This section provides the displacements and corresponding rotations that occurred from the experimental blast testing. The data was collected at four locations on the upper quarter of the wall (centre, ¾ wall height, top and ¾ wall width / ¾ wall height). This was done to capture the entire wall deformation by projecting the upper quarters

displacements to the other three quarters, assuming double symmetry, resulting in the complete wall deformation profile. The positive values show that the wall is deflecting towards the back of the test bunker. Figure 4.9 shows the horizontal absolute displacement profile for the upper half of each wall at its mid span vertical section.

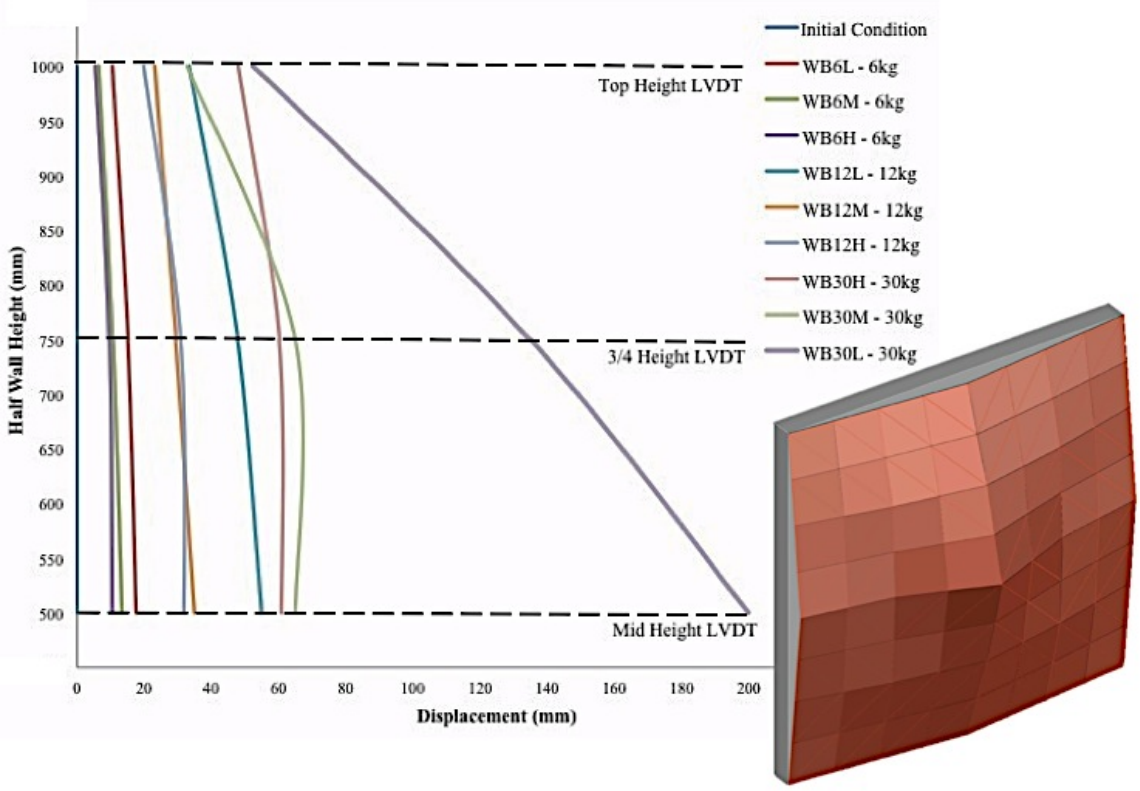

Figure 4.9: Comparison of maximum relative mid height displacements

The wall top end displacements were taken from the top linear displacement potentiometers as mentioned before and are not equal to zero because the wall was allowed to slide while arching in the vertical as well as the horizontal direction as shown in Figure 4.9. As expected the deflection tends to increase with the decrease in the

reinforcement ratio (weaker and less stiff walls) as well as the increase in explosive charge weight. The rotation was taken at the arc tangent over the ratio of maximum displacement to half the wall height/length. A sample displacement-time history from wall WB30L with a 30 kg explosive charge is shown in Figure 4.10.

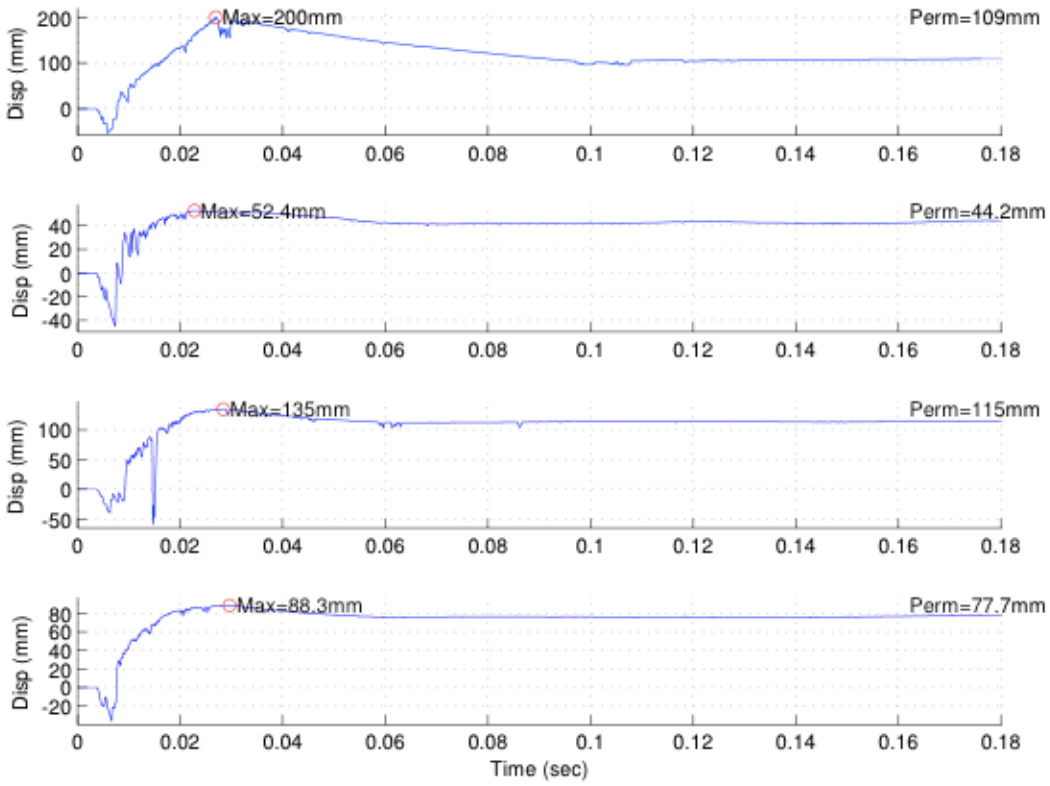

Figure 4.10: Sample displacement readings of specimen WB30L from Shot 9 – 30 kg

Figure 4.10 above, shows a sample from Shot 9, for the 4 linear potentiometers readings from the experimental blast event. As can be seen from the figure, there were significant permanent deflections present, after the blast event. The positive values on the displacement-time histories indicate that the test specimen is deflecting inward towards

the back of the test bunker. Due to occasional erroneous linear potentiometer readings, the maximum central displacement had to be estimated in some shots. The estimation took into account actual post blast measurements, the top linear potentiometer (at ¾ wall height) and to the right (at ¾ wall width / ¾ wall height) measurements.

As mentioned previously, the blast load was chosen to cause different damage and deflection levels based on the Canadian CSA S850 (2012) and the American ASCE 59 (2011) blast standards. It can be difficult to quantitatively categorize the level of damage of the masonry wall specimens on just the crack patterns and deflection levels from blast loading. Thus, the Canadian CSA S850 and the American ASCE 59-11 blast standards quantitatively categorize the damage by the out-of-plane rotation at the top of the wall. There are 5 expected damage levels for flexural reinforced masonry infill walls in the Canadian S850 and the American ASCE 59 blast standards. The five damage levels are: Superficial damage, Moderate damage, Heavy damage, Hazardous damage, and Blowout. The lateral maximum displacement profiles along the vertical axis and the corresponding Canadian and American blast standards damage levels for the nine tested masonry wall specimens are presented in Table 4.2.

Table 4.2: Experimental Measurements

Blast Shot Number	TNT Charge Weight (kg)	Specimen	Maximum Central Deflection (mm)	Rotation at top of wall (degrees)	Predicted Damage Level (CSA S850-12)
1	6	WB6L	17	2.0	Moderate Damage
2	6	WB6M	13	1.5	Moderate Damage
3	6	WB6H	*10	1.2	Moderate Damage
4	12	WB12L	*55	6.3	Heavy Damage
5	12	WB12M	35	4.0	Heavy Damage
6	12	WB12H	*32	3.6	Heavy Damage
7	30	WB30L	61	7	Heavy Damage
8	30	WB30M	65	7.4	Heavy Damage
9	30	WB30H	200	22	Blowout

* Estimated central displacement based on other potentiometers due to incorrect centre linear potentiometer readings

The first sets of walls tested were all subjected to a 6 kg blast load at a 5m standoff distance. Wall WB6L was the first wall tested in Group I and has the lowest reinforcement ratio and the next two walls tested had increased in reinforcement ratios. The 6 kg of TNT shots produced maximum displacements ranging from 10 to 17 mm with corresponding rotations of 1.2° to 2°. When looking at the horizontal displacements for these groups of walls, one can observe a similar displacement level demonstrating that the wall was indeed acting in a two-way action. In the CSA S850-12 standard, the response limits for reinforced masonry with a rotation 2° and under falls in the moderate

damage category. All three walls that were tested under a 6 kg blast load are classified as moderate damage failures as shown in Table 4.2.

The second group of walls were tested with 12 kg of TNT at a 5m standoff distance. This group of walls were all categorized as a heavy damage failure classification ranging from 32 mm at maximum central displacement with the highest reinforcement ratio to 55 mm at maximum central displacement with the lowest reinforcement ratio.

Finally, the last group of walls were tested with the 30 kg of TNT at a 5m standoff distance. Wall WB30H with the highest reinforcement ratio developed a 61 mm maximum central deflection with a corresponding rotation of 7° placing this wall in the heavy damage category. The next wall tested at 30 kg of TNT was wall WB30M. This wall produced a very similar deflection of 65 mm and was classified as a heavy damage failure. The final wall tested in the experimental program was wall WB30L that has the lowest reinforcement ratio and was subjected to the highest blast load of 30 kg of equivalent TNT. This test wall resulted in a 22° rotation, which places it in the blowout damage category for flexure. Although wall WB30L had very high rotations and was placed within the blowout damage category, the only part of the wall that actually blew out was the left and right sides where the arching mechanism took place. Visual inspection inside of the bunker after the blast event showed that no large debris was blown inside of the test frame.

In the CSA S850-12 standard, the response limits for reinforced masonry predicted damage levels correspond to the support rotation. Another way the support rotation could be calculated is by the net central deflection. The predicted damage levels are listed below in Table 4.3. When using the Net Central deflections, the predicted damage levels are classified as lower damage levels.

Table 4.3: Experimental Measurements with Net Deflections

Blast Shot Number	TNT Charge Weight (kg)	Specimen	Maximum Net Central Deflection (mm)	Rotation at top of wall (degrees)	Predicted Damage Level (CSA S850-12)
1	6	WB6L	7.15	0.8	Superficial Damage
2	6	WB6M	6.81	0.8	Superficial Damage
3	6	WB6H	*5	0.6	Superficial Damage
4	12	WB12L	*21.6	2.5	Heavy Damage
5	12	WB12M	11.8	1.4	Moderate Damage
6	12	WB12H	*12.1	1.4	Moderate Damage
7	30	WB30L	13	1.5	Moderate Damage
8	30	WB30M	32.2	3.7	Heavy Damage
9	30	WB30H	147.5	16.4	Blowout

* Estimated central displacement based on other potentiometers due to incorrect centre linear potentiometer readings

A more suitable way to calculate the predicted damage levels from the CSA S850-12 standard, is by taking the maximum effective deflected length. The effective length was

selected to be half the diagonal distance form the centre of the wall to the support. This effective distance is to be considered a more appropriate estimate. The estimated damage levels are shown in Table 4.4 below.

Table 4.4: Experimental Measurements with Diagonal Chord

Blast Shot Number	TNT Charge Weight (kg)	Specimen	Maximum Central Deflection (mm)	Diagonal Chord Rotation at top of wall (degrees)	Predicted Damage Level (CSA S850-12)
1	6	WB6L	17	1.4	Moderate Damage
2	6	WB6M	13	1	Superficial Damage
3	6	WB6H	*10	0.8	Superficial Damage
4	12	WB12L	*55	4.5	Heavy Damage
5	12	WB12M	35	2.8	Heavy Damage
6	12	WB12H	*32	2.6	Heavy Damage
7	30	WB30L	61	4.9	Heavy Damage
8	30	WB30M	65	5.3	Heavy Damage
9	30	WB30H	200	15.8	Blowout

* Estimated central displacement based on other potentiometers due to incorrect centre linear potentiometer readings

Figure 4.11 a) below, shows the effects of the test parameters in the experimental testing. These different parameters are; support rotation, scaled distance and reinforcement ratio. Figure 4.11 b) shows slices of the surface shown in Figure 4.11 a) and presents 3

particular scaled distances comparing support rotation vs. reinforcement ratio. Figure 4.11 c) shows the perpendicular slices of the surface, but with specific reinforcement ratios comparing support rotation vs. scaled distance. From these plots, some trends in the wall response can be observed. The scaled distances in Figure 4.11 b) show that a lower scaled distance gives you a higher damage level, but at a higher scaled distance, you have very little variation in the walls damage. This figures also shows that the lowest reinforced wall has a steeper slope indicating that these walls are more susceptible to damage within such low range of scaled distance.

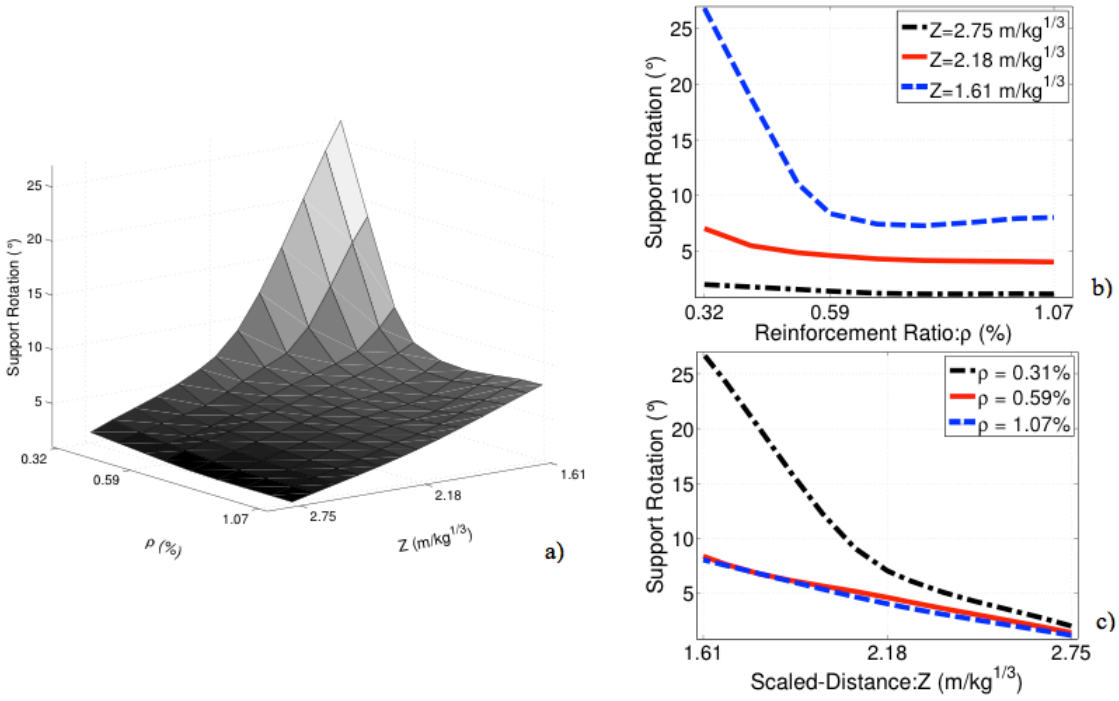

Figure 4.11: Effect of Test Matrix Parameters: a) Surface Plot; b) Scaled Distance; c) Reinforcement Ratio

4.5 Summery and Conclusions

The blast response of the two-way arching reinforced masonry walls was evaluated through experimental testing of nine third scaled walls with three different reinforcement ratios. The blast loads ranged from 6 – 30 kg of equivalent TNT at a 5 m stand-off distance. At the lowest blast load of 6 kg the infill walls rotations ranged between 1.2° and 2° which were which the Canadian CSA S850-12 and the American ASCE 59-11 blast standards quantitatively categorize the infill walls damage as Moderate damage. The walls tested at the blast load of 12 kg exhibited rotations between 3.6° and 6.4° categorizing the damage as Heavy damage. Finally, the highest blast load at 30 kg resulting in rotations between 6° and 22°. These infill walls were categorized as Heavy Damage to Blowout Failure.

5 Finite Element Modeling

5.1 Introduction

This chapter discusses the concepts used for modeling the reinforced masonry walls with the boundary conditions forcing a two-way arching mechanism. The Finite Element (FE) model is produced to check and verify the experimental results from the blast testing in Chapter 4. This FE model must accurately represent the masonry wall specimens and blast pressures. FE models are valuable tools that can be used to simulate and compare experimental

With the advancement of different material models, high speed computers, and more efficient numerical solution techniques FEA has been relied on for verifying experimental work and understanding complex inelastic behavior under dynamic loading. Experimental and numerical analyses can be performed on reinforced masonry specimens; however, high cost, time, and safely limit the number of tests that can be conducted. LS-DYNA is a advanced nonlinear dynamic finite element software by Livermore Software Technology Corporation (LSTC).

The detailed focus of this section will be to compare the failure modes and crack patterns obtained from experimental testing with a Finite element model. Using the results of the earlier reported nine two-way arching reinforced masonry walls, confined by four rigid supports. The validation of the model will be reviewed and its significance to the experimental testing.

5.2 Development of the Finite Element model

The development of the FE model contains significant preparation before it can be used as an accurate model for predicting the capacity and response of the masonry test specimens. There are many materials and factors within the FE model that need to be addressed specifically in order to precisely develop the FE model. The FE model constructed in LS-DYNA, discussed in the chapter, replicates the experimental, blast-tested walls from Chapter 4.

5.2.1 Unit System

It is important to initiate and maintain a consistent unit of measurement throughout the entire analysis as there is no way to predict the units used within the LS-DYNA model process. The following table below, Table 5.1, provides the consistent units used in the FE model.

Table 5.1: LS-DYNA Units

Unit	Measurement
Length Unit	Millimetre (mm)
Time Unit	Millisecond (ms)
Mass Unit	Gram (g)
Force Unit	Newton (N)
Gravity	9.81E+03
Stress	MPa
Energy	N-mm

5.2.2 Geometry and Dimensions

As presented earlier in this paper, Chapter 2 and Chapter 4, the masonry wall specimen's sample geometry is 1000 mm x 1000 mm x 63.33 mm thick, fully grouted reinforced masonry. There were three different types of walls subjected to three different blast charge weights totaling nine walls. These nine walls were experimentally tested and then replicated in LS-DYNA attempting to duplicate the behavior of the experimentally constructed walls.

5.2.3 Parts

In the LS-DYNA FE model, three parts were considered, which are defined in LS-DYNA under the PART tab. The first part in the model represents the concrete masonry. For this simple FE model, the masonry blocks and mortar were not individually defined because of the complexity of the model. This was thought to be a valid assumption especially for fully-grouted masonry. The second part in the model being the reinforcing bars, and the final part in the FE model is the steel C-Channels. These C-Channels are rigid plates surrounding the entire perimeter of the masonry wall but not welded. The interaction between the masonry wall and the C-Channels was modeled using contact surfaces, which will be discussed in Section 5.2.7. In the LS-DYNA input deck, each of the *PART tabs created are further identified under the section (*SECTION) and material (*MAT) tabs. These secondary tabs link the element properties and material to the specific part.

5.2.4 Meshing Strategy

Within LS-DYNA there are several meshing options available, in this FE model the concrete masonry element were meshed. The method used for this FE model was a 12-line solid element mesh, in the LS-DYNA input deck, *SECTION_SOLID tab for the concrete masonry. The mesh size started with a 32 mm cube element. The results of the 32 mm cube element were then compared to the experimental tests. These results were in close agreement with one another. The mesh size was then halved to 16 mm cube elements. When the mesh was cut into half it resulted in 5% difference improving the experimental results predictions. This mesh size was then used because of the closer predictions while still having a reasonable computation time. The wall was divided into 60 elements high x 60 elements wide x 4 elements thick, thus creating a cube element, approximately 16 mm in size throughout the wall. The aspect ratio of the mesh elements is 16 mm cubed which is desirable in finite element mesh. As a result of the meshing technique, each masonry wall contains a total of 14 400 elements as shown in Figure 5.1.

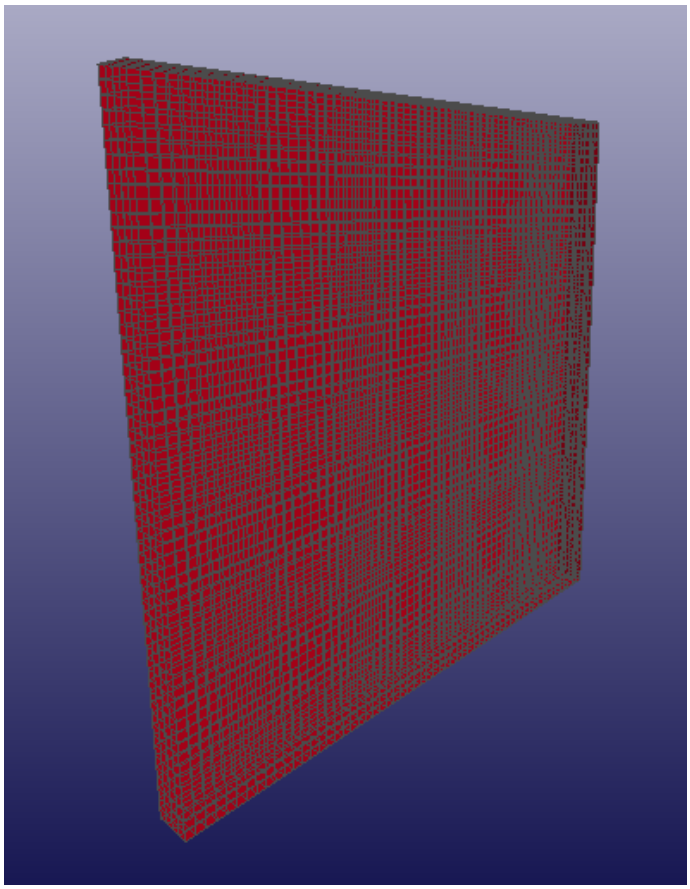

Figure 5.1: Concrete Masonry Wall Mesh

A further meshing element to be defined in the modeling within LS-DYNA was the rigid steel C-Channels, installed around the perimeter of the masonry wall used to enforce the two way arching. The C-Channels were meshed using a 4-line plate shell, containing 120 x 12 x 120 x 12, doubling the initial number of elements used in the masonry wall. Figure 5.2, shows the rigid C-Channels meshed around the perimeter of the masonry wall.

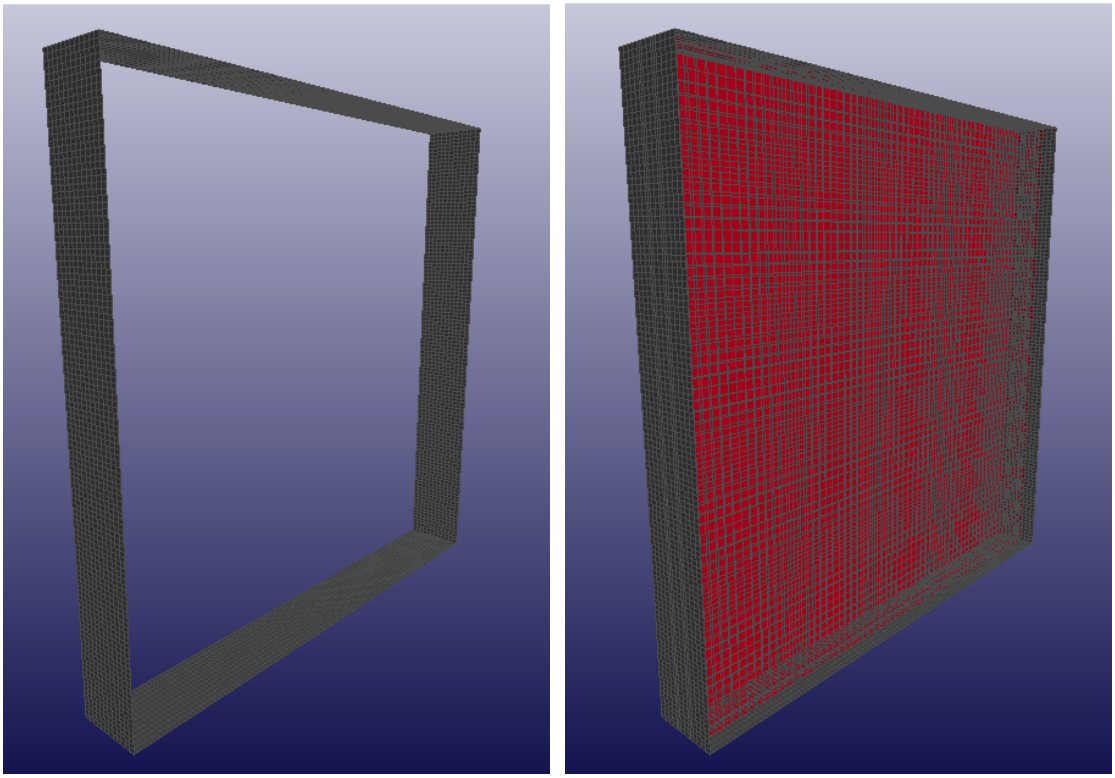

Figure 5.2: Rigid C-Channels Meshed

Lastly the steel reinforcement was meshed into elements. The *SECTION_BEAM was used for the reinforcement. The determination of the mesh size for the reinforced steel bars was selected to coincide with the nodes from the concrete mesh elements. This enforces the fact that complete bonding between reinforcements and concrete material is maintained during the analysis. Subsequently, the mesh for the beam elements (reinforcement), which runs along the length of the beam, was assigned and two different beam elements created for the horizontal and vertical reinforcement. Figure 5.3 shows the beam elements meshed in the FE model in the horizontal and vertical directions.

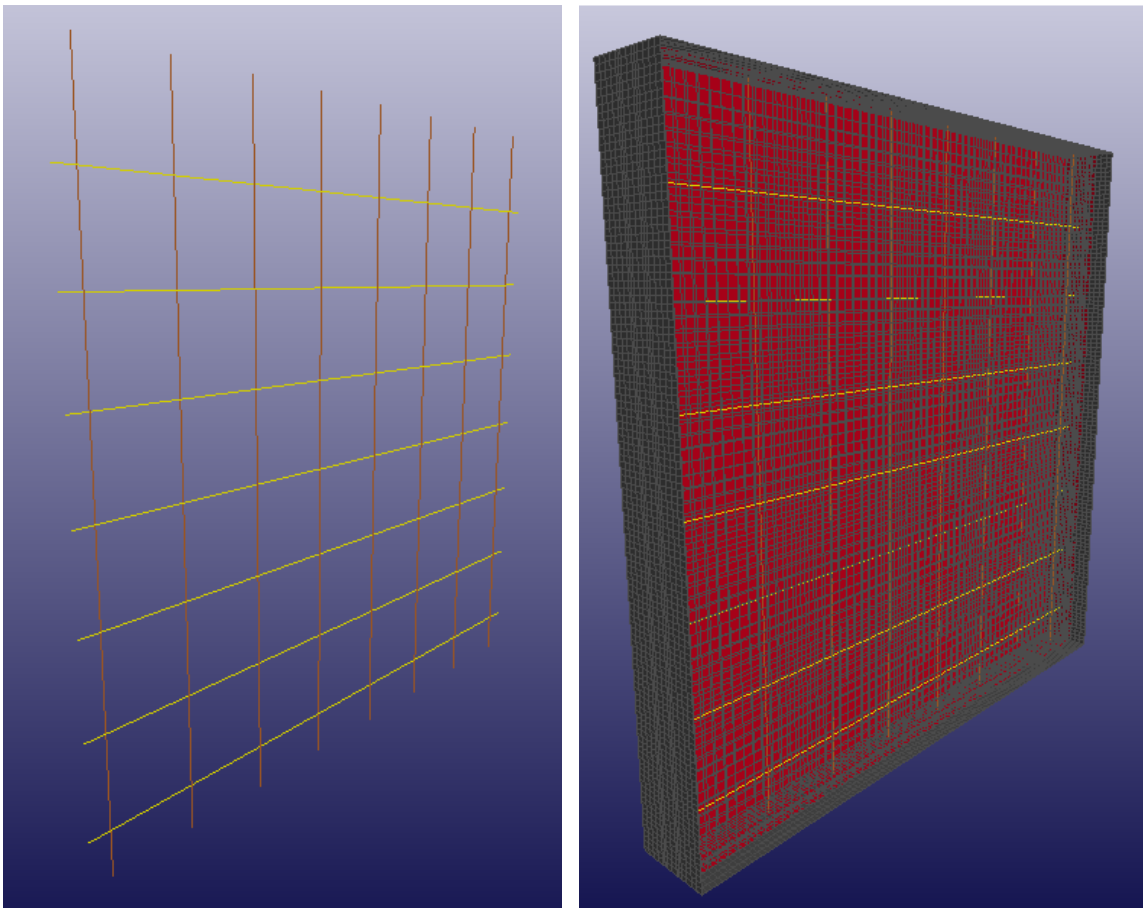

Figure 5.3: Reinforcement Mesh

5.2.5 Material Models

In LS-DYNA, there is a large database for material model selection, enabling you to choose the correct material model for the appropriate situation. The materials are selected in the *MAT tab and all the material models are defined in the user manual for LS-DYNA.

5.2.5.1 Material Model for Reinforcing Steel

In the three different types of experimental walls, one type of reinforcement was used for the vertical and horizontal steel, since the wall specimens are acting in two-way so therefore the reinforcement is symmetrical in both vertical and horizontal directions. As mention earlier in Chapter 2, the steel reinforcement used was D4 and D7 steel which was heat-treated with a cross sectional area of 26 mm^2 and 45 $mm^{2,}$ respectively. The rest of the reinforcement properties are in Table 5.2 below.

Table 5.2: Reinforcement Properties

Steel Size	Poissons Ratio (*PR*)	Yield Stress (σ_y, MPa)	Strain Rate (*SRS*)
D4	0.333	478	$1x10^{-4}$
D7	0.333	484	$1x10^{-4}$

The steel reinforcement material model used in LSDYNA is PLASTIC_KINEMATIC (MAT_003). Since this material is subjected to blast loads and is affected by large strains, which can lead to failure, this was an appropriate material to use. Depending on the blast intensity, material and structural behavior become very different from their quasi-static behavior and strain rate effects become dominant in blast events. With the Plastic Kinematic material, strain rate effects and isotropic and kinematic hardening of the material (Hao and Zhongxian, 2009) can be included.

5.2.5.2 Material Model For Concrete Masonry

Eighteen random one-third scale masonry blocks were tested and the average compressive strength *(f'_m)* was 20.3 MPa with a coefficient of variation (COV) of 11% according to CSA A165.1 and S304.1-04. The masonry blocks compressive strength was based on the average net cross-sectional area 4789 mm^2 from clause 5.1.3.4.3 in S304.1-04. On average grout cylinders were 23.3 MPa with a COV of 9% based on CSA A179. Type-S mortar cubes were tested according to the CSA A179 with an average of 28.4 MPa with a COV of 3.7%. The four course high, fully grouted masonry prims were built and tested in accordance to ASTM C1314-11a, with an average compressive strength of 18.7 MPa with a COV of 10.2%. The masonry material properties for the FE model are summarized in Table 5.3 below.

Table 5.3: Masonry Material Properties for FE Model

Mass Density (*RO*) (g/mm^3)	**Youngs Modulus (*E*) (MPa)**	**Poissons Ratio (*PR*)**	**Tensile Strength (MPa)**	**Compressive Strength (f'_m) (MPa)**	**3/8"Aggregate Size scaled to 1/3 (mm)**
$1.8x10^{-9}$	14278	0.2	2.65	18.7	3.0

In LS-DYNA there are several concrete material models to choose from. Based on former research studies (Schwer, L. and L. Malvar (2005) and Crawford et al. (2012)), the Concrete Damage Material Model Release 3 (MAT_CONCRETE_DAMAGE_REL3) was chosen for this study.

This material model is used to study steel reinforced concrete structures subjected to impulse loading, having the capacity of self-parameter generation based on the unconfined strength of concrete. MAT_CONCRETE_DAMAGE_REL3 is a three invariant plasticity and damage based constitutive model, which is used for lightweight and normal concrete applications to compute quasi-static and blast loads on structures (LSTC, 2007).

5.2.6 Strain Rate Effect

Blast Loads typically produce very high strain rates and would dynamically alter the material properties. The strain rate material characteristic becomes an important parameter in blast loading since the dynamic loading duration is very small. Both concrete and reinforcing steel materials show greater strengths, at a high strain rate of loading. A higher strain rate gives the steel reinforcement a higher yield and ultimate load, and gives a higher compressive strength of the concrete (UFC 340-02). The strain rate effect for the steel was based on Crawford et al. (2012) and Schwer and Malvar (2005).

5.2.7 Contact Interfaces

Contact surfaces are necessary in modeling the experimental research properly. There are various interactions in the experimental wall specimens between the rigid steel C-Channels and the masonry walls mortar, such as friction and separation. The choice of which contact type to use depends on the behaviour of the individual elements. LS-

DYNA identifies contact by checking for potential penetration of a slave node set through a master node set. Penetration algorithms perform this check at each time step.

The rigid steel shell element was set as the master, while the masonry wall was set to be the slave. Because the shell segments thickness was considered in the geometry, an automatic type of contact was used. The *CONTACT_AUTOMATIC_SURFACE_TO_SURFACE was used to define the contact between the rigid steel boundary elements and the masonry wall.

5.2.8 Boundary Conditions

The experimental masonry test specimens are used to simulate an exterior steel framed structure with masonry infill wall panels. These infill wall panels are pin-supported boundary conditions forcing a two-way arching effect; this is why the reinforcement is symmetrical in both directions. As detailed in Chapter 2, the test specimens were constructed with 5 x 9 C-Channel. The C-Channel was used as a base for the masonry wall to be built on. When the masonry wall construction was completed, another C-Channel was mortared in place on top of the wall. The next step was to weld the two side C-Channels to the top and bottom making it one. Gypsum was placed in the top corners to ensure there was no sliding of the wall during the blast load. There was a 25 mm gap on each side of the C-Channel to the wall. The reinforcement was not welded to the C-Channels allowing it to slide back and forth on the C-Channel before it was mortared in

place. 2 inch round stock was welded around the entire perimeter of blast frame to allow perfect contact from the wall to blast frame during the testing.

In order to be consistent with the boundary conditions used in the experimental testing, the following FE model boundary conditions were adopted. To model the wall specimen in LS-DYNA a simplified model had to be made. The first step was to model the 5 x 9 C-Channels welded around the entire wall specimen with some type of friction contact. This was done by using a contact from the plate steel (C-Channels) sitting on top of the masonry wall and adding in contact in LS-DYNA. The contact used was *AUTOMATIC SURFACE_TO_SURFACE CONTACT as was previously described in Section 5.2.7 of this thesis. The C-Channels were set up as the master and the wall as the slave, to ensure the wall moves but the rigid C-Channels do not move. These rigid C-Channels will also enforce the masonry wall to arch.

The next step is to create a node set in LS-DYNA to fully define the boundary conditions. There were two node sets generated, these can be found in the *SET_NODE tab in LS-DYNA. The first node set generated, was be fixing the corners. The corners had a translational constraint in the X, Y and Z directions. This node set was then simplified by fixing the nodes completely at the front and the back of the wall, only at the corners. Precisely where the hydrostone would be in the experimental test walls. Figure 5.4. a) below, shows the corners fixed in the LS-DYNA FE model. The second node set created in LS-DYNA is the front face node set, which was created under the *SET_SEGMENT

tab. The front face node set is created to direct the blast load at the front face of the masonry wall and can been seen in Figure 5.4 (b).

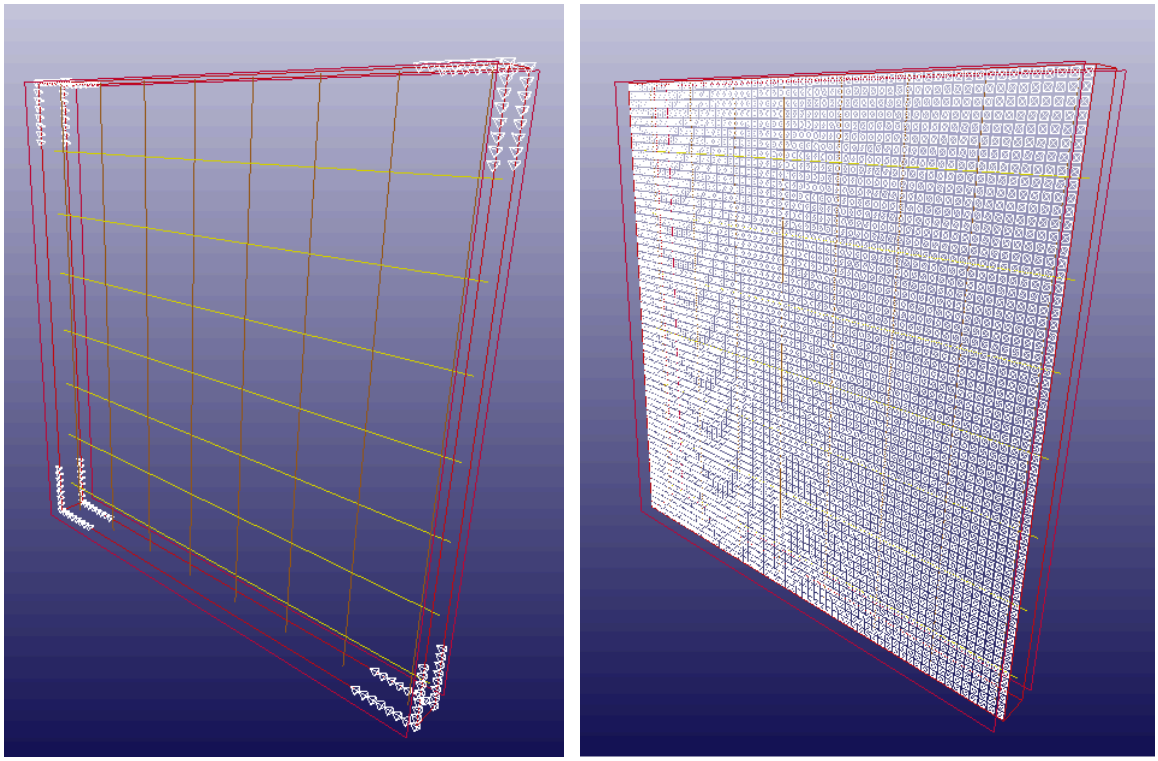

Figure 5.4: Boundary Conditions of FE Model: a) Four Fixed Corners *SET_NODE; b) Front Face *SET_SEGMENT

5.2.9 Blast Loading

As mentioned previously, as apart of the larger test program, the three selected TNT equivalent charge weights were 6 kg, 12 kg and 30 kg. The experimental blast wave parameters were then verified from ConWep. ConWep predictions compare well to the experimental recorded blast wave parameters in Chapter 4 of this dissertation. A modified Friedlander equation (Baker et al. 1983) described in chapter 4, was used to fit

the experimental blast wave pressure profiles to then use in the FE model. Three loads having various charge stand-off combinations were used. An average of the time histories, peak pressures, and impulses of the three loads are given below.

The first group of recorded blast reflected pressure profiles for the 6 kg charge weight averaged 367 kPa (COV = 13.8%). Figure 5.5 below, shows the recorded reflected pressure profile used for the first blast load in LS-DYNA. The modified Friedlander fit curve was imported into LS-DYNA for the blast load on the first three walls.

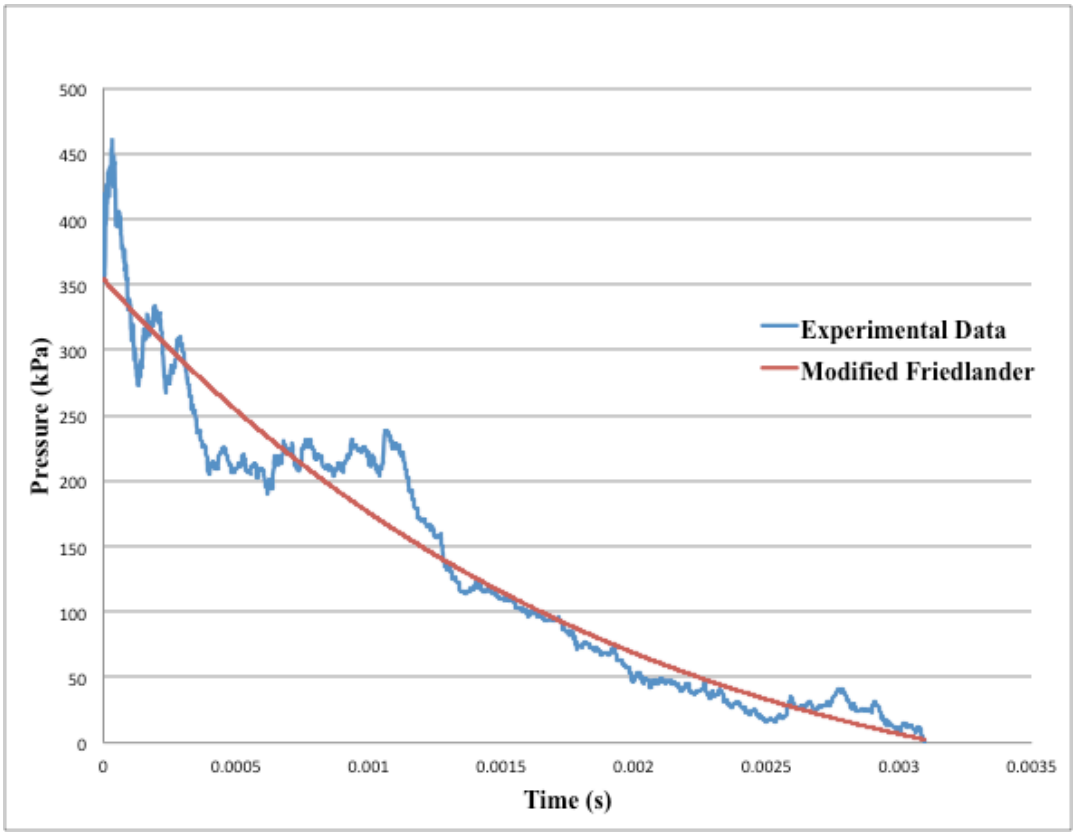

Figure 5.5: Pressure – Time History for Blast Load 1

The second group of recorded blast reflected pressure profiles for the 12 kg charge weight averaged 872 kPa (COV = 5.7%). Again, the modified Friedlander fit curve was imported into LS-DYNA for the blast load on the second group of three walls and is shown in Figure 5.6 below.

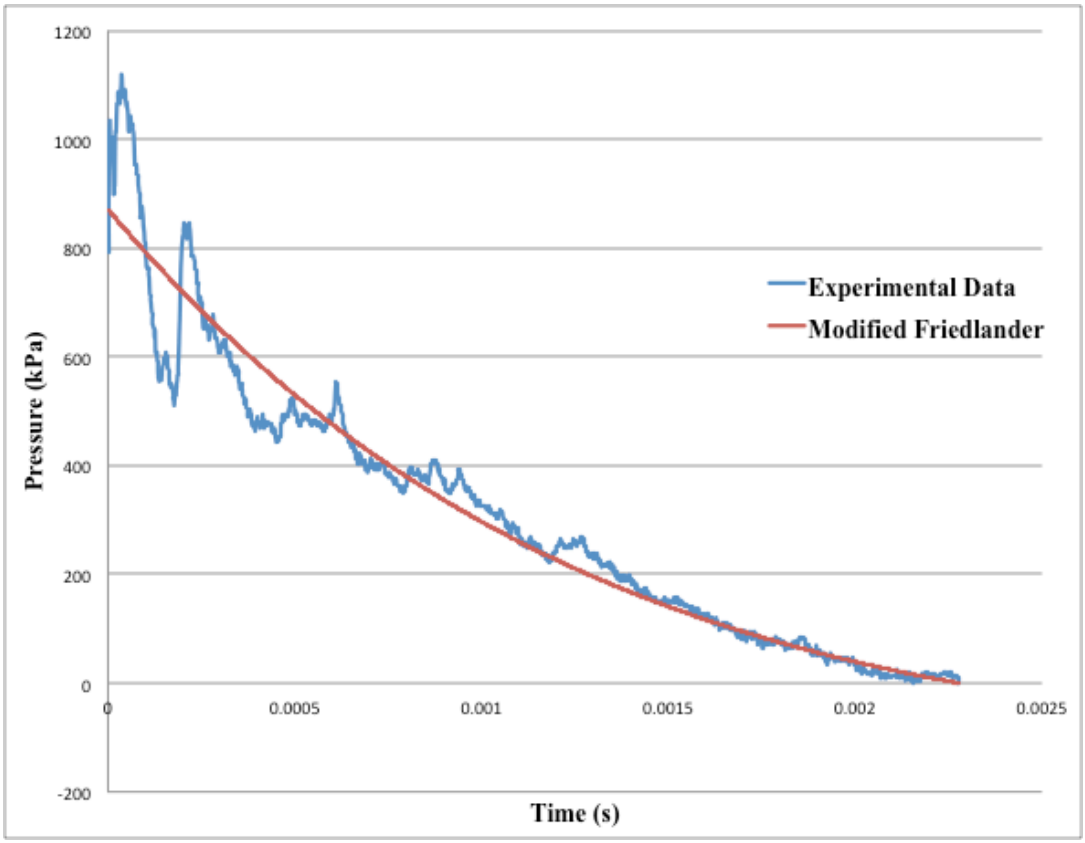

Figure 5.6: Pressure – Time History for Blast Load 2

The last group of recorded blast reflected pressure profiles for the final 30 kg charge weight averaged 1882 KPa (COV = 18.6%). Figure 5.7 below, shows the recorded reflected pressure profile used for the third blast load in LS-DYNA.

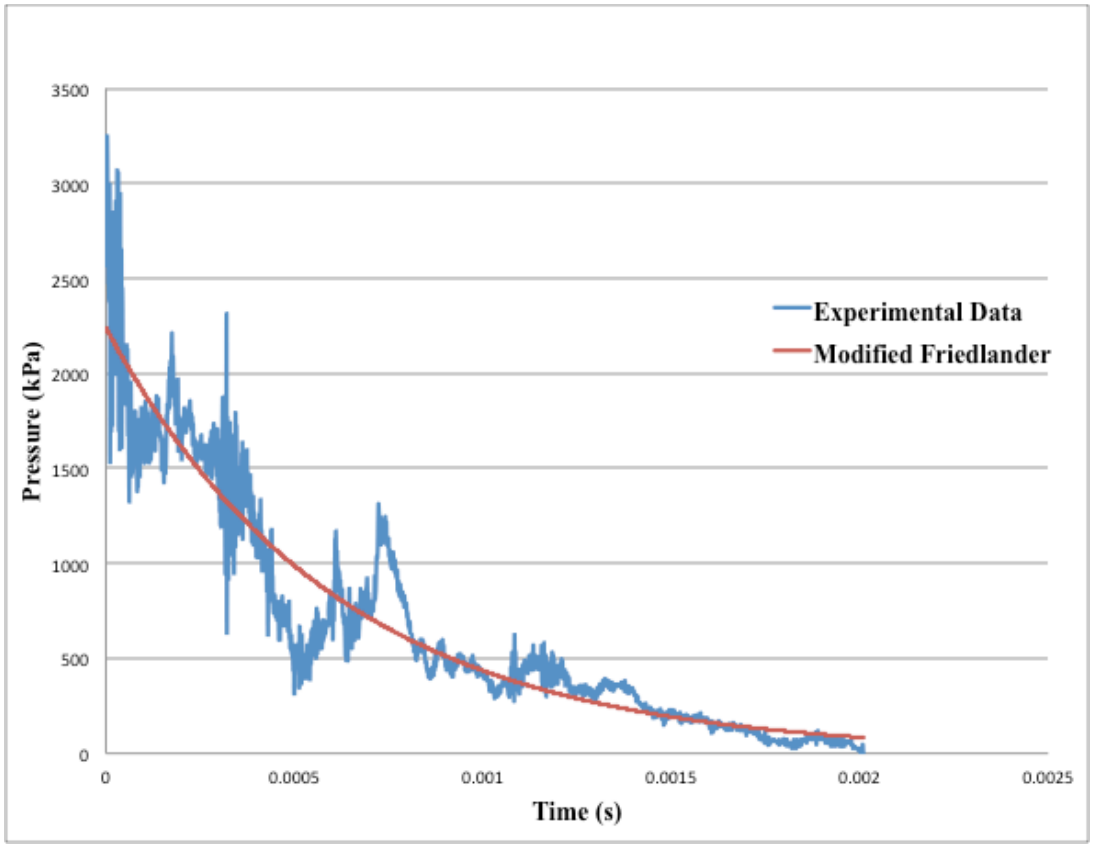

Figure 5.7: Pressure – Time History for Blast Load 3

In the FE model, the blast load was loaded into LS-DYNA into *DEFINE_CURVE tab. The modified Friedlander curve was used to apply the reflected pressure to the masonry wall model. The blast load curve *DEFINE_CURVE needs to be used in coincidence with the *SET_SEGMENT (SSID) which is set to the front face of the masonry wall on which the blast pressure will be applied.

5.3 Model Verification

5.3.1 Comparison of Experimental and Numerical Results

The LS-DYNA FE model was developed to predict the experimental blast test failure modes and damage patterns (Chapter 3). This chapter confirms the developed FE model compares well to the experimental testing in Chapter 3. This model was also developed to verify its reliability on predicting similar blast tests in future analysis without the expense of experimental testing and ensuring it is computationally efficient. The experimental testing is compared with the FE model by the general overall failure modes and damage patterns. The FE model was also used to predict peak deflections to compare to the experimental results recorded by the centre LVDTs. The predictions were in close agreement for walls for the low level blast tests but had convergence problems with the higher levels.

5.3.2 Comparison of Failure Modes/Damage

It is significant for the FE model to be able to predict the correct failure modes and damage patterns for the wall specimens. In the FE simulations the masonry walls experienced different failure mechanisms, exactly as the experimental testing. There was flexure failure, shear at supports, punching shear failure and in most cases, crushing of the masonry in the boundary regions, and a combination of all above failure mechanisms. It is important to predict the correct failure mechanism with correct damage patterns. To compare the experimental walls damage to the FE simulation in LS-DYNA, the plastic strain was used to capture the damage in the FEM. The effective strain establishes the

weakest parts of the walls and their location by the highest strain areas, which in the physical experimental testing produced crushing and large cracks in the masonry. The main experimental failure modes in the masonry walls were crushing of the masonry at boundary regions, a development from the arching action, visible in the FEM as a high damage around the perimeter of the frame. Other failure modes involved high damage around the wall corners (diagonal cracks), and the typical cross hair flexure failure patterns.

Figure 5.8 shows a sample masonry wall, WB6L, subjected to 6 kg of TNT equivalent explosive damage evolution predicted by the FE software LS-DYNA. The damage index is zero for no damage, and undamaged concrete and takes the value of 2.0 for completely damaged concrete, making the LS-DYNA damage index range from 0 to 2.0. The damage from the FEM first developed in localized zones at the corners of the masonry wall, as shown in Figure 5.8 a), where the wall had stiff corners. After the corner damage developed, tensile cracks developed in both vertical and horizontal directions at the centre of the wall. This damage in the FEM and large crack in the experimental testing propagated the entire length of the wall from one side to the other (Figures 5.8 a) – g)). The damage patterns continued to worsen due to the arching mechanism and bending in both directions. This crack pattern is a typical flexure "cross hair" failure mode that was produced in the lowest explosive blast load.

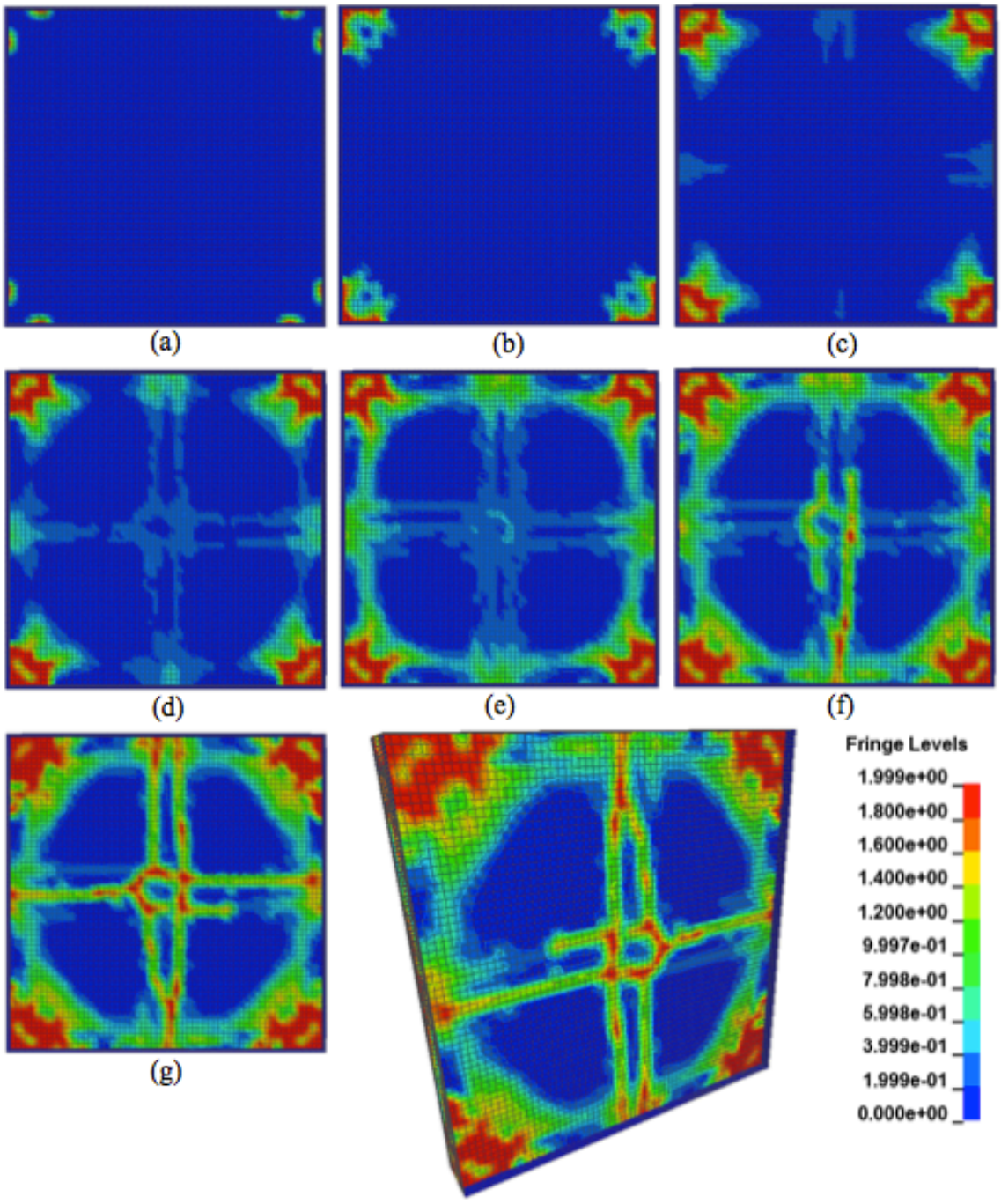

Figure 5.8: Damage evolution of FEM WB6L, subjected to 6 kg of TNT equivalent

5.3.2.1 6 kg of TNT equivalent – WB6L, WB6M, and WB6H failure patterns

The LS-DYNA models first group of walls predicted was from the lowest blast load at 6 kg of TNT equivalent. Figure 5.9 shows a comparison between the damage pattern from the experimentally tested wall WB6L and the predicted damage pattern from the FE analysis. All three-wall types had very similar predicted crack patterns from LS-DYNA. The lowest reinforcement ratio walls crack patterns were more pronounced, as shown in the comparison below.

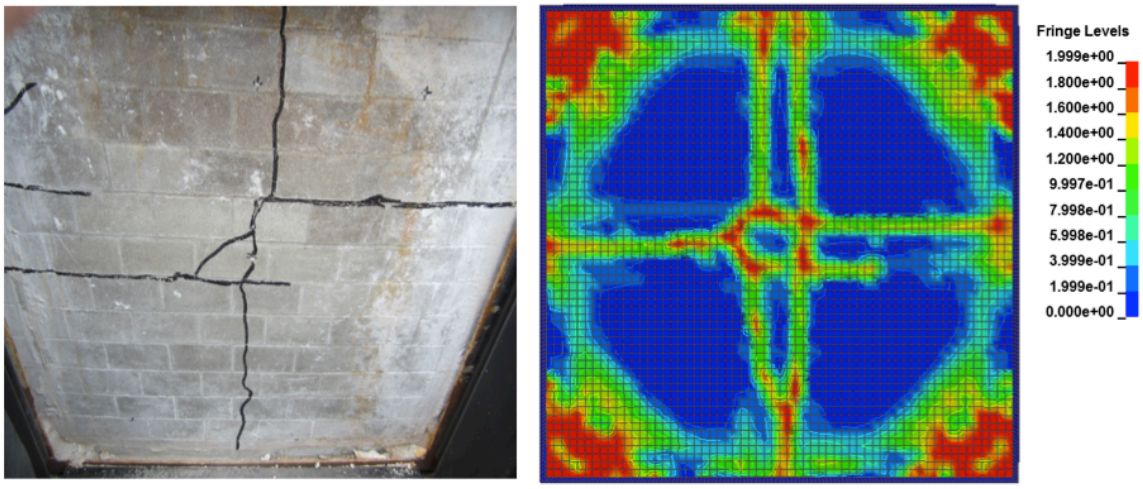

Figure 5.9: Damage comparison of FEM WB6L, subjected to 6 kg of TNT equivalent: a) Experimental; b) FEM

Figure 5.9, wall WB6L, which has D4 reinforcement in every other cell, had almost identical crack patterns as the experimentally tested wall of the same. The damage from the FEM first developed in localized zones where stiff hydrostone was used at the corners

of the masonry wall. After the corner damage developed, a large damage pattern developed on the model in both vertical and horizontal directions at the centre of the wall. The damage in the FEM propagated the entire length of the wall from one side to the other. The high damage was also around the perimeter of the wall, where the wall was arching and continued to increase due to the arching mechanism and the two-way bending. This crack pattern is a typical flexure "cross hair" failure mode and was produced in the lowest explosive blast load to all three walls.

5.3.2.2 12 kg of TNT equivalent – WB12L, WB12M, and WB12H failure patterns

The second group of walls were modeled and compared to the 12 kg of equivalent TNT experimental blast load. This group of walls all performed similarly with more prominent flexural cracks in the horizontal and vertical axis spanning from one side of the wall to the opposite side. They also displayed shear cracks in the diagonal corners of the wall. The FEM model predicted the cross hair flexure failure mode with the horizontal and vertical damage patterns as well as having the high diagonal damage in the top corners. The FEM damage patterns are completely symmetrical again, ensuring that the wall is acting two-ways. The wall specimen in Figure 5.10 developed a flexure failure with combined shear failure in the corners. Figure 5.10 shows a comparison between the damage pattern from the predicted LS-DYNA model for wall WB12M at a 12 kg of TNT equivalent blast load and that observed from the experimental test with the same wall and charge weight.

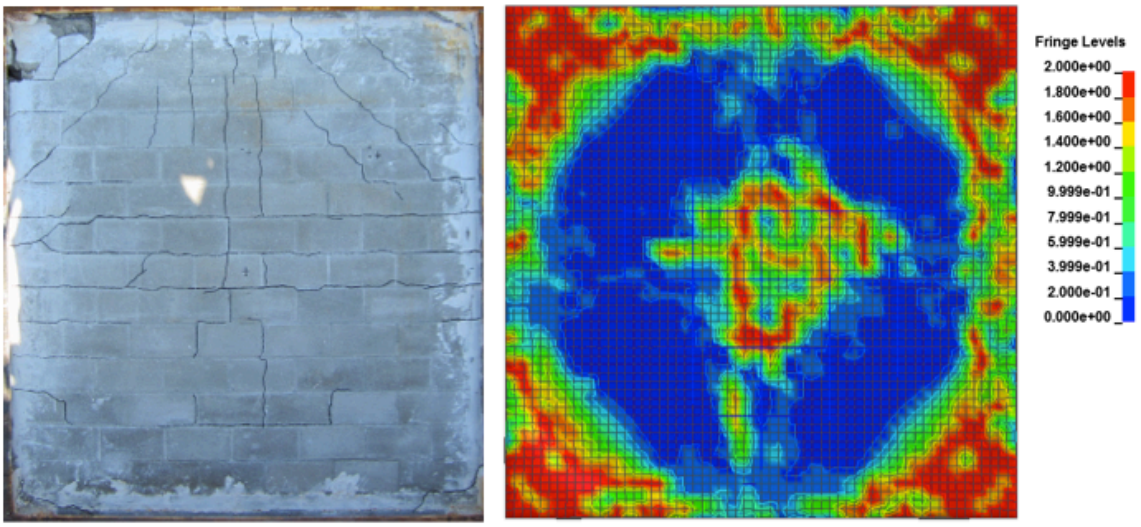

Figure 5.10: Damage comparison of FEM WB12M, subjected to 12 kg of TNT equivalent: a) Experimental; b) FEM

5.3.2.3 30 kg of TNT Equivalent – WB12L, WB12M, and WB12H Failure Patterns

The last group of walls were modeled and subjected to a 30 kg of equivalent TNT blast load in LS-DYNA. WB30L was the first wall modeled in LS-DYNA. Figure 5.11 shows a comparison of wall WB30L showing the damage predicted by the FEM in LS-DYNA and the observed damage from the experimental blast tests.

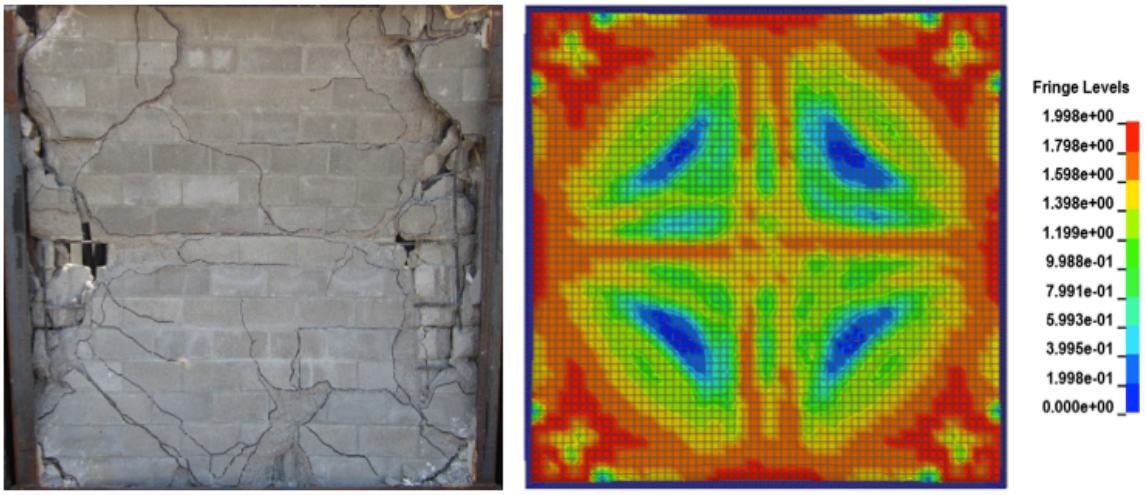

Figure 5.11: Flexure failure Damage FEM WB30L, subjected to 30 kg of TNT equivalent: a) Experimental; b) FEM

The LS-DYNA FEM damage confirms that WB30L is acting in two ways and most importantly, the wall is arching. As shown in the figure above, the wall had very large damage around its perimeter and where the walls arching effect developed. This was the main failure mode for wall WB30L in the experimental test. The simulation also showed a flexure failure mode and the high damage diagonally, shearing at the corner supports. This FE simulation compared well to the experimental test with the combined shear and flexure failure and the high arching force and rotation around the perimeter. WB30L was completely destroyed during the experimental and had a high amount of damage in the FE model. Wall WB30M with the middle reinforcement ratio had similar results to the first wall, although there was not the same extent of crushing of the masonry from the arching effect. The last wall WB30H from the experimental test with the largest reinforcement ratio had the top corner of the wall blown out. This was caused from the high explosive

charge and the top weld in the C-Channel breaking apart. The last FE model WB30H showed the same results as the first two walls but with less of pronounced damage patterns.

5.3.3 Comparison of peak deflections

The objective of the FEM was to predict the failure mechanism and damage patterns. Nevertheless, the FEM did generate the wall displacement history and thus, the maximum central displacements. In LS-DYNA, a D3Plot file is generated by the LS-DYNA solver and opened in LS-PrePost to acquire the simulation's solution. The centre mid-point node in the FEM is selected, then plotted to compare with the experimental centre LVDT for each tested wall specimen. This is important as, in most blast standards, the damage level is based on wall chord rotation, which can be correlated to the maximum central displacement. Reviewing similar research in FE modelling of blast loading of structures, Dennis et al. (2002), Seyedrezai (2011), and Chaimoon and Attard, (2007), reported a range from 10% to 30% central displacement error. For the FEM in this section of the thesis, the 30% error threshold was used as the upper bound for the FE model. This error threshold was chosen due to the fact that only one wall was experimentally tested at each scaled distance and the uncertainty of blast loading to the two-way arching masonry walls. Although, for the low level blast, the FEM analysis yielded much less error, as the damage level increases, it is very difficult to predict and simulate the experimental behavior of masonry walls under high impulsive loads due to solution convergence problems.

5.3.3.1 6 kg of TNT equivalent – WB6L, WB6M, and WB6H deflections

Wall WB6L was the first wall analyzed in Group I, which had the lowest reinforcement ratio. The next two walls modeled, had an increase in their reinforcement ratios. It can be observed from Figure 5.12, that the maximum displacement from the FE simulation for wall WB6L is 17.25 mm. This is in very close agreement with the experimental displacement at 17.65 mm, which gives a 2.3% error. The displacement response closely resembles the shape from the experimental data with both FEM and experimental walls and both having close permanent deflections.

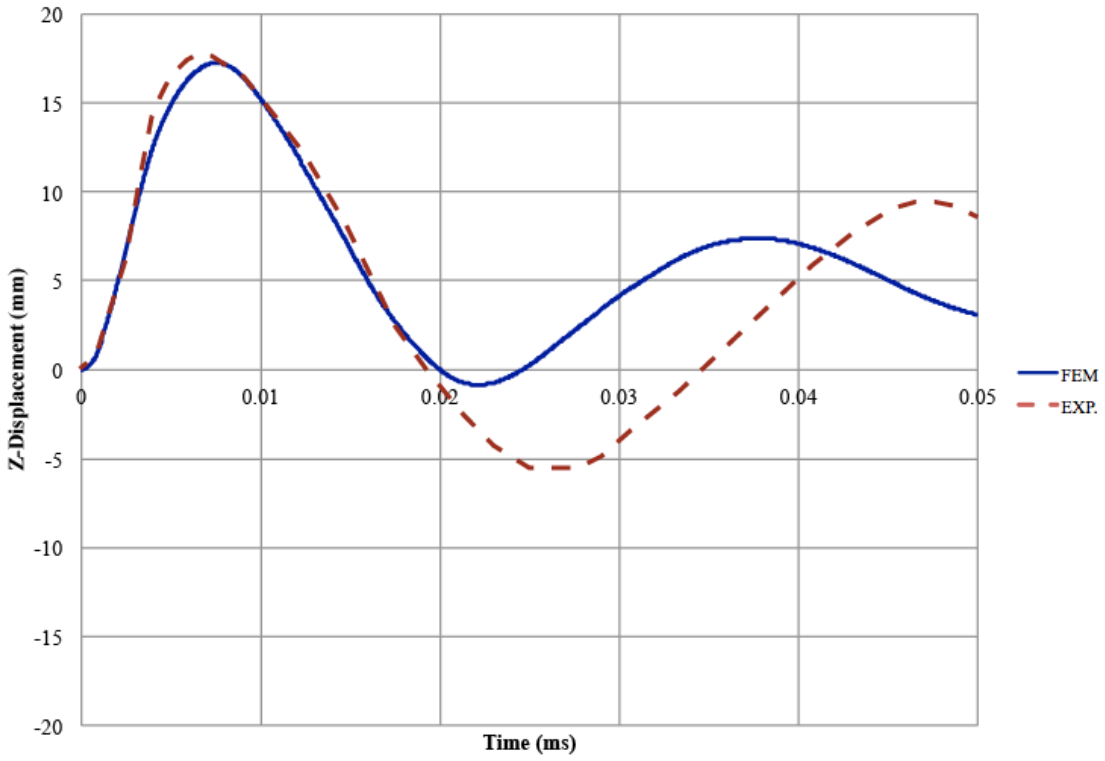

Figure 5.12: Displacement Time History WB6L – 6 kg of TNT Equivalent

The next two FE simulations WB6M and WB6H, at the 6 Kg of TNT, produced maximum displacements, ranging from 12.0 to 9.8 mm, respectively. They both

compared well to the experimental test walls with peak deflection of 13.3 mm for WB6M and 10.5 mm for wall WB6H. When picking different quadrant nodes in the FE model, for example, at ¾ height and to the right at ¾ wall width in the FEM model, one can see similar displacements to the experimental tested walls. Also, picking different quadrant nodes and plotting them authenticates that the wall is in fact, acting in two-ways as shown in Figure 5.13.

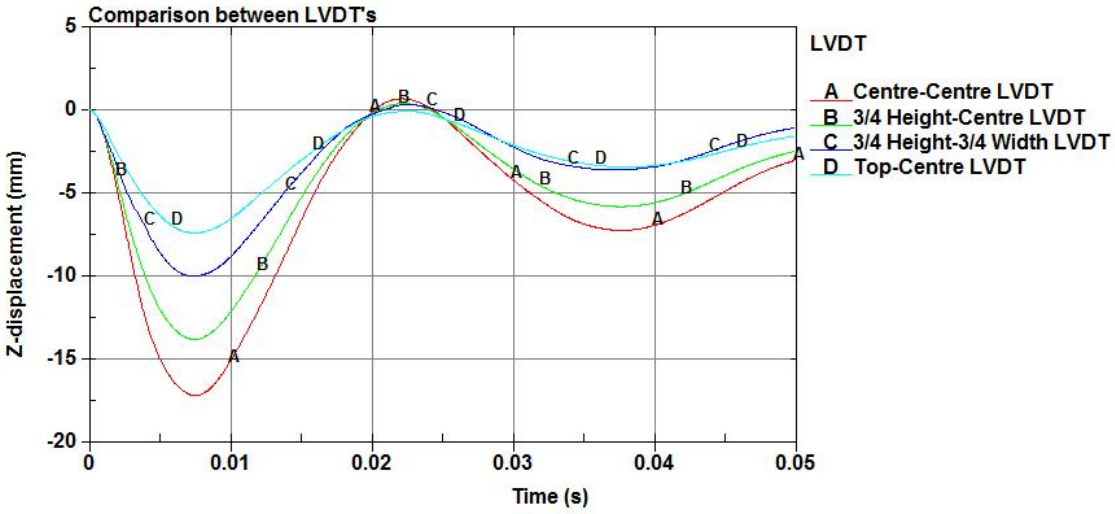

Figure 5.13: Displacement Time History in LVDT location of wall WB6L – 6 kg of TNT Equivalent

5.3.3.2 12 kg and 30 kg of TNT equivalent

The next group of walls predicted from LS-DYNA, were subjected to 12 kg and 30 kg blast load at a 5m stand-off distances. With the higher blast loads of 12 kg and 30 kg of TNT equivalent, artificial damping had to be added so the walls did not continue to deform and there was a permanent deflection. The artificial damping significantly

minimized the convergence problem with the larger blast loads and the walls having a large accumulation of damage. The *DAMPING_GLOBAL tab was added in LS-DYNA with a 15% system damping constant. These walls modeled in LS-DYNA gave significant convergence issues with the model. Although the peak deflections were in the 30% error threshold the trend of the FEM does not however match that of the experimental results.

Overall, when comparing the peak deflections of the FE simulations from the two-way arching reinforced masonry walls to the experimental testing, the lowest blast load predicted well within the 30% error threshold set initially. The overall response of the walls was closely captured with the lowest blast load. When the larger blast loads were used, there was a significant variation to the overall response of the wall. This variation was due to convergence issues with the FE model, which will require further analysis.

5.5 Summary and Conclusions

The FE model's focus was to predict the experimental wall's behaviour in terms of damage patterns and it's failure mechanisms. The FE model's predictions were accurate in failure modes and damage patterns. The FEM also predicted the centre, mid-height displacements. The maximum displacements for the low-level blast loads gave good results compared to the experimental blast tests. With the higher-level blast loads, the maximum displacements had significant convergence issues with the FE model. These convergence issues made the overall response of the walls not match the experimental.

6 Conclusions and Recommendations

6.1 Conclusions

In addition to exploring alternative construction techniques of blast-resistant reinforced masonry walls, it is important to evaluate the blast performance of current reinforced masonry construction, determine its limitations and provide potential improvements in order to continue to promote its use as a viable, cost-effective building system. The thesis discussed the experimental results tests and numerical model results of nine, third-scale, two-way arching, masonry walls were experimentally investigated under different levels of free field blast loads and scaled distances. This study demonstrates the effectiveness of two-way arching on enhancing the performance of masonry infill walls as well as a cost effective system for building envelopes. The reported experimental results demonstrate the beneficial effect of two-way arching on the out-of-plane response of reinforced masonry walls under blast loads. The governing failure mode of the experimental wall specimens was flexure with some signs of shear in the corners as well as with the higher explosive charges; there was severe masonry crushing around the perimeter of the wall specimen from the arching effect. Forcing arching action to develop by-design presents a cost-effective way to enhance the capacity of reinforced masonry wall against blast loading. The arching effect can also limit the amount of flying debris, which in turn can increase public safety and minimize the hazard level for building occupants. Within the larger MBPD project, the experimental test results are expected to contribute to quantifying the arching response of masonry walls under blast. This study would also contribute to the CSA S850 future editions.

The following conclusions can be made from the static test experimental results, post blast results and analysis:

1. The out-of-plane capacities were conducted using an air bag system to observe the overall capacity of the masonry walls. This static capacity (and corresponding resistance function) can be used later in a SDOF analytical analysis. Wall WBL experimental static capacity was 157 kPa, wall WBM was 167 kPa, and wall WBH was 230 kPa.
2. The out-of-plane flexural capacity of each of the three masonry wall types were determined using simple yield line approach as well as the flexural out-of-plane wall equation and the MSJC (2013) arching infill wall capacity prediction approach to capture the flexural and arching failure mechanisms. These calculated capacities of the reinforced masonry infill walls determined that the out-of-plane analysis significantly underestimated the out-of-plane capacity of the infill walls that was verified by static testing. These infill wall capacity predictions did not take into account all the failure mechanisms and it is thus imperative that these results be used in further development to future blast and masonry infill wall design provisions and should be further investigated.
3. Two-way arching reinforced masonry walls significantly reduces structural damage and increases out-of-plane resistance, which in turn enhances overall structural integrity and ultimately building preservation.

4. Both the Canadian CSA S850 and the American ASCE 59-11 blast standards do not account for the arching action, which can considerably enhance the performance of the masonry infill wall.
5. The governing failure modes of the nine experimental wall specimens were a combined flexure and shear failure. The CSA S850-12 blast standard does not give performance limits for shear or combined shear and flexure failures.
6. When subjected to a free field blast, two-way arching mechanism can considerably reduce debris and dispersal of debris, in turn increasing public safety and minimizing hazard levels.
7. The two-way arching reinforced masonry walls behavior was modeled using Finite Element software, LS-DYNA. The model was analyzed from the failure modes and damage patterns predicted from the FE analysis. The objective was to predict the experimental blast testing in the form of a dynamic model. It can be concluded that the FE model's predictions gave good indications of the walls failure modes and damage patterns. Although the FE model can be used to predict the peak deflections, the overall wall response history was not accurately captured with the FEM. The FE model had significant variation to the wall response with the higher blast loads. This variation was due to convergence issues with the FE model, which will require further analysis.

7.2 Recommendations

This thesis studied the beneficial effect of two-way arching on the flexural behaviours of reinforced steel masonry walls under impulsive loading. While significant progress has been outlined, there are areas requiring more extensive experimentation, and analytical modeling. While this research paper explored the use of Finite Element modeling, a simplified SDOF analytical model should be explored and evaluated. Further research and sensitivity analysis for this FE model should be expanded and should be further researched, i.e. comparing Concrete Damage REL 3 to the Winfrith Concrete model. Pressure Impulse (P-I) diagrams and/or ISO Damage Curves should be generated for infill walls for practical application by structural designers. Producing P-I Diagrams consist of several damage contour lines that would correspond to different levels of damage and failure. These in turn, can be used to develop blast standards for engineers to deign structures subjected to different levels of blast loading.

References

Abou-Zeid, Badr M., El-Dakhakhni, W., Razaqpur, A.G., and Foo, S. (2011) *"Response of Arching Unreinforced Concrete Masonry Walls to Blast Loading."* ASCE journal of structural engineering., 137(10), 1205-1214.

American Society of Civil Engineers (ASCE). (2011), *"Blast Protection of Buildings ASCE 59-11."* Reston, Virginia, USA.

American Society for Testing Materials (ASTM), (2011) A615-12. *"Standard Specification for Deformed and Plain Carbon-Steel Bars for Concrete Reinforcement."* Conshohocken, PA, USA.

American Society for Testing Materials (ASTM). (2011), C1314-11a. *"Standard Test Methods for Compressive Strength of Masonry Prisms."* Conshohocken, PA, USA.

B.R. Banting, P. Heerema, and W.W. El-Dakhakhni. (2010) *"Production and Testing of 1/3 Scale Concrete Blocks."* 8th International Masonry Conference. Dresden, Germany.

Baker, W.E. (1973) *"Explosions in Air"* University of Texas Press, Austin, TX, USA.

Baker, W.E., Cox, P.A., Westine, P.S., Kulesz J.J., and Strehlow., R.A. (1983)

"Explosion Hazard Evaluation." Elservier Scientific Publishing Company. Oxford, New York, USA.

Baylot, James T., Bullock, Billy, Slawson, Thomas R., and Woodson, Stanley C. (2005) *"Blast Response of Lightly Attached Concrete Masonry Unit Walls."* Journal of Structural Engineering 131, no. 8. 1186-1193.

Canadian Standards Association (CSA) A165.1. (2004) *"CSA Standards on Concrete Masonry Units."* Mississauga, ON, Canada.

Canadian Standards Association (CSA) A179-04. (2004) *"Mortar and Grout for Unit Masonry."* Mississauga, ON, Canada.

Canadian Standards Association (CSA) S850-12, (2012). *"Design and Assessment of Buildings Subjected to Blast Loads."* Mississauga, ON, Canada.

Chaimoon, Krit, and Attard, Mario M. (2007) *"Modeling of Unreinforced Masonry Walls under Shear and Compression."* Engineering Structures 29, 2056-2068.

Crawford, J.E., Wu, Y., Choi, Y., Magallanes, J., and Lan, S. (2012) *"Use and Validation of the Release III K&C concrete material model in LS-DYNA."* Karagozian & Case Structural Engineers, Report TR-11-36.5. California.

Dawe, J. L., and Seah, C. K. (1989). *"Out-of-plane Resistance of Concrete Masonry Infilled Panels."* Can. J. Civ. Eng., 16, 854-864.

Dennis, Scott T., Baylot, James T., and Woodson, Stanley C. (2002) *"Response of 1/4-Scale Concrete Masonry Unit (CMU) Walls to Blast."* Journal of Engineering Mechanics 128, no. 2. 134-142.

Dynasupport (2011) *"Hourglass (HG)."* LS-DYNA Support, http://www.dynasupport.com/howtos/element/hourglass, accessed August 1, 2013.

Eamon, Christopher D., Baylot, James T., and O'Daniel, James L. (2004) *"Modeling Concrete Masonry Walls Subjected to Explosive Loads."* Journal of Engineering Mechanics 130, no. 9. 1098-1106.

Federal Emergency Management Agency (FEMA). (2000). *"Prestandard and commentary for the seismic rehabilitation of buildings."* FEMA 356, Federal Emergency Management Agency, Reston, VA. USA.

Forsen, R. (1985) *"Airblast Loading of Wall Panels."* FOA Rep. C 20586-D6. National Defence Research Institute, Stockholm, Sweden.

Hamed, E. and Rabinovitch, O. (2006) *"Supporting Conditions Effects in The Out-of-Plane Behavior of URM Walls Strengthen with Externally Bonded FRP Strips."* Proceedings of Third International Conference on FRP Composites in Civil Engineering (CICE 2006), Miami, Florida, December, 519 – 522.

Hamid, A.A., and Drysdale, R.G. (2005) *"Masonry Structures: Behaviour and Design, Canadian Edition."* Mississauga, ON, Canada.

Hao, D., and Zhongxian, L., (2009). *"Numerical Analysis of Dynamic Behavior of RC slabs Under Blast Loading."* Transactions of Tianjin University., 15, 61-64.

Harris, H. G., and Sabnis, G. M. (1999). *"Structural Modeling and Experimental Techniques."* 2nd Ed., CRC Press, Boca Raton, FL.

Hopkinson, B. (1915). *"British Ordinance Board Minutes"* 13565.

Hrynyk, Trevor D. and Myers, John J. (2008). *"Out-of-Plane Behavior of URM Arching Walls with Modern Blast Retrofits: Experimental Results and Analytical Model."* ASCE journal of structural engineering, October. 134:10, 1589-1597.

Hyde, D.W. (1990) *"Conventional Weapons Effect (CONWEP) - Application of TM5-855-1."* US Army Engineer Waterways Experiment Station. Vicksburg, MS, USA.

Landry, K. L. (2003) *"The blast resistance of unreinforced, ungrouted, one-way, concrete masonry unit walls."* PhD dissertation, Rensselaer Polytechnic Institute, Troy, N.Y.

Li, Z., and Hao, H. (2012) *"Advances in Protective Structures Research."* Taylor and Francis Group. London, England.

LSTC, Livermore Software Technology Corp. (2007) *"LS-DYNA Keyword User's Manual – Version 970 and 971."* Livermore, California.

Masonry Standards Joint Committee. (MSJC). (2013). *"Building Code Requirements for Masonry Structures."* TMS 402/ASCE 5/ACI 530, The Masonry Society, American Society of Civil Engineers, Boulder, New York/American Concrete Institute, and Detroit, USA.

Masonry Society. (1989) *"Proceedings of an International Seminar on Evaluating, Strengthening, and Retrofitting Masonry Buildings"* Arlington, TX, USA.

Mays, G. C. and Smith, P. D. (1995). *"Blast Effects on Buildings."* Thomas Telford Publications. London, England.

McDowell, E. L., Mckee, K. E. and Sevin, E. (1956). *"Arching Action Theory of Masonry*

Walls." J. Struct. Div., 82(2), 1-8.

Myers, J., Belarbi, A., and Khaled, A. (2004) *"Blast Resistance of FRP Retrofitted Un-Reinforced Masonry (URM) Walls with and without Arching Action."* TMS J., 22(1), 9-26.

Park, R. and Gamble, W. L. (2000). *"Reinforced Concrete Slabs: Second Edition."* John Wiley & Sons Inc. New York City, New York, USA.

Randers-Pehrson and Bannister (1997) *"Airblast Loading Model for DYNA2D and DYNA3D"* Army Research Laboratory. ARL-TR- 1310.

Schwer, L. and L. Malvar (2005) *"Simplified concrete modeling with *MAT_CONCRETE_DAMAGE_REL3."* In proceedings. LS-DYNA Anwenderforum, Bamberg.

Seyedrezai, Seyedehshadi (2011) *"Modeling of Arching Unreinforced Masonry Walls Subjected to Blast Loadings."* M.A.Sc. Thesis. McMaster University. Hamilton, ON, Canada.

Smith, P.D., Hetherington, J.G., Burlington (1994) *"Blast and Ballistic Loading of Structures."* Butterworth-Heinemann, London.

Strehlow, Roger A., and Baker, Wilfred E. (1976) "*The Characterization and Evaluation of Accidental Explosions."* Progress in Energy and Combustion Science 2, no. 1 27-60.

Varela-Rivera, Jorge, Moreno-Herrera, Joel, Lopez-Gutierrez, Ivan, and Fernandez-Baqueiro, Luis (2012) *"Out-of-Plane Strength of Confined Masonry Walls."* ASCE Journal of Structural Engineering, November. 138,1331-1341.

Zongiin, Li (2011) *"Advanced Concrete Technology."* John Wiley and Sons Inc. Hoboken, New Jersey, USA.